Study of pattern formation in drying colloidal suspensions with varying pH and different parameters on different substrates.

Thesis submitted for the Degree of Doctor of Philosophy (Science)

In **Physics**

By

Samiul Haque

Post Graduate and Research Department

of

Physics

St. Xavier's College (Autonomous), Kolkata

Affiliated to the **University of Calcutta**

2023

St. Xavier's College, Kolkata
Kolkata-700016
INDIA
Post Graduate and Research Department of Physics

CERTIFICATE FROM SUPERVISOR

I, certify that the thesis entitled **"Study of pattern formation in drying colloidal suspensions with varying pH and different parameters on various substrates**." submitted by **Samiul Haque** for the degree of Doctor of Philosophy (Ph.D.) in Physics in the area of Soft Matter Physics is the record of research work carried out by him during the period from 28.06.2018 to 15.09.2023 under my guidance and supervision and that this work has not formed the basis for the award of any Degree, Diploma, Associateship, Fellowship, Titles in this University or any other University or other similar institution of Higher learning.

Signature of Supervisor

Dr. Tapati Dutta
Associate Professor
Physics Department
St. Xavier's College, Kolkata
Kolkata-700016

" IN THE NAME OF ALLAH, THE MOST GRACIOUS AND MOST MERCIFUL"

Dedicated to
Ammara Khatun (my wife)
Sulekha Khatun (my mother)
Md Ajijul Haque (my father)

ACKNOWLEDGMENTS

The research work of this thesis entitled **"Study of pattern formation in drying colloidal suspensions with varying pH and different parameters on different substrates"** has been carried out at the Department of Physics of St. Xavier's College, Kolkata-700016 under the principal guidance of **Dr. Tapati Dutta**. I enrolled my name on 29-06-2018 and registered on 11-05-2019 with Registration No: *PHD/18/PHY/05(2018-19)*. At the end of this phase of my academic career, I would like to use this space to express my gratitude for all the assistance and support during this entire journey.

I will remain grateful forever to **Dr. Tapati Dutta** for my entire research work. She has a wonderful personality and is a very good teacher, a guide for anything. During this long period, she listened to all my problems with her incomparable patience and showed me the solution with her knowledge and experience. Her insightful suggestions pushed me to new ideas and sharpened my thinking always. Her enormous enthusiasm and encouragement made this journey enjoyable.

I am grateful to **Prof. Sujata Tarafdar** who gave her valuable time for my research work. Her valuable suggestions, advice, and her insistence on clarity always show new sight to explore the problem. I express my deep gratitude for her excellent behavior and all type of helps during this journey.

I am thankful to Tajkera di, who first introduced me to this research area and helped me a lot at the beginning of this course. I would like to thank Dr. Saswati Majumder, Moutushi di, and Abhro da who spent their valuable time providing valuable suggestions and other help.

I extend my gratitude to our respected Father principal Dr. Dominic Savio S.J for giving me the opportunity to pursue my work at St. Xavier's College, Kolkata. I am also grateful to Dr. Samrat Ray,

Ph.D. coordinator of our college for extending his helpful hand for academic purposes.

I sincerely acknowledge all our professors in the Department of Physics. Whenever I needed help, they extended their helping hand.

I am thankful to Rahul sir and Indranil sir for giving me their valuable time and suggestions.

The working environment of the Central Research Facility (CRF) is obviously to be mentioned. I express my thanks to the director of CRF Dr. Rina Ghosh for her support in the Laboratory. The help and support I got from Mr. Arup Mandal and Mr. Pallab Palta who are the staff members of CRF must be mentioned. They help me a lot during lab work. Thanks to the staff members of the Physics Department and Chemistry Department for providing me required materials facility when I needed them.

I would like to mention the names of Ruhul, Anamika di and Ashadul Haldar with whom I have worked during the tenure of my works. Special thanks to Ruhul who always extended his helping hand to solve any technical problem that I faced during this academic journey.

I express my wholehearted gratitude to my parents for their enormous support, sacrifice, and blessings throughout my life. This thesis would be unfinished if I don't convey my gratitude to my wife Ammara Khatun who has given me constant encouragement and mental support in all possible ways during this academic journey. At the early stage of this journey, she helped me a lot in laboratory work. Lastly, I make a special and most worthy mention of my only son Adnan Sami who is just two months old.

Samiul Haque

Contents

Contents ix

List of Figures xiii

List of Tables xvii

1 Introduction 1
- 1.1 Introduction to colloidal suspension . . . 4
- 1.2 Introduction to Laponite clay . . . 5
- 1.3 Charge distribution of a Laponite particle . . . 6
- 1.4 Patterns depend on interface geometry . . . 9
- 1.5 Concepts of Fracture mechanics . . . 11
  - 1.5.1 Basic modes of fracture and stress intensity factor . . . 13
- 1.6 The Griffith Theory . . . 14
- 1.7 Formation of desiccation crack . . . 16
  - 1.7.1 Effect of capillary pressure and clay layer thickness . . . 19
- 1.8 Theoretical concept: Drying dynamics of an evaporating droplet . . . 20
  - 1.8.1 Surface Tension and Youngs' equation . . . 20
  - 1.8.2 Nature of surface and wetting phenomenon . . . 22
  - 1.8.3 Different flows inside the droplet . . . 24

2 Impact of preparation protocol of colloidal suspension on drying droplet on different substrates 30
- 2.1 Introduction . . . 30
- 2.2 Review of related work . . . 32
- 2.3 Materials and Experimental Methods . . . 36
- 2.4 Results . . . 37
  - 2.4.1 Evaporation rate on glass and acrylic substrates . . . 38
  - 2.4.2 Role of substrate on evaporation rate . . . 38
  - 2.4.3 Final pattern after complete drying . . . 39
- 2.5 Effect of changing ultrasonication time . . . 42
- 2.6 Explanation . . . 46
- 2.7 Conclusion . . . 51

3 Pattern formation of aqueous Laponite droplet on different substrates with varying pH 58

3.1 Introduction . . . 58
3.2 Earlier work related to Laponite . . . 60
3.2.1 Laponite particle and its characterization . . . 60
3.3 Materials and Experimental Methods . . . 63
3.4 Different forces at play . . . 65
3.5 Experimental results and discussions . . . 66
3.5.1 Pattern formation on PMMA: Hydrophobic substrate . . . 68
3.5.2 Pattern formation on Glass and Quartz: Hydrophilic substrate 73
3.6 Cavity formation in acidic pH on PMMA substrate . . . 76
3.7 Conclusion . . . 77

4 Role of pH and concentration on desiccation crack of aqueous Laponite suspension 83
4.1 Introduction . . . 83
4.2 Review of earlier related work . . . 84
4.3 Materials and Experimental Methods . . . 87
4.4 Results and discussions . . . 88
4.4.1 Variation of pH . . . 88
4.5 Effect of concentration variation on the crack pattern . . . 93
4.6 Effect of variation of film thickness . . . 97
4.7 Lace crystallization pattern . . . 98
4.8 Conclusions . . . 100

5 Fabrication of Transparent Conducting Sheet tailoring the pH-regulated desiccation crack network. 106
5.1 Introduction . . . 106
5.2 Review of earlier related works . . . 107
5.3 Fabrication of transparent conducting film by modulating the desiccation crack. . . . 109
5.4 Fabrication method of Transparent Conducting Sheet (TCS) . . . 110
5.4.1 Determination of optical properties of TCS . . . 112
5.5 Result . . . 112
5.6 Discussions . . . 114
5.7 Conclusion . . . 118

6 Summary and Future Outlook 123

7 The end after ending: Aggregation patterns of copper sulphate salt via droplet drying: Mediation by surface hydrophobicity and salt concentration 128
7.1 Introduction . . . 128
7.2 Materials and Methods . . . 132
7.3 Theory . . . 133

7.4 Results and Discussions 135
7.5 Characterization through Euler characteristics 136
7.6 Wetting and Drying 139
7.7 Conclusion 144

List of Figures

1.1 The schematic diagram of tetrahedal sheet and octahedral sheet of Laponite particle. 6
1.2 The schematic diagram of atomic arrangement of Laponite particle. . 7
1.3 Increasing size of the droplet. Curved surface changes to the flattened surface with increase in size. 10
1.4 Schematic diagram of three different fracture modes. 13
1.5 Formation of mud crack in a cultivated land. Both T junction and Y junction cracks are observed 18
1.6 Youngs' equation: Force balance at the Triple Phase Contact Line . . 21
1.7 Droplet on different substrates. a) Hydrophilic b) Hydrophobic c) Superhydrophobic 23
1.8 Typical evaporation modes of a drying droplet. 23
1.9 Flow inside the droplet: a) Capillary flow b) Marangoni flow c) Flow due to DLVO force 25

2.1 a) Evaporation rate on hydrophilic substrate(glass) for SetI and SetII experiments. b) Evaporation rate on the hydrophobic substrate(acrylic) for SetI and SetII experiments. 37
2.2 a) Comparison of evaporation rate on both substrates for SetI (stirring by Magnetic stirrer) experiments. b) Comparison of evaporation rate on both substrates for SetII (stirring by Ultrasonicator) experiments. 38
2.3 Final pattern of dried droplet on a)acrylic substrate b) on glass substrate for SetI experiment (stirring by Magnetic stirrer). Final pattern of dried droplet on c)acrylic substrate d) on glass substrate for SetII experiment (stirring by Ultrasonicator) 40
2.4 Final pattern of the dried droplet on hydrophobic substrate(acrylic) for different ultrasonication times varying from 5 min to 45 min in step of 5. 41
2.5 Final pattern of the dried droplet on hydrophilic substrate(glass) for different ultrasonication times varying from 5 min to 45 min in step of 5. 42
2.6 Time development of a drying droplet on glass substrate for both set of experiments 43
2.7 a) Variation of ring width at the TPCL with the variation of ultrasonication time. b) Variation of average crack spacing at the ring with the variation of ultrasonication time 44

2.8 Time development of a drying droplet on acrylic substrate for SetI experiment . . . 46
2.9 Time development of a drying droplet on the acrylic substrate for SetII experiment . . . 47

3.1 Contact angle of aqueous Laponite droplet on a)glass b)quartz and c)PMMA substrate. d) Surface tension at the TPCL. e)Rate of change of contact angle of Laponite droplet on PMMA substrate for different pH values. The region between the vertical and dotted lines is the time duration for constant contact angle. . . . 63
3.2 Bottles are contained with aqueous Laponite suspension with 1% concentration for different pH values, after 90 hours since sample preparation time. pH values are from left to right: 0.95, 1.18, 1.88, 5.65, 6.5, 7, 9, 12, 12.3. . . . 64
3.3 Final pattern of the dried droplet of aqueous Laponite droplet on PMMA substrate of different pHs a)0.95 b)1.18 c)1.88 d)5.6 e)6.5 f)7 g)9 h)12 i)12.3. The scale bars are of 200μm . . . 67
3.4 Time development of drying droplet of aqueous Laponite with pH value 0.95 on PMMA substrate. The scale bar mentioned in the figures is 200μm . . . 68
3.5 Time development of drying droplet of aqueous Laponite with pH value 12.3 on PMMA substrate. The scale bar mentioned in the figures is 200μm . . . 70
3.6 Final pattern of the dried droplet of aqueous Laponite droplet on the glass substrate of different pH values a)0.95 b)1.18 c)1.88 d)5.6 e)6.5 f)7 g)9 h)12 i)12.3. The scale bars are of 200μm . . . 72
3.7 Deposition of crystal in a dried droplet of aqueous Laponite on glass substrate at pH=12.3 a) center of the droplet b) pattern near the contact line. c) crystalline deposit at pH 12.3 on PMMA substrate. The scale bars are of 200μm . . . 73
3.8 Final pattern of the dried droplet of aqueous Laponite droplet on a quartz substrate of different pH values a)0.95 b)1.18 c)1.88 d)5.6 e)6.5 f)7 g)9 h)12 i)12.3. The scale bars are of 200μm . . . 75
3.9 Pattern of aqueous Laponite droplet at pH 1.88 in different magnifications on different substrates. a) and b) pattern on PMMA substrate. c) and d) pattern formation on a glass substrate. . . . 76

4.1 Desiccation crack patterns of aqueous Laponite suspension with varying pH. a)0.445 b)0.765 c)1.68 d)3.43 e)5.93 f)6.73 g)9.25 h)12.25 i)13.05 j)13.45 . . . 88
4.2 Area versus perimeter curve of the peds of the films for different pHs. a)pH=0.765 b)pH=1.68 c)pH=13.05 d)pH=13.45 . . . 90

4.3 Variation of fractal dimension of the crack interface d_f with pH. Films of the pH range 3.43 to 12.25 are peeled off from the substrate. Calculation of d_f in this pH range is uncertain. The uncertain region is marked by an arrow line. 91
4.4 a)Schematic diagram of the crack formation of the films around a house-of cards structure at pH value < 11.5 b)Schematic diagram of the crack formation of the films around a stack-coin arrangements at pH value > 11.5 92
4.5 a)Variation of ped number of the films in the basic range of pH. b)Variation of time of first crack appearance of the films with pH. c)Variation of Conductivity of the suspensions with pH. 94
4.6 Desiccation crack pattern of aqueous Laponite suspension on Polypropylene petri dish of diameter 7.25 cm. (a)2% (b)3% (c)4% (d)6% (e)8% (f)10%. 95
4.7 a)Variation of total crack length and ped number with the concentrations of the suspension. Solid green points represent the number of peds and open blue circle represents the crack length. b)Variation of the first crack appearance time with the concentrations of the suspension. 96
4.8 Desiccation crack formation of aqueous Laponite suspension of pH 13.3 on Polypropylene petri dish with varying thickness. (a)0.30 cm (b)0.35 cm (c)0.40 cm (d)0.45 cm . The diameter of the petri-dish is 7.25 cm. 97
4.9 Absence of crystallization pattern at relative humidity of a)30% b)40% d)65%. c) Crystallization pattern at relative humidity 48%. Different magnified portions of the lace pattern are shown. 1) On the branch portion 2) Transparent portion between two branches 3) Lawn portion 4) Lawn portion from where it starts branching. 98
4.10 1) Horizontal images at the top show the SEM and EDAX of the Branch portion as shown in Fig.4.9c. 2) Horizontal images at the bottom show the SEM and EDAX of the base portion between two branches as shown in Fig.4.9c 100
4.11 3) Horizontal images at the top show the SEM and EDAX of the lawn like portion as shown in Fig.4.9c. 4) Horizontal images at the bottom show the SEM and EDAX of the lawn portion from where it starts branching as shown in Fig.4.9c 101

5.1 Flow chart: Image processing procedure of a crack template 111
5.2 Images of the TCSs obtained from the crack template formed with the pH values (a) 7.8 (b) 8.7 (c) 11.2 (d) 11.8 (e) 12.2 (f) 12.5 (g) 12.7 (h)The hierarchical crack patterns are displayed for pH value 12.7. The black dotted lines represent the primary cracks, the red dashed lines represent the secondary cracks and the green lines are for tertiary cracks 113

5.3 Variation of optical properties of TCSs with wavelength in the visible region. a) Variation of Transmittance of the TCSs with wavelength. b) Variation of Reflectance of the TCSs with wavelength. c)Variation of total total crack length and resistance with pH of the suspension. . 114
5.4 a)Variation of resistance and tortuosity with pH b)Variation of Euler number of TCS with pH c) Variation of transmittance of the TCS at 0.54μm d)Variation of Figure of Merit with pH 116

7.1 Droplet deposition pattern of 3% salt solution on different substrates: glass, quartz and polypropylene (PP) are displayed column-wise. The rows display the pattern for two salt concentrations-3% and 5% . . . 135
7.2 Binary images of deposition pattern after optimal thresholding of images. The upper row depicts images for 3% salt concentration and the lower row shows images for 5% salt concentration, The columns denote the different substrates. 137
7.3 Variation of Euler characteristic χ(r) with r (pixel) for 3% and 5% salt concentration. Figures a, b and c indicate the variation for glass, quartz and PP substrates, respectively 138
7.4 Droplet profile of 3% salt solution on different substrates: (a) glass (b) quartz (c) polypropylene(PP). Droplet profile of 5% salt solution on different substrates: (e) glass (f) quartz (g) polypropylene(PP). . . 140
7.5 (a)Rate of evaporation for 3% salt concentration. (b)Rate of evaporation for 5% salt concentration. 142

List of Tables

4.1 Effect of variation of initial thickness of the film 97

7.1 Contact angle for different substrates and salt concentrations 141

Chapter 1

Introduction

Colloidal suspensions form an integral part of our daily life starting from human body fluids, to paint, pharmaceutical, food, printing, and many other industrial applications. Colloidal particles are constituted of large-sized molecules that can range from a few nanometers to a few microns in size. When mixed with a suitable solvent, particles that are of the order of a few nm may mix so homogeneously as to be totally invisible to the naked eye - these are referred to as colloidal solutions. However, if the particles are greater than 1000nm in size, they may be seen as finely suspended in the host solvent and are referred to as colloidal suspensions. Hence the difference between a colloidal solution and a colloidal suspension is determined by the size of the colloidal particle itself. Examples of colloidal suspensions are slurries of clay, while teard-rops, serum and blood are examples of colloidal solutions. The point of interest in my thesis starts from the study of patterns of the particles that are left behind on substrates when colloidal solutions or colloidal suspensions are left to dry. Even under normal ambient conditions, the desiccation patterns observed can be varied in their geometry of crystal aggregation and deposition pattern. The patterns can form as uniform layers or deposit as concentric rings or can have a wrinkled look, form blisters, and even cracks. The deposition layer may not have uniform

thickness, cracks can be isolated or form a crack network having a particular preferred geometry. Over the last three decades, there has been tremendous research in an effort to understand the fundamental principles responsible for desiccation patterns. Principles of fluid dynamics and mass transfer processes along with thermodynamics and rheological properties have been used in tandem to understand the complex dynamic processes responsible for pattern formation by desiccating colloidal suspensions. Much modelling and simulation has been done based on experimental and theoretical understanding of the effect of parameters that affect the patterns. As colloidal particles develop surface charges in solution, the role of external electric [1], [2] and magnetic fields [3] on the drying colloidal solutions has been studied. The colloidal solutions showed crack patterns on the desiccation residue that have a clear correlation to the applied field [4], [5]. Mechanical stirring of the solution in a specific direction has been shown to affect desiccation crack patterns on dried colloidal films. The size and shape of colloidal particles [6], and the wetting and spreading properties of the colloidal solution on a substrate have all left their mark on the patterns. However, one of the lesser-studied aspects has been the role of solution pH on the desiccation pattern of drying colloidal solutions.

In this thesis, I have studied the effect of pH in aqueous Laponite suspension by varying its pH from acidic to the basic range. As desiccation dynamics is very dependent on the interface curvature, I have experimentally investigated the effect of varying pH on two different geometries of the interface of aqueous Laponite suspension: (1) a desiccating droplet and (2) desiccating film. In planar geometry, even though the evaporation flux is uniform across the interface, intricate crack patterns were observed that varied distinctively with the solution pH. In a droplet geometry, the interface curvature complicates matters further by introducing a non-uniform evaporation flux along the interface. This creates complex mass transfer processes driven by gradients of concentration, surface tension, and temperature. I have exposed the importance of aqueous solution preparation protocol and its profound influence on final desiccation patterns, especially, in the case of drying droplets. Lastly, as an

application of the role of pH in the desiccating film of aqueous solutions of Laponite, I have reported a novel technique of preparing economically viable Transparent Conducting Sheet (TCS) by modulating the pH of the aqueous Laponite suspension. I have demonstrated that the pH-modulated crack network can be tailored to obtain TCSs of different conductivities and optical properties.

In the following sections, I shall briefly discuss some essential material properties, and review our understanding of fluid flow in colloidal solutions due to differential evaporation flux across the interface and elements of fracture physics that shall be encountered quite often in the study.

The study of the physics of fracture and droplet evaporation has captured the interest of the research community over the last few decades. As cracks occur frequently in the desiccation pattern of colloidal solutions, understanding crack physics was important. As mentioned earlier, the difference in the radius of curvature of the interface of a colloidal film and a colloidal droplet affects the drying dynamics of a colloidal solution profoundly, it was important to understand the physics of droplet drying and its connection to pattern formation. Droplet physics and desiccation crack patterns are significantly different in the geometry of their exposed surface. My own interest in the physics of droplet drying dynamics was stimulated by the varied spreading and wetting properties of different solutions on different substrates [7]. The famous 'Coffee Ring Effect' [8] explained by Prof. Deegan and his group impressed me with the interplay of simple physics and complex coupled dynamics in a micron-sized system. Today sessile droplet and their evaporation have become an active area of research because of their great impact on our daily life, to name a few - printing technology, medical diagnosis, etc.

In our surroundings, we notice cracks or fractures in many things. Normally crack causes difficulties. In drying colloidal solutions cracks may also appear due to external effects like electric field [1], [2], magnetic effect [3], different mechanical mechanical energy like vibration, rotation, and oscillation [4], [5]. The mode by which

residues of drying colloidal solutions crack may be different and is guided by the method of strain accumulation in a material. Thus an understanding of the physics of fracture was important to me. Today apart from the academic interest, the study of desiccation crack patterns is a very useful topic to research because of its many applications in our everyday life [9].

1.1 Introduction to colloidal suspension

Most of the part of this dissertation is concerned with the colloidal suspension of a synthetic clay. So, we start with the general idea of the colloidal suspension. To know about the colloidal suspension, we need to know about the solution and suspension. One way to identify a solution is by the rule that a solution is a mixture of a solute in a solvent where the state of the mixture is determined by the bigger bulk of the two components, usually the solvent. For example, if we add some sugar to water then the sugar is completely dissolved into water and the state of water determines the state of the solution. The size of the particles in the solution is less than $1nm$. Unlike the solution, a suspension is a heterogenous mixture in which the solid particles are distributed through the bulk material, usually solvent. The size of the particles in suspension is greater than $1000nm$ and most of the particles can be seen with the naked eye. Due to the large size of the particles it sediments with time and the mixture is therefore unstable over a long time. The solute particles can then be filtered in time. For example, sand in water is an example of suspension.

Colloidal particles usually form suspensions. However, a *colloidal suspension* is a heterogenous mixture that follows the properties intermediate to those of solution and suspension. Particle size distribution is between $1nm$ to $1000nm$. Some of the colloidal solutions may look like a true solution with the naked eye but if we see it under a microscope, it is observed to be heterogenous in nature. Particles in

the colloid can be solid, liquid, or gas and particles are suspended in the continuous medium. Hot chocolate is a colloidal suspension. In human blood, red blood corpuscle, white blood corpuscle, and lymphocytes are suspended in plasma which is a perfect example of colloidal suspension (solid particles in liquid phase). Body spray (liquid particles suspended in air), and butter (solids are suspended in a solid medium) are also colloidal suspensions.

Another method to distinguish between solution, suspensions and colloidal suspensions is to study the Tyndal Effect of light through the mixture. Light through the true solution passes without any affect. If we pass light through the colloidal solution, light gets scattered whereas the light through the suspension gets reflected.

1.2 Introduction to Laponite clay

A major part of the experiments of this dissertation was performed with an aqueous colloidal suspension of Laponite clay. Laponite is a synthetic clay belonging to the hectorite family. It is available in a dry powder state with white colour. The primary particles of Laponite are disk-shaped with a diameter of $\sim$ 25–30 nm and thickness $\sim$ 0.92 nm. The chemical formula of this particle in dry state is $Na_{0.7}Si_8Mg_{5.5}Li_{0.3}O_{20}(OH)_4$.

Any synthetic clay is formed with a tetrahedral layer of silica and an octahedral layer of magnesia (or aluminium). One Laponite particle consists of two tetrahedral silica layers and one octahedral magnesia layer. H. van Olphen [10] describes the basic structure of Laponite as described below. Silicon atom is present at the centroid of the tetrahedron while the four corner points are occupied by four different oxygen atoms as shown in Fig.1.1 . Among the four oxygen atoms of the tetrahedron three oxygen atoms are shared by the three nearest neighbour tetrahedron and the rest oxygen atom is shared by the octahedral magnesia sheet as shown in Fig.1.2.

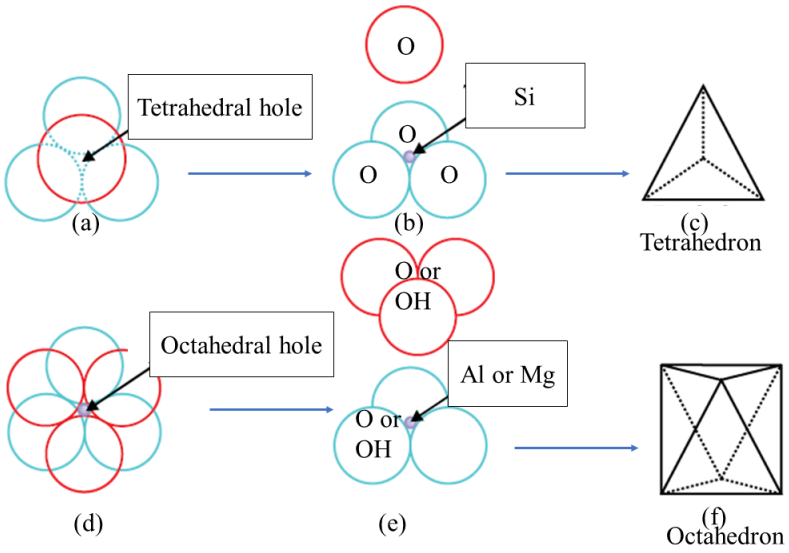

Figure 1.1: The schematic diagram of tetrahedal sheet and octahedral sheet of Laponite particle.

In an octahedral magnesia sheet the six corner points are occupied by oxygen atom or hydroxyl (OH) group. In an octahedron, these oxygen atoms and OH groups form two parallel planes and the magnesium ion is located at the centroid of the octahedron as shown in Fig.1.1. Depending on the shearing method of the sheets the synthetic clay can be classified into different groups. Amongst them, Laponite is a 2:1 layer silicate synthetic clay. In the dry state, a Laponite particle is formed by one octahedral magnesia sheet sandwiched between two tetrahedral silica sheets. The unit cell of the Laponite atom is shown in Fig.1.2. One layer of the particle is formed with thousands of such unit cells.

1.3 Charge distribution of a Laponite particle

In order to understand the role of pH in desiccation of aqueous Laponite we should have clear knowledge about the behavior of Laponite particle in aqueous medium. Laponite is a disk-shaped particle having one octahedral magnesia layer sandwiched by two tetrahedral silica layers on either side. In general, a higher valence atom

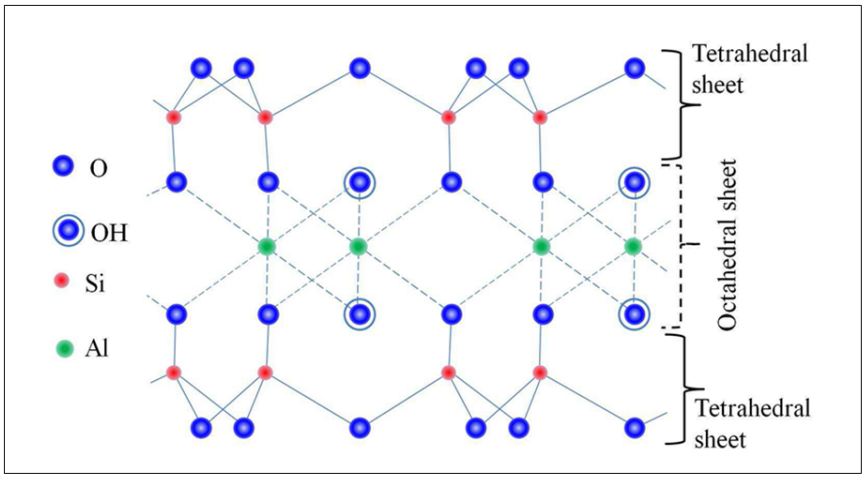

Figure 1.2: The schematic diagram of atomic arrangement of Laponite particle.

is replaced by a lower valence atom for most of the clay and this substitution is called isomorphic substitution. This isomorphic substitution of atoms into the clay structure turns the sample negatively charged. For example in the case of Laponite in the octahedral layer, some of the magnesium ions are substituted by lithium ions by isomorphic substitution creating a deficiency of positive charge. Similarly, the Si atom is present at the centroid of the tetrahedron and it is substituted by the Al atom, which creates a surplus of electrons and turns the particle negatively charged. Consequently, the opposite faces of particles have surplus electrons that they share with the sodium atoms and make the clay negatively charged. Nature of charge of Laponite particles in the edge surfaces and faces is governed by the pH of the solution strongly.

Definition of pH

pH scale (ranges from 0-14) is a tool to measure acids and bases. The mathematical definition is more useful in general. If $[H^+]$ is defined as the H^+ concentration in moles per litre then its negative logarithmic is called the pH (power of hydrogen ion)

of the solution.

$$pH = -log_{10}10[H^+]$$

Litmus paper is the indicator to identify whether a substance is an acid or base. Whether the blue litmus paper turns to red in acidic medium, the red litmus paper turns to blue in alkaline medium. The strength of an acid or base depends on the concentration of H^+ or $(OH)^-$ ions. pH 7 is neutral and below pH 7, the substance is acidic and acidity decreases with an increase in the pH value from 0 to 7. pH above 7 is basic and basic nature increases with increasing pH from 7 to 14.

Charge on the face surface of the Laponite particle

In most cases, clay minerals are neutral. The clay remains neutral because of its adsorption of cations like Na^+, K^+, Ca^{2+}, etc from the atmosphere during manufacturing by Laponite faces and neutralizes the negative charges. These cations cannot enter into the clay due to their bulk size and reside on the surface of the clay. When Laponite is dissolved into water the cations are diffused into the sample because of its low concentration and cations are free to move in the sample and a negative layer is formed on the surface. On the other side, there is an electrostatic attraction force between these negative faces and cations. These cations are attracted to the surface due to electrostatic attraction to form a cloud layer of cations. So, there are completely opposite trends of compensating cations that form a cloud in a diffuse layer at the exterior of the surface of the layer of Laponite which is known as **Double Layer**. The compensation cations act as counter ions having exchange capacity which is the most important feature of the clay. Due to the formation of this type of Double Layer and *exchange capacity* of the cations the faces of the Laponite particles show negatively charged. We will discuss how the double layer is formed and the way it exchanges its nature of charge.

Charge on the edge surface of the Laponite

The double layer of the edge face is also important in many aspects. For example, the desiccation crack patterns change their nature with pH which actually depends on the nature of the charges of the edge surface [11]. At the edge of a Laponite particle, the surface of the Si and Al are exposed because the primary bonds are broken [12]. The charge of the double-layer surface of the edge faces is dependent on the pH of the solution. The edge surface of Laponite creates a positive double layer when the solution is acidic and Mg^{2+} acts as a potential determining ion. Similarly, the edge surface of the Laponite creates a negative double layer in an alkaline solution and hydroxyl ion acts as potential determining ions. It must be noted that the point of zero charge is not necessarily at neutral pH. **The Iso Electric Point** (IEP) for the crystal of Mg^{2+} (potential determining ion) is at pH 12.5 while that of the *Si crystal* is around at pH 2 [12]. So, the point of zero charges is at pH 12.5, and below this pH, the edges of Laponite where the MgOH crystal is located are expected to possess a positive charge, and above this pH, it is expected negative charges. Roughly we can say that the edge of the Laponite particle forms a positive double layer in acidic medium and Mg^{2+} ions act as a potential determining ion and it possesses a negative double layer in an alkaline medium and hydroxyl ion acts as a potential-determining ion. The ionized state of the colloidal laponite solution is responsible for the electrostatic forces that exist between the particles. This, in turn, determines the morphology of the sol or gel state, swelling behaviour, rheological properties like viscosity and elastic modulus, electrokinetic response to external electric or magnetic fields, and eventually their cracking patterns upon desiccation.

1.4 Patterns depend on interface geometry

Liquid possesses some extra ordinary properties. For example, sometimes they beat the gravitational force or they can rise up in a capillary tube with a very small diameter. Various patterns are left by a liquid droplet on different substrates for various types of solutions or suspensions. The dynamics of drying on a surface for

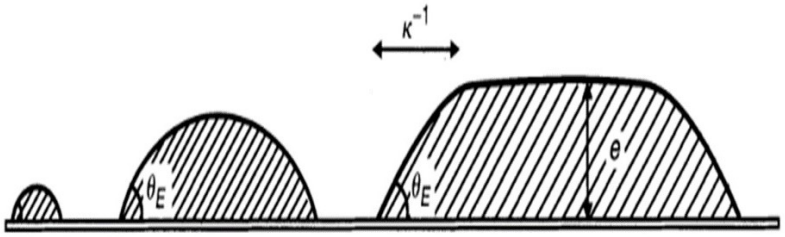

Figure 1.3: Increasing size of the droplet. Curved surface changes to the flattened surface with increase in size.

any liquid strongly depends on the size of the deposited. If the size of the deposited is very small, gravitational effect is not considerable to the drying dynamics. So, there is a characteristic length namely capillary length, denoted by inverse of κ. The mathematical formula for capillary length can be derived using Laplace pressure and hydrostatic pressure and is given by

$$\kappa^{-1} = \sqrt{\frac{\gamma}{\rho g}}$$

where γ is the surface tension and ρ is the density of the liquid.

Depending upon the radius of the deposit, the geometry of the exposed surface is changed from a curved to a uniform flat surface as shown in Fig.1.3. Hence, we have focused our investigation on two different regimes. If the size of the deposited is so small that $r < \kappa^{-1}$, where r is the radius of the deposited liquid then we consider it as a droplet and the liquid is in an environment where there is no gravitational effect. In this case, the capillary effect dominates over the gravitational effect. This geometry of the curvature creates complex mass transfer processes driven by the gradient of concentration or thermal or surface tension. We will discuss later how these factors affect the dynamics of droplet evaporation and hence left interesting patterns after complete drying.

Another aspect is when the radius of the deposited is greater than the capillary length i.e. $r > \kappa^{-1}$ then the gravitational effect comes into consideration. In this

case, a major portion of the exposed surface is flattened and drying dynamics are completely different. So, the study of the patterns formation and evaporation dynamics of the film is the second part of our study. Mainly we have studied the crack pattern of colloidal suspension changing different parameters. We will discuss the factors which control the desiccation patterns after complete drying.

1.5 Concepts of Fracture mechanics

The study of the crack pattern is a very active and interesting research area for the last few decades not only for academic purposes but also because of its profound implication in our daily life [9]. From cosmetics and pharmaceuticals, printing and paint, to medical diagnostics and the cement industry, crack patterns provide an insight into the composition of the colloidal solution, fundamental principles of mass transfer that dictate flow patterns during drying, and rheological changes that occur in the solution with drying. In most cases, crack is problematic in our life. Colloidal films or paintings has leaning towards cracking during drying. Colloidal films are used in ink-jet printing as a coating on papers and the formation of cracks is undesired in these cases. The study of crack patterns can guide us to prevent undesired cracks and therefore invited a lot of research [13] in this field.

In recent times researchers are interested in making useful applications of crack patterns. Crack patterns of different colloidal films can be controlled and tailored to design fantastic designs on a coating of paint, on wooden furniture, on metal surfaces, and used to provide templates for producing transparent conducting films [14] and other nanodevices. Crack patterns of drying droplets of blood or blood serum are used in the diagnosis of different diseases in pathological laboratories [15].

The wide application of cracks in our life makes it a serious topic of research among researchers. In research, synthetic clay such as Laponite and Bentonite are often used for their known structure and purity of compositions. One of the most common

synthetic clay in the research area is Laponite clay which belongs to the hectorite family. It possesses very interesting phase changes in different cases. The previous studies which were done by various research groups show us there are many phase determinations factors of aqueous Laponite suspension with respect to salt concentrations [16], pH [17], aging effects [18] etc., we have seen the absence of attention to link the role of pH and particle concentration to the desiccation crack patterns or in evaporation of sessile droplet.

The fracture of a solid takes place in different forms like buckling of matter, deformation of a substance, or fracture of a solid. Here we are interested in a fracture of a substance. Fracture mechanics is mainly studied as an engineering subject dealing with the reason for a crack and various criteria of cracks and the dynamics of crack propagation. There are two basic criteria of happening crack in a matter. One of them is the local approach namely "crack tip stress filed" and another one is the global approach namely the "energy balance approach".

Crack tip stress and its critical value

Irwin [19] established the criteria of critical value of stress. In this approach stress at the crack tip varies according to $r^{-1/2}$, where r is the distance from the tip. There is a singularity problem at the tip where, $r = 0$ and due to this situation stress field criteria are not applicable at the tip. Irwin accepts this singularity and resolved the fact by proposing that stress at the tip cannot exceed a certain stress value and this limiting value is **yield stress** or **cohesive force** between the atoms of a material. He studied the stress near the tip of a crack of a linear elastic body and gave a criterion for the crack of a solid. According to this criteria, fracture growth happens when the stress intensity factor (K_I) reaches a critical value (K_{lc}) i.e.

$$K_I = K_{lc}$$

. Where K_{lc} is called 'fracture toughness' and it can be measured experimentally for any material. All the analysis done by Irwin based on linear elasticity and stress

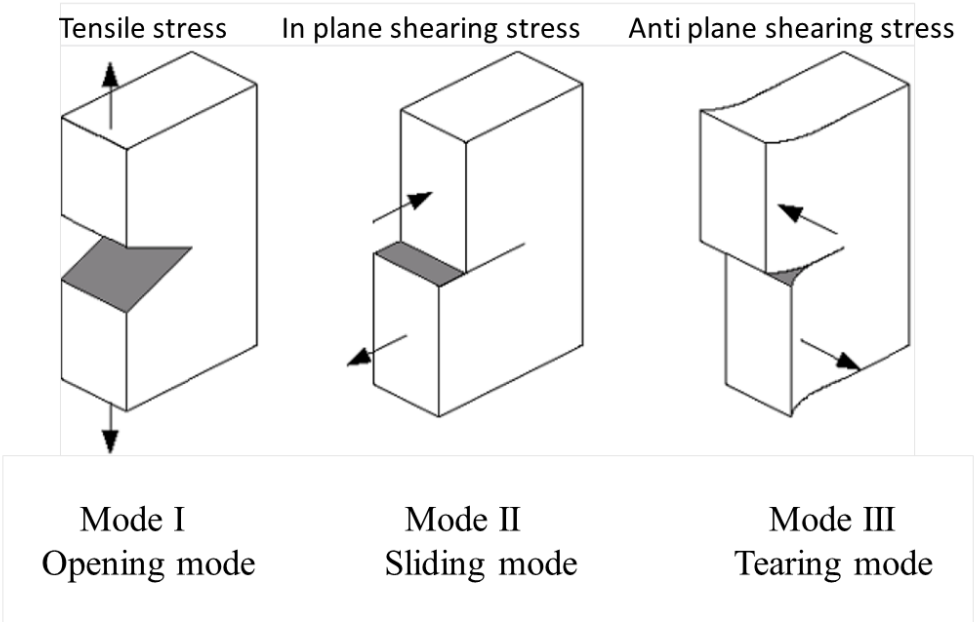

Figure 1.4: Schematic diagram of three different fracture modes.

intensity factor is well defined in this study. There is a limitation in this study that the real fracture mechanics can not be explained by linear elasticity theory.

1.5.1 Basic modes of fracture and stress intensity factor

The stress field around a crack tip is the reason for the brittle fracture of a solid. So, the study of the stress field is a very important factor for the analysis of brittle fracture and the method of the elasticity is the key to studying the stress field. A crack body is actually two faces material. These two faces lie in the same plane before deformation. When the crack body is subjected to external forces, these two faces move with respect to each other. Depending on the forces, the movement of lower and upper faces are different.

Total fundamental classical modes are classified by Irwin into three different modes. These fundamental modes are called MI, MII, and MIII. Al the cracks that happen in nature can be described by one of these modes or combinations of these modes.

Mode I: It is known as the 'opening mode' of fracture. In this mode, the crack surfaces depart from each other symmetrically as seen from the undeformed plane as shown in Fig.1.4. A tensile stress which acts normally to the plane of the crack is responsible for this mode of fracture.

Mode II: This type of fracture mode is known as 'sliding mode'. In this mode, shear stress is acting parallel to the crack surface and perpendicular to the crack front. In this mode, the crack surfaces slide along the stress applied and perpendicular to the crack front as shown in Fig.1.4

Mode III: The last mode is Mode III which is known as 'tearing mode'. A shear stress which is parallel to the plane of the crack surface and perpendicular to the crack front is responsible for this fracture mode. In this case, the plane moves along the crack surface plane as shown in Fig.1.4.

1.6 The Griffith Theory

Theoretical strength

The theoretical strength of a solid is defined as the required stress to fracture a perfect crystal by breaking its bond along the fractured surface. It can be calculated in two different ways. One of them is considering the atomistic model. If a_0 is the atomic separation of a solid and if σ is the force required to separate the atoms at a distance 'a', $a > a_0$ then the value of σ depends on the bonding force of the solid [20]. If Y is the elastic modulus of the solid then,

$$\sigma_c = \frac{Y}{2\pi}$$

where σ_c is the theoretical strength. Theoretical strength can also be calculated using surface energy consideration in addition to the atomistic model. In this model

critical value of theoretical strength (σ_c) is

$$\sigma_c = \frac{Y}{10}$$

Practically it is seen that commercially produced materials can be fractured by applying stress value 10-100 times below the theoretical strength value. This type of discrepancy is seen due to the existence of grain boundaries in polycrystalline.

Griffith Energy balance theory of Fracture Mechanics

Griffith was motivated by the discrepancy between theoretical strength and practical strength value and worked on brittle glass. In order to resolve this discrepancy, Griffith argued that in the fracture process of the matter, the weakness of the matter dominates over the strength of a matter. In real cases, glass shows more complex fracture behavior containing numerous microcracks which were simplified during the calculation of theoretical strength value using cohesive strength. In this work, Griffith assumed that a bulk glass material composes of a huge number of flaws that acts as stress concentration generators. This approach composed of *'energy release'* started the revolutionary journey of fracture mechanics.

Griffith argued that a continuous propagation of cracks in any material must be associated with a decrease in the strain energy of the materials. Consider a material with crack extension da and due to this crack, the increase in energy regarding this crack is dE. When a crack is propagating in the material and a new surface is generated, consider the energy associated with the new surface to be dE_s. Griffith suggested that a crack can only propagate when the energy related to the extension of crack dE is greater than or equal to energy related to new surface generated dE_s [20]. That is,

$$dE \geq dE_s$$

This equal sign suggests the critical value for the propagation of cracks in any material. Surface energy can be calculated if the surface energy density γ is given. If

the crack length is 2a then the surface energy required to create a new surface is

$$E_s = 2(2a)\gamma$$

The extra 2 factor comes due to the fact that, when a crack propagates, two new surfaces are generated. Griffith used Inglis' [21] solution to obtain critical strength value and showed that this critical value is much less than the theoretical strength value and he was able to explain qualitatively the reason behind the lower value of actual strength compared to theoretical strength value.

Relation amongst the different energies

The Griffith theory for perfectly brittle matter is established on the basic principle of energy conservation. During crack propagation, let da be the crack extension and dE_e be the work done due to external force. Due to crack propagation, the new surface is generated and dE_s is the increase in energy due to surface increment, then

$$dE_s + dU = dE_e$$

where dU is the increment of strain energy. For the conservative force field, the above expression can be written as

$$d(E_s + U + V)/da = 0$$

where V is the total potential corresponding to the external applied force. When dV is negative, work done is positive and dW is work done by external forces.

1.7 Formation of desiccation crack

Desiccation crack is a very common problem in many aspects of nature. Most of the crack patterns in desiccation are composed of two types of crack geometry; cracks

meet either at 'T' junctions or at 'Y junctions.' [22]. In the orthogonal crack, cracks meet with each other at right angles. Primary cracks make the soil into some blocks of soil and secondary cracks meet the primary cracks at a right angle. The junction point of the crack looks like 'T' as shown in Fig.1.5 and hence it is called **T Junction**. In the case of soft cohesive soil when the drying is very slow the orthogonal crack pattern is observed. This type of crack is very common in soil. In the natural desiccation of soil non-orthogonal crack is not seen.

If the desiccation rate is very high and deposition of soil thickness is very low then a non-orthogonal crack pattern is seen. In this case, the cracks meet with each other at an angle of 120° and a hexagonal pattern is seen. The junction point of the cracks looks like 'Y' as shown in Fig.1.5 and hence it is called **Y Junction**. Fang and Danniels [23] first observed that hexagonal patterns in desiccation which is seen in the case of homogeneous soil and suggest that when the soil is heterogenous then hexagonal peds become almost round shaped. One of the most common phenomena of desiccation crack is mud crack (1.5). If the soil is exposed to natural weather, then due to the evaporation of water from mud the crack is seen. The study of the desiccation process is a very difficult task because it concerns many nonlinear parameters like humidity, wetting dewetting, temperature, etc. Investigation on desiccation was started almost 100 years back. At the early stage of research qualitative analysis was done and in modern days quantitative analysis, crack mechanism, modelling, etc. are more concerned to the researchers.

Why do desiccation cracks happen?

We are concerned about the natural crack that happens in the soil, dried water resources, clay slurry, etc. Based on the factor that causes cracks in these cases, Fang [24] proposed four common reasons and corresponding types of cracks namely: shrinkage, fracture cracks, thermal and tensile. The most common crack is "shrinkage". When soil or clay is exposed to the environment then the liquid in the material evaporates from the exposed surface and solidification happens and shrinks the soil

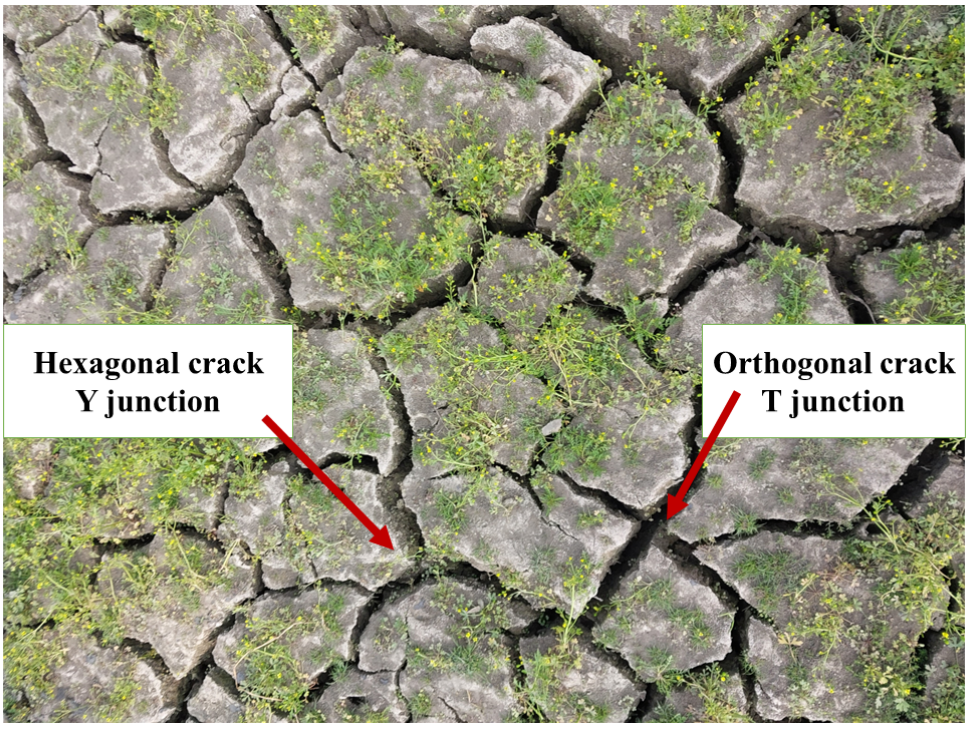

Figure 1.5: Formation of mud crack in a cultivated land. Both T junction and Y junction cracks are observed

and induced stress cracks the soil. Evaporation rate [25] and film thickness [26] provides also the stress in this case. Thermal stress developed due to thermal changes in the material. When rapid heating and cooling occurs in the material then thermal stress is developed in the material and cracks happen. One important thing is that in case of cracks in soil, the main reason cannot be identified whether it is caused by thermal stress or stress due to shrinkage. Stress that causes cracks in soil is due to both thermal and shrinkage stress and both are very mutually influenced. Obviously, thermal stress is relatively less effective than stress due to shrinkage. Sometimes cracks happen due to tensile stress and the corresponding crack is called tensile crack. External pressure is applied for structural loading that causes tensile cracks. Sometimes cracks in soil happen due to fracture stress developed due to fracture load. During desiccation, pore of water is generated in the soil, and fluctuation of the pore water pressure, shrinkage, and thermal variation is the reason for fracture load.

Normally shrinkage crack is more related to the desiccation of soil rather than the temperature change. However, there are some materials in which shrinkage pressure is mostly dependent on the cooling of the material. A good example of a crack due to cooling is hexagonal basalt column formation.

1.7.1 Effect of capillary pressure and clay layer thickness

Poroelasticity is the combined properties of porosity and elasticity of a matter. When a porous media is elastically deformed or buckled then it is called poroelastic deformation [9]. Soil is an example of porous media having elastic properties. The main driving force behind poroelastic deformation is capillary pressure. Normally when two immiscible fluid and a third material exists then capillary pressure exists. During the drying of soil, a water layer is introduced due to cohesive attraction between two particles. This gives rise to negative capillary pressure [27]. This existing capillary pressure causes a crack in a layer. The thickness of a layer is a very important parameter in crack formation. Lakshmikantha and his group [28] observed that when the clay thickness is increased, the area of the crack ped and width of the crack increases but the rate of desiccation decreases. Again, for the same thickness of different materials, the crack area and width of the crack are not the same. Corte and Higashi noticed that area of the crack ped is larger for the wooden base than for the glass base indicating that the substrate adhesion that can vary from one material to another, can affect the crack ped [22]. Capillary pressure is always not able to crack a film. There is a critical capillary pressure above which elastic energy overcomes the energy required to create the surface then cracks happen. There is also a critical thickness of the film above which crack happens. A notable point is that when a water-air interface is formed inside the film then the thickness of the film is not dependent on the film thickness [29, 30]. If the water-air interface is formed outside the film, then this *critical capillary pressure*,

p_c^{cr} is dependent on the film thickness according to the relation

$$p_c^{cr} \sim \gamma G^{2/5} h^{-3/5}$$

Where G is the shear modulus. From the relation we see the power of h is negative. If h is getting down then crack formation is more difficult. So there is a particular value of thickness below which crack formation is not possible and this thickness is called critical thickness [31].

1.8 Theoretical concept: Drying dynamics of an evaporating droplet

Pattern formation of evaporating droplets has a great scientific interest because it involves lots of physics inside the droplet and has wonderful applications for humans. When a droplet containing various solutes and solvent allows drying it leaves a final pattern that not only depends on the compositions but also on the drying dynamics which depends on some nonlinear factors like substrate, temperature and relative humidity, etc. people are interested to understand the phenomena of dried patterns and their evaporation dynamics for a technical application like painting technology, printing technology, etc. By studying the pattern formation of droplets containing nanoparticles, researchers are able to design inexpensive and easily feasible nanoparticle deposition. One of the most exciting and interesting applications of droplet evaporation is to detect diseases. Analysis of final deposition patterns of biofluid helps us to detect the disease [15]. The sessile shape of the droplet is very interesting because of their exposed curvature which creates complex mass transfer during drying. The basic fluid properties, physics of thermodynamics, and ambient conditions of the environment control the mass and energy transfer. We will shortly

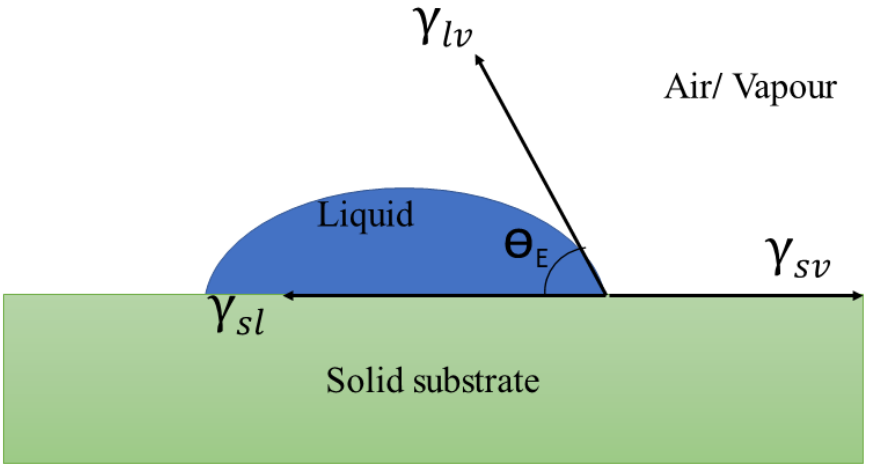

Figure 1.6: Youngs' equation: Force balance at the Triple Phase Contact Line

discuss some important physics that works inside the droplet to create the final deposition pattern.

1.8.1 Surface Tension and Youngs' equation

The most important phenomenon which is studied for the last hundred years in droplet physics is capillary action. The main tool for this study is the excess free energy developed to create an interface between two phases and this is called 'surface tension'. If a droplet of aqueous solution is deposited on a solid substrate it spreads on that substrate immediately after the deposition which depends on the nature of the substrate and surface tension of the solution. We have shown a schematic diagram of a deposited droplet on a substrate and components of interfacial tension in Fig.1.6. A lower value of surface tension means greater spreading on the substrate. When a droplet spreads partially, its contact line is pinned on the substrate and pinned line is called *Triple Phase Contact Line* (**TPCL**). "Surface tension" of a liquid is actually the interfacial tension between the liquid and air medium which

is given by γ_{lv}. Another two surface tensions are γ_{sl} ("interfacial tension" between substrate and liquid) and γ_{sv} ("interfacial tension" between solid and air) are shown in Fig.1.6. The relation between the cosine value of the contact angle (θ_E) and "interfacial tension" is called the Youngs equation which is given by

$$\gamma_{sl} + \gamma_{lv} \cos\theta_E = \gamma_{sv}$$

. It is simply the mechanical force balance equation of TPCL.

1.8.2 Nature of surface and wetting phenomenon

The wetting phenomenon is very important in many aspects like in the food industry, painting technology, etc. Young's equation has a direct impact on wetting phenomena. Depending on the wetting characteristics a surface may be partially wet, completely wetting, or completely drying. In the case of a completely wetting substrate, the droplet spreads all over the surface. For partial wetting, it spreads and is pinned on the substrate and the characteristic measurement of the spreading is called contact angle θ_E. Depending on the value of "contact angle" substrates can be classified in three different natures namely hydrophilic, hydrophobic, and superhydrophobic substrate as shown in Fig.1.7. If the "contact angle" of a water droplet on a substrate is acute angle i.e. $< 90°$ then the substrate is called water-loving or **Hydrophilic substrate**. On this substrate water droplet is pinned to the substrate and the substrate is partially wetting substrate. Glass and quartz are examples of hydrophilic substrates. When the contact angle of a water droplet on a substrate is $> 90°$ then the substrate is called water-hating or **Hydrophobic substrate**. It is also a partially wetting substrate. Polypropylene is an example of hydrophobic substrate. If the contact angle is more than 150° then the substrate is called **superhydrophobic** substrate. Lotus leaf is an example of a superhydrophobic substrate. On this surface, some textures are present and consist of an array of pillars of heights and distances of some micrometer order. This array of pillars is

coated with thin hydrophobic metal to prepare a superhydrophobic substrate. The super hydrophobic substrate can be made at home. If a metal spoon is held on a burning candle for some time then a thin layer of carbon is coated and forms a superhydrophobic substrate. This carbon acts as a pillar [32]

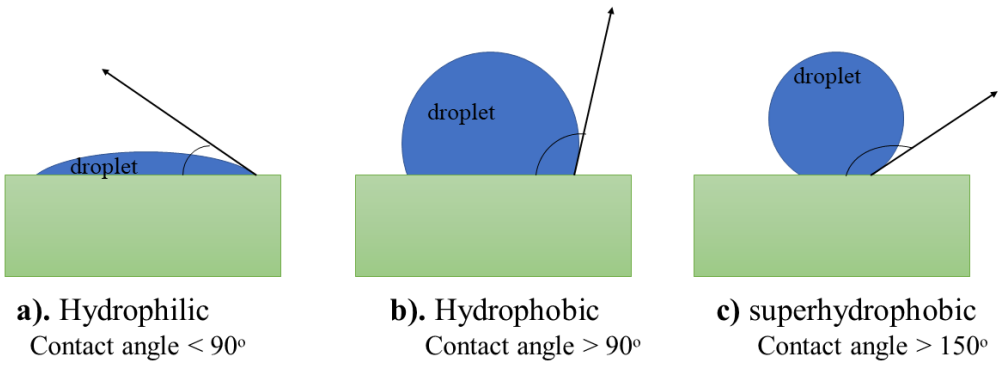

Figure 1.7: Droplet on different substrates. a) Hydrophilic b) Hydrophobic c) Superhydrophobic

Evaporation modes of a drying droplet

Evaporation of a sessile droplet means the escaping of solvent from the droplet and decreasing the size/volume of the droplet with time. There are two types of evaporation mode during drying, *Constant Contact Angle* mode **(CCA mode)** and *Constant Contact Radius* mode **(CCR mode)** [33]. Schematic diagrams of these modes of evaporation are shown in Fig.1.8. In the CCR mode of evaporation height of the droplet decreases gradually and also contact angle decreases until the contact angle reaches a value which is called receding contact angle. In CCR mode contact area is fixed during this mode of evaporation. Normally on a hydrophilic substrate, CCR mode of evaporation is seen. In the CCA mode of drying radius of the droplet decreases gradually keeping the contact angle constant. This mode of evaporation happens normally after CCR mode. During the period of drying, if the contact angle reaches a certain value called receding contact angle then the droplet slips to a new position with a small radius, and then the CCA mode of evaporation happens which is depicted in a schematic diagram in Fig1.8b.

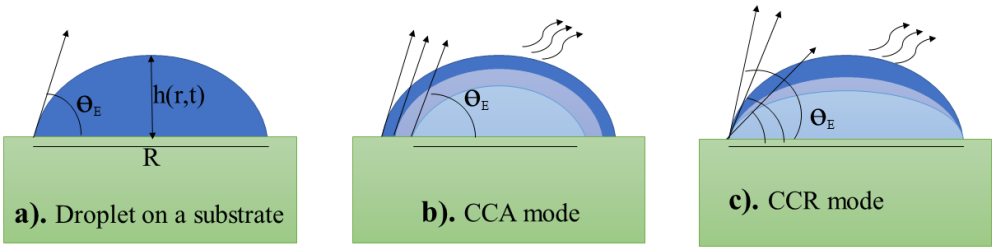

Figure 1.8: Typical evaporation modes of a drying droplet.

1.8.3 Different flows inside the droplet

Consider a sessile droplet of nonvolatile solvent on a substrate. For a hydrophilic substrate, the droplet TPCL is pinned to the substrate. Due to the curvature of the exposed surface, the evaporation flux is uneven to the different portions of the droplet. At the TPCL, evaporation flux is much greater than at the droplet apex. Due to this gradient of evaporation flux a flow of solvent is observed from the apex to the TPCL as shown in Fig.1.9a. This is called capillary flow. After complete drying of the droplet, a ring-like residue is observed on the substrate which is called **Coffee Ring** [34]. One interesting thing is observed in the ring under a microscope. Initially, deposition is very slow, and very ordered deposition is observed. During drying of the droplet surface tension gradient is developed by some reasons like temperature gradient or the presence of chemical species called surfactant, which lower the surface tension of the solvent. Due to this surface tension gradient, a flow pattern is observed inside the droplet during drying which is called **Marangoni Flow**. There are two types of Marangoni flow, thermal Marangoni flow, caused by temperature gradient and due to concentration gradients, solutal Marangoni flow. Due to the surface tension gradient higher surface tension area pulls the interface of the lower surface tension area. This is called Benard Marangoni flow or "Marangoni flow" which flows the liquid towards the higher surface tension from the lower surface tension. The direction of the Marangoni flow depends on the comparative value of

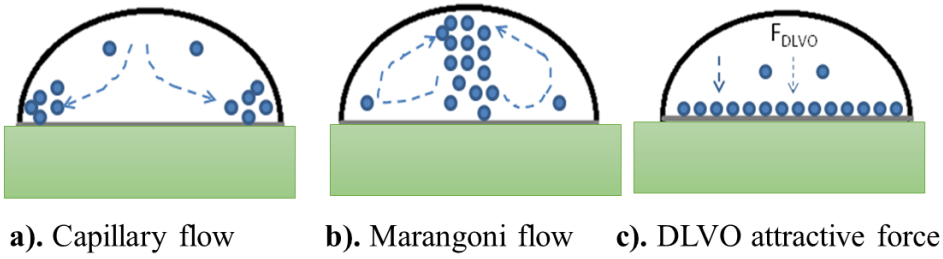

Figure 1.9: Flow inside the droplet: a) Capillary flow b) Marangoni flow c) Flow due to DLVO force

"thermal conductivities" of the substrate and the liquid. If the thermal conductivity of the substrate is much higher than that of the liquid then the droplet TPCL is warmer than the droplet apex and flows towards the TPCL from the apex. If the thermal conductivity of the substrate is much lower than that of the liquid then opposite trends are observed and liquid flow towards the middle of the droplet from the TPCL as shown in Fig.1.9b. Each type flow can lead to different patterns after complete drying [35]

Flow inside the droplet pattern is also controlled by DLVO attractive force which is given by

$$F_{DLVO} = F_{el} + F_{vdw}$$

WhereF_{el}= electrostatic force between the particles and F_{vdw}= van der Waal's force between particles and substrates Due to this DLVO attractive force particles inside the droplet can be attracted to the substrate directly as shown in Fig.1.9c. DLVO force is strongly dependent on the zeta potential of the substrate and solution [36]. pH of the solution can greatly affect the zeta potential. We will discuss in details about DLVO force later.

The next five chapters describe the body of work that is tandem to the title of the thesis. But sometimes there comes another end after ending. In that spirit I have included another chapter even after the 'Summary' to showcase another study I have

done during this time. Pattern formation of desiccating droplets of copper sulphate salt that not only looked beautiful , but introduced me to the topological tools of Euler Characteristics that I have used to analyze the patterns.

Bibliography

[1] T. Khatun, T. Dutta and S. Tarafdar, *"Crack formation in laponite gel under ac fields"*, *Applied Clay Science* **86** 125-128 (2013).

[2] T. Khatun, M. D. Choudhury, T. Dutta and S. Tarafdar, *"Electric-field-induced crack patterns: Experiments and simulation"*, *Phys. Rev. E* **86** 016114 (Jul, 2012).

[3] L. Pauchard, F. Elias, P. Boltenhagen, A. Cebers and J. C. Bacri, *"When a crack is oriented by a magnetic field"*, *Phys. Rev. E* **77** 021402 (Feb, 2008).

[4] A. Nakahara and Y. Matsuo, *"Transition in the pattern of cracks resulting from memory effects in paste"*, *Phys. Rev. E* **74** 045102 (Oct, 2006).

[5] Y. Matsuo and A. Nakahara, *"Effect of interaction on the formation of memories in paste"*, *Journal of the Physical Society of Japan* **81** 024801 (2012).

[6] L. Onsager, *"The effects of shape on the interaction of colloidal particles"*, *Annals of the New York Academy of Sciences* **51** 627--659 (1949).

[7] P. G. de Gennes, *"Wetting: statics and dynamics"*, *Rev. Mod. Phys.* **57** 827--863 (Jul, 1985).

[8] R. D. Deegan, O. Bakajin, T. F. Dupont, G. Huber, S. R. Nagel and T. A. Witten, *"Capillary flow as the cause of ring stains from dried liquid drops"*, *Nature* **389** 827--829 (1997).

[9] L. Goehring, A. Nakahara, T. Dutta, S. Kitsunezaki and S. Tarafdar, *"Desiccation cracks and their patterns: Formation and modelling in science and nature"*, .

[10] V. H. Olphen, *"An introduction to clay colloid chemistry, 2nd edition."*, *Jhon Wiley, New York, 2nd edition*, (1977).

[11] S. Haque, S. Tarafdar and T. Dutta, *"Desiccation cracks formed in laponite suspensions of varying ph: aid to analyzing clay microstructure"*, *Phys. Scr.* **95**, (2020).

[12] W. Stumm, *"Chemistry of the solidliquid interface."*, *John Wiley & Sons, New York.*, (1992).

[13] A. F. Routh, *"Drying of thin colloidal films"*, *Reports on Progress in Physics* **76** 046603 (mar, 2013).

[14] S. Sadhukhan, A. Kumar, G. U. Kulkarni, S. Tarafdar and T. Dutta, *"A spring network simulation in three dimensions for designing optimal crack pattern template to fabricate transparent conducting electrodes"*, *Bulletin of Materials Science* **42** 197 (2019).

[15] D. Brutin, B. Sobac, B. Loquet and J. Sampol, *"Pattern formation in drying drops of blood."*, *J. Fluid Mech.* **667**, (2011).

[16] S. Sircar, M. D. Choudhury, S. Karmakar, S. Tarafdar and T. Dutta, *"Crack patterns in drying laponite–nacl suspension: Role of the substrate and a static electric field"*, *Langmuir* **34** 6502-6510 (2018).

[17] S. Jatav and Y. M. Joshi, *"Chemical stability of laponite in aqueous media"*, *Applied Clay Science* **97-98** 72-77 (2014).

[18] R. Bandyopadhyay, D. Liang, H. Yardimci, D. A. Sessoms, M. A. Borthwick, S. G. J. Mochrie et al., *"Evolution of particle-scale dynamics in an aging clay suspension"*, *Phys. Rev. Lett.* **93** 228302 (Nov, 2004).

[19] G. R. Irwin, *"Analysis of Stresses and Strains Near the End of a Crack Traversing a Plate"*, *Journal of Applied Mechanics* **24** 361-364 (06, 2021), [arXiv:https://asmedigitalcollection.asme.org/appliedmechanics/article-pdf/24/3/36

[20] C. T. Sun and Z. H. Jin, *"Chapter 2- griffith theory of fracture,"*, *Elsevier* 11-24. (2012).

[21] C. INGLIS, *"Stresses in a plate due to the presence of cracks and sharp corners"*, *Trans Inst Naval Archit* **55** 219-241 (1913).

[22] A. Corte and A. Higashi, *"Experimental research on desiccation cracks in soil-research report 66"*, *Wilmette, Illinois: US Army Snow Ice and Permafrost Research Establishment*, (1960).

[23] H.-Y. Fang and J. L. Daniels, *Introductory geotechnical engineering: an environmental perspective*. CRC Press, 2006.

[24] H. Y. Fang, *Introduction to environmental geotechnology*. CRC Press LLC, 1997.

[25] Y. Y. Tarasevich, *"Simple analytical model of capillary flow in an evaporating sessile drop"*, *Phys. Rev. E* **71** 027301 (Feb, 2005).

[26] H. N. Yow, M. Goikoetxea, L. Goehring and A. F. Routh, *"Effect of film thickness and particle size on cracking stresses in drying latex films"*, *Journal of Colloid and Interface Science* **352** 542-548 (2010).

[27] V. Slowik, M. Schmidt and B. Villmann, *"Capillary shrinkage cracking–experiments and numerical simulation"*, *Fracture mechanics of concrete and concrete structures-assessment, durability, monitoring and retrofitting of concrete structures. Seoul: Korea Concrete Institute*, (2010).

[28] M. Lakshmikantha, P. Prat and A. Ledesma, *"An experimental study of cracking mechanisms in drying soils"*, in *5th ICEG Environmental Geotechnics: Opportunities, Challenges and Responsibilities for Environmental*

Geotechnics: Proceedings of the ISSMGE's fifth international congress organized by the Geoenvironmental Research Centre, Cardiff University and held at Cardiff City Hall on 26–30th June 2006, pp. 533–540, Thomas Telford Publishing, 2006.

[29] G. MASON and D. W. MELLOR, *"Simulation of drainage and imbibition in a random packing of equal spheres"*, *Journal of Colloid and Interface Science* **176** 214–225 (1995).

[30] W. Man and W. B. Russel, *"Direct measurements of critical stresses and cracking in thin films of colloid dispersions"*, *Physical Review Letters* **100** 198302 (2008).

[31] K. B. Singh and M. S. Tirumkudulu, *"Cracking in drying colloidal films"*, *Phys. Rev. Lett.* **98** 218302 (May, 2007).

[32] X. Deng, L. Mammen, H.-J. Butt and D. Vollmer, *"Candle soot as a template for a transparent robust superamphiphobic coating"*, *Science* **335** 67--70 (2012).

[33] J.-H. Kim, S.-B. Park, J. H. Kim and W.-C. Zin, *"Polymer transports inside evaporating water droplets at various substrate temperatures"*, *The Journal of Physical Chemistry C* **115** 15375–15383 (2011), [arXiv:https://doi.org/10.1021/jp202429p].

[34] R. D. Deegan, O. Bakajin, T. F. Dupont, G. Huber, S. R. Nagel and T. A. Witten, *"Capillary flow as the cause of ring stains from dried liquid drops"*, *Nature* **389** 827--829 (1997).

[35] Y. Choi, J. Han and C. Kim, *"Pattern formation in drying of particle-laden sessile drops of polymer solutions on solid substrates"*, *Korean Journal of Chemical Engineering* **28** 2130--2136 (2011).

[36] A. M. Gallardo-Moreno, V. Vadillo-Rodríguez, J. Perera-Nunez, J. M. Bruque and M. L. González-Martín, *"The zeta potential of extended dielectrics and conductors in terms of streaming potential and streaming current measurements"*, *Physical Chemistry Chemical Physics* **14** 9758--9767 (2012).

Chapter 2

Impact of preparation protocol of colloidal suspension on drying droplet on different substrates

2.1 Introduction

In the last few decades, scientists have involved themselves to study the complex drying dynamics inside a microliter size droplet and now it still remains a basic problem to understand the roles of the nonlinear parameter like temperature, ambient weather, nature of surfactant, and substrates in the drying process of the droplet properly [1], [2], [3], [4]. Pattern formation left by a sessile droplet of colloidal suspension is an amazing field of application in medical science, the cosmetic industry, lubricant, pharmacy, etc [5], [6], [7]. Instead of understanding the complex mass behavior, the wonderful application of droplet physics in our life is still motivation for researchers to study the physics inside the droplet.

Curvature of sessile droplet which is a factor responsible for complex mass transfer. Surface tension at the interfaces of three phases- liquid, air, and solid, substrate and

the nature of the solution play a role in the generation of curvature. This curvature is responsible for nonuniform evaporation flux which in turn generates temperature and concentration gradient along the droplet interface hence thermal and solutal Marangoni flow build inside the droplet. Different flow inside the droplet carries the suspended particles even in the microliter size droplet if the suspended particles are very light. When the evaporation proceeds the amount of solvent is reduced and hence viscosity increases inside the droplet. Viscous drag force developed inside the droplet which depends on the shape and size of the solute particles. So according to the shape and size of the droplet deposition during drying changes. Sometimes desiccation energy is released by the crack formation inside the droplet. So, the final pattern bears a signature of all the effects discussed here. The exact effect of the parameters cannot be explained properly and hence it remains a fundamental problem to the scientists.

The size of the particles in the colloidal solution is of the order of nanometers. These nanoparticles in the colloidal solution gain charges and form aggregates. Depending on the size of the aggregates final dried patterns changes. In this work, we have revealed that depending on the preparation method, final dried patterns changes. Normally a solution is prepared using the stirring process to make it homogeneous. Now the question is how much time do we have to stire the solution to make it homogeneous? What will change in the final pattern of the dried droplet if we change the stirring time or preparation protocol? We have prepared suspension using two different processes namely stirring by Ultrasonicator and stirring by Magnetic stirrer. In this chapter, we will systematically demonstrate that there is standard time t_{std} for a particular mixing process of a colloidal solution for a given solvent-solute pair. We will discuss the patterns formed in different substrates with different hydrophobicities and how the dynamics of flow pattern changes with aggregate sizes

.

2.2 Review of related work

The evaporation of droplets is a very simple observation in our surroundings gives us a very interesting topic to study. Lots of nonlinear factors like humidity, temperature, the motion of TPCL, some thermodynamic phase changes, etc. participate to give interesting dynamics and hence a final pattern. Although there is a great challenge to explain the variety of patterns left by droplets after complete drying, research on droplet physics has drawn huge attention because of its wonderful application in medical diagnosis, painting, printing technology, nanotechnical application, etc. Maxwell in 1877 studied the basic droplet evaporation and found that droplet evaporation is controlled by the diffusion process. Diffusion is caused by the difference in vapor pressure concentration in the different parts of the droplet [4]. Evaporation flux is maximum at the TPCL and hence a capillary-driven force is developed. The revolutionary observation in droplet evaporation is coffee ring formation at the TPCL of the droplet. During the evaporation in CCR mode, capillary-driven force carries the suspended or dissolved particles to the droplet contact line and form a "coffee ring" [8]. Every time droplet does not leave the coffee ring after drying. Hu and Larson observed that due to higher evaporation rate at TPCL makes it a cooler region than the other part of the droplet [9]. Again, due to capillary-driven flow, increasing concentration at the contact line creates a surface tension gradient which in turn develops a Marangoni flow that drives the particles from the TPCL to the droplet apex. So, in order to form a coffee ring at the contact line Marangoni effect should be less effective than capillary flow.

Pinning and depinning of the droplet affect the deposition pattern greatly. Pinning of the droplet leads to the coffee ring effect. Depinning of the droplet strongly depends on the evaporation time [10]. Depinning of the droplet can be caused by the factors like solutal concentration, shape, and size of the particle surface tension of the solution, heterogeneity of the substrate, etc. The final deposition pattern depends on the particle size of the solute. Weon shows how the particle size affects the deposition

pattern [11]. He used a 20-micrometer polystyrene bead and the same bead with a lower size and examined the final deposition pattern of the aqueous solution using these. In the case of larger particles maximum deposition is formed at the droplet center whereas for lower particle size coffee ring is observed. Similarly, the shape of the particles remarkably changes the droplet patterns after drying. Yunker and his group showed that using elliptical particles instead of spherical ones with an aqueous-based solution formed uniform deposition rather than the coffee ring effect. The anisotropic shape of the particle does not allow to create the coffee ring. Due to the shape, the interaction between the particles changes and leads to that wonderful change in the final deposition pattern. [12]. Some of the research groups claimed that the size and aspect ratio of the particles cannot modify the final pattern. They argued that DLVO force can affect the patterns and creates the uniform deposition pattern [13] [14] [15]. DLVO force can be changed by changing the pH of the solution and by changing the pH, uniform deposition can be achieved. Robert Malinowski et.al experimentally controlled the deposition pattern by changing the vapor source. During drying, there is vapor near the surface of the droplet. They changed the solvent with different volatility to change the vapor source and observed the different deposited patterns [16].

The deposition pattern of drying droplets can be changed by changing the temperature of the substrates [17]. Sometimes droplet is heated from the top and hence apex of the droplet gets warmer than the contact line of the droplet and thermal Marangoni convection drives the particle to the TPCL and creates a coffee ring [18]. In most cases of the printing and painting technology coffee ring effect is problematic. The coffee stain effect is a very common phenomenon. Researchers were able to suppress this effect. Some of them are discussed here. Eral et. al was able to suppress the coffee ring by electrowetting process by using AC electric field. Time-dependent electric field prevents pinning of the droplet and flow generated in the droplet helps to prevent radial outward flow [19]. The polymer-like surfactant can

also be used to avoid the coffee ring deposition in droplet drying. Polyethylene Glycol was successfully used to prevent coffee ring deposition [20]. The coffee ring effect can also be avoided by using a hydrosoluble polymer. This acts by changing the viscosity of the droplet to control the motion of the contact line and flow inside the droplet [21].

Effect of substrate: The substrate plays a vital role in the final deposition pattern. The heterogeneity of the substrate, the roughness of the substrate, surface energy, thermal conductivity, etc. affect the adhesion of the droplet to the substrate. Changing the substrate, DLVO force can also be changed. A smooth hydrophilic substrate leads to coffee ring deposition. Depending on the roughness of the substrates Contact Angle Hysteresis (CAH) is changed. Feng Li and his group used two different substrates of different CAH for copper sulphate solution. Silica glass shows weak CAH and a droplet of copper sulphate solution on this substrate shows a concentrated stain. On the other side Graphite substrate shows strong CAH and ring-like deposition [22]. Different kinds of patterns are also observed due to the transition of mode of evaporation from CCR to CCA mode which is actually stick slip motion of the contact line. The droplet slip to a new position after the contact angle reaches to receding contact angle. This happens when the advancing contact angle and receding contact angle differ with some limiting value [23]. The heating effect of the substrate changes the final pattern depending on the nature of the substrates. N. D. Patil and his group investigated through experiments. They used glass substrate as a hydrophilic substrate. For nonheated cases, a ring-like deposition is observed. When the substrate is heated, a thermal Marangoni flow developed and deposition throughout the droplet was observed with the addition of a thin ring-like pattern. They used a Silicon substrate as a hydrophobic one. For nonheated cases the evaporation mode is governed by the CCA mode and the central deposition pattern is observed after complete drying. But in the case of heating of the substrate CCR mode is dominated and the heating effect prevents the transition from CCR to CCA method. The final pattern is observed as a thin ring with inner deposition. The

hydrophobic substrate has less adhesion properties and it helps for less adhesion of dirty things or oil on a surface. Normally droplet on a hydrophobic substrate, evaporation mode is dominated by CCA mode and stick-slip motion of the contact line. Hence this substrate has self-cleaning properties [24]. For this kind of usefulness, research has been done on the method of preparation of the hydrophobic substrate. Some techniques are improving nanotubes or nanopillars or coating of hydrophobic layer on substrate [25] [26].

Porous substrates are composed of holes or capillary tubes on their surface. It takes more evaporation time than the normal surface. Pattern formation on these substrates depends on the adhesion of the particle, the motion of the particle to the substrate, etc. If the time taken to reach the particle to the TPCL is less than the time taken for infiltration of the particle to the pores then coffee ring effect is seen. On the other hand, if the time taken to reach the particle to TPCL is greater than the time taken to infiltrate then the coffee ring is suppressed [27] [28]. The coffee ring effect received most of the attention in sessile droplet dynamics. A hanging droplet is known as a pendant droplet. The study of hanging droplets is also very important because of its application in spray in fertilization and in the adhesion of contamination on the wall or any surface. Hampton et. al studied droplets of silica nanoparticles on a hydrophilic substrate. In the case of sessile droplet, a prominent coffee ring with thin-like deposition is observed. When the droplet is deposited on the substrate in pendant form, it lost its symmetry. At the downward, thickness is much greater than that of the upper portion of the droplet. They observed a thin coffee ring with a bump of deposition [29].

Cao et. al studied the effect of substrate elasticity which changes the drying dynamics of the evaporating droplet. They used polymeric droplets to study the equilibrium condition of the droplet. They showed that there is an interaction between capillary force and elastic force which controls the equilibrium shape of a sessile droplet [30]. Dynamics of the contact line change with changing the elasticity of soft substrates.

Hence the final pattern of dried droplet changes with changing the Young modulus of the substrate [31].

2.3 Materials and Experimental Methods

We have done two sets of experiments in this study. 0.1 gm of silica flakes was added to 10 ml of HPLC water and the mixture is stirred at different times 5 min, 10 min, 15 min, 20 min, 25 min, 30 min, 35 min, 40 min, and 45 min. Depending on the stirring process we have divided the experiments into two different sets. Experiments were done at different times to find the minimum time for stable droplets for both sets of experiments.

SetI: In this set of experiments, stirring is done by a magnetic stirrer. **SetII:** Stirring is done by ultrasonicator in this set of experiments.

After the preparation of the suspension, droplet of 5-7 microliter is deposited on two different substrates. Glass substrate as hydrophilic and acrylic substrate as hydrophobic is used for droplet desiccation which was already cleaned with extran detergent and then by acetone and deionized water.

An image of the final pattern for both sets and substrates was taken by an inverted microscope fitted with a Magnum MagCumMU2.3MP camera with a 0.5× C-Mount Adapter. The frame width and height of the video were 1920 and 1200 and the rate captured frame was 30/sec. A complete video of the drying of the droplet was captured by this camera. The image of the droplet was sliced off from the drying video for analysis as needed.

Angle contact was measured on both glass and acrylic substrates. The photograph was taken with a Canon 700D camera and measured the contact angle using ImageJ software. Measurement was repeated five times for each of the droplets.

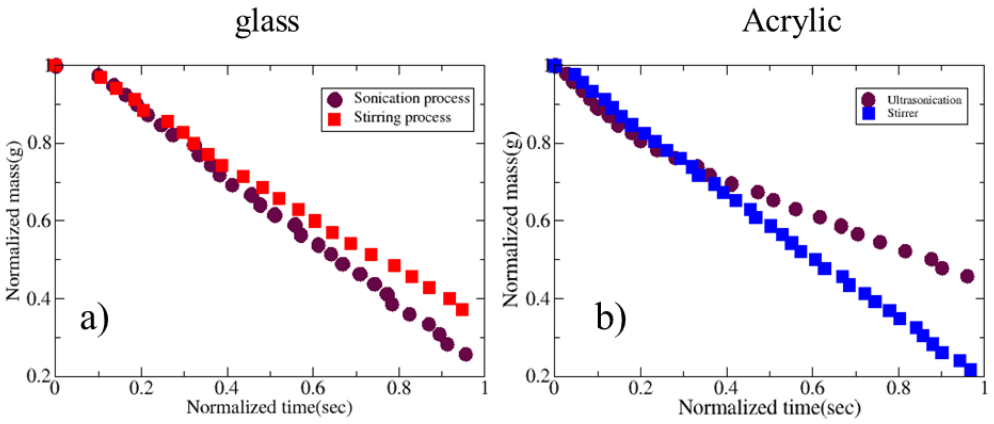

Figure 2.1: a) Evaporation rate on hydrophilic substrate(glass) for SetI and SetII experiments. b) Evaporation rate on the hydrophobic substrate(acrylic) for SetI and SetII experiments.

To check the rate of mass loss during the evaporation, droplet mass was measured during evaporation at the interval of some duration for both glass and acrylic substrates and for both sets of experiments. The mass of the droplet as well as the time of evaporation is normalized by the mass of the droplet at the commencement of deposition of the droplet and the total time of evaporation respectively.

2.4 Results

The angle of contact on both of the substrates- glass, and acrylic was measured for both sets of experiments. On a glass substrate, the angle of contact is 37° and for an acrylic substrate, it is 78° and hence glass is treated as a hydrophilic substrate whereas acrylic is treated as a hydrophobic substrate. It is seen that for both sets of experiments for a particular substrate, there is no significant change in the angle of contact.

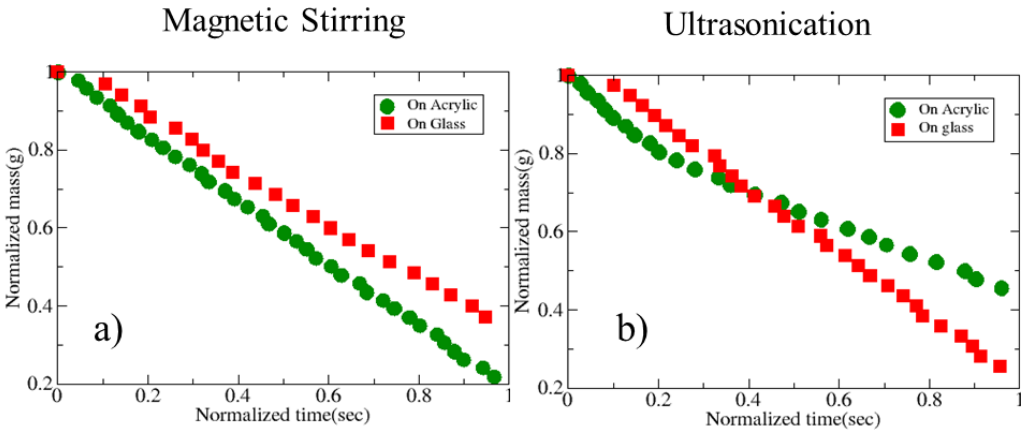

Figure 2.2: a) Comparison of evaporation rate on both substrates for SetI (stirring by Magnetic stirrer) experiments. b) Comparison of evaporation rate on both substrates for SetII (stirring by Ultrasonicator) experiments.

2.4.1 Evaporation rate on glass and acrylic substrates

The rate of mass loss on both substrates was measured to check the evaporation rate. The total time taken for an aqueous silica droplet on a glass substrate is 15 minutes for complete drying in an ambient condition of temperature $23 - 26°C$ and relative humidity of 40-45%. For the same drying condition with the same droplet, total drying time on the acrylic substrate is about 55 minutes. The rate of mass loss was plotted for both substrates and for both sets of experiments. For better comparison, the mass of the droplet at any instant is normalized by the initial mass of the droplet. Similarly, the time of evaporation is normalized by total drying time. The details are discussed below step by step.

2.4.2 Role of substrate on evaporation rate

Examining Fig.2.1 it is evident the role of both hydrophilic and hydrophobic substrates for different preparation protocols. Fig2.1a shows the evaporation rate on glass substrate for both sets of experiments. It is interesting to note that rate of mass loss during evaporation is faster for the ultrasonication process (SetII) than

for stirring by magnetic stirrer (SetI). It is also noted that the rate of mass loss for SetII experiment is almost linear whereas for SetI experiments rate of mass loss is nonlinear in nature. The complete opposite trend is seen on the hydrophobic, acrylic substrate Fig.2.1b. On this substrate, the evaporation rate during drying evaporation is faster for SetI experiment than for SetII experiment. Not only that rate of mass loss is linear for SetI experiments and nonlinear behaviour is seen for SetII experiments. So completely different response in evaporation is seen on different substrates of different hydrophobicities.

The role of the preparation method is evident from Fig.2.2(a and b). For the SetI experiment rate of evaporation is higher for acrylic substrate than glass substrate. Glass substrate exhibits higher water retention than acrylic substrate. Different behaviour is seen for the SetII experiment. Initially, hydrophilic substrate shows higher water retention during the evaporation and at a later time rate of mass loss gets higher than in acrylic substrate.

2.4.3 Final pattern after complete drying

Final deposition patterns after complete drying for SetI (stirring by Magnetic stirrer) experiments on hydrophobic substrate acrylic, and hydrophilic substrate glass are shown in Fig.2.3(a and b) respectively. Similarly, for SetII (stirring by Ultrasonicator) experiment final dried patterns are shown in Fig.2.3(c and d) for hydrophobic substrate acrylic, and hydrophilic substrate glass respectively. For any given substrate say acrylic, the difference in deposition pattern for the solution prepared by different methods is striking. Examining Fig.2.3a which is the final deposition pattern on the acrylic substrate for the solution prepared by stirring with a magnetic stirrer gives some interesting features in it. A thin-ring like deposition is observed at the TPCL with micro-cracks that emerge from the TPCL to the inner ring of the deposition. A gradient in ped size is clearly noticed where small peds are near the ring deposition and ped size increases gradually towards the center of the droplet.

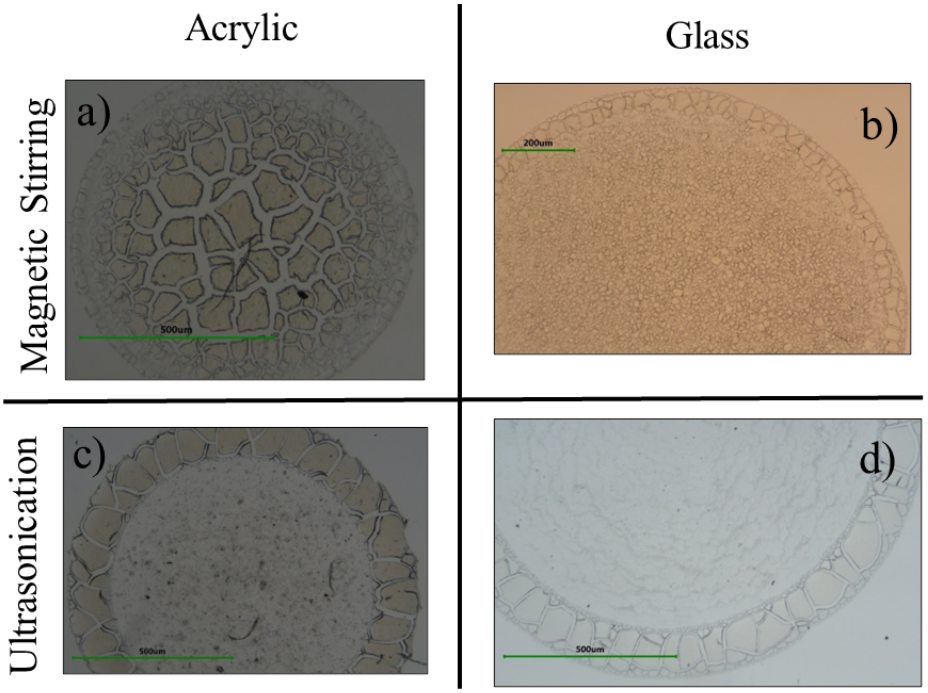

Figure 2.3: Final pattern of dried droplet on a)acrylic substrate b) on glass substrate for SetI experiment (stirring by Magnetic stirrer). Final pattern of dried droplet on c)acrylic substrate d) on glass substrate for SetII experiment (stirring by Ultrasonicator)

Due to the gradation of ped size, the crack width is higher to the inner portion of the droplet than the crack width near the ring. Even with the naked eye, one can see the thick deposition at the droplet apex than the deposition near the boundary.

In the same substrate acrylic, the droplet shows a different pattern after drying when the solution is prepared by stirring with an ultrasonicator as shown in Fig.2.3c. A wide ring-like deposition is formed at the TPCL with periodic cracks. The peds in the deposited ring are almost the same size and hence the cracks at the ring seem periodic. A very thin uniform deposition is observed on the interior of the droplet. Any considerable gradient in ped size is not observed at the interior portion of the droplet as seen in the case of the SetI experiment on the hydrophobic substrate.

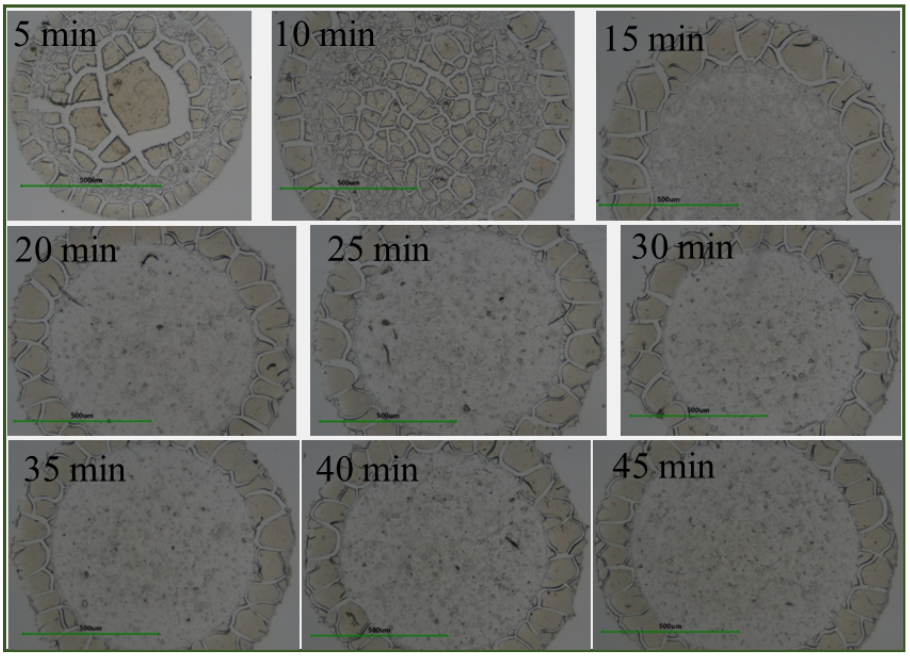

Figure 2.4: Final pattern of the dried droplet on hydrophobic substrate(acrylic) for different ultrasonication times varying from 5 min to 45 min in step of 5.

The final patterns of the dried droplet on hydrophilic substrate glass are shown in Fig.2.3(b and d) for SetI and SetII experiments respectively. Almost similar patterns are formed as seen in the case of hydrophobic substrate. In this case, however, no gradient in ped size to the interior portion of the droplet is seen Fig.2.3b when the solution is prepared by a magnetic stirrer and deposited on a glass substrate as seen on the hydrophobic substrate. Fig.2.3 b shows uniform deposition with uniform ped size. When the solution is prepared by ultrasonicator the peripheral border shows a wider ring with thick deposition. The ring at the border shows a faint crack with uniform distance. No such ped is formed in this case and a comparatively thin layer is formed at the interior of the droplet.

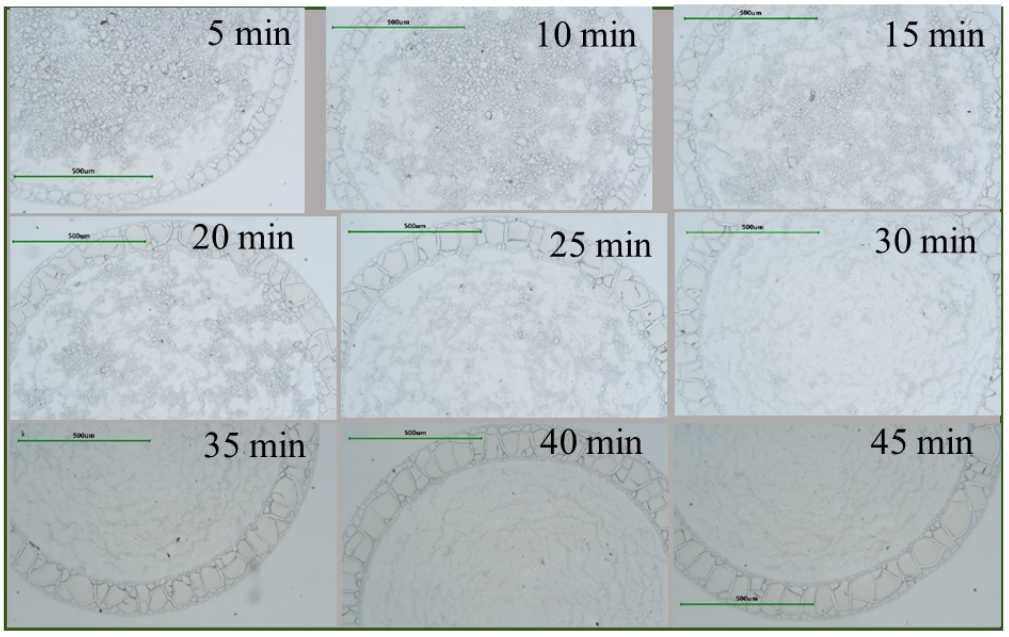

Figure 2.5: Final pattern of the dried droplet on hydrophilic substrate(glass) for different ultrasonication times varying from 5 min to 45 min in step of 5.

2.5 Effect of changing ultrasonication time

Applying the knowledge from the mentioned experiments, solutions are customized for a given combination of solute and solvent keeping fixed the other parameters. Especially for a microliter droplet when the solute size changes in the order of nanometer, the final deposition pattern changes considerably. Stirring the mixture of solvents means to breakdown the original aggregates by degrees. Stirring by ultrasonication or magnetic stirrer is similar by means of their functioning in the preparation of the solution. In the experiments, it is seen that the final patterns differ with preparation protocols (SetI and SetII) mentioned earlier on both substrates. It suggests that different processes break their aggregates to different degrees. In order to find a standard solution that yields a stable and reproducible pattern that would not change with further stirring, it is important to call a process for stirring the solute and solvent. As a way of dealing with this SetII (stirring by ultrasonication)

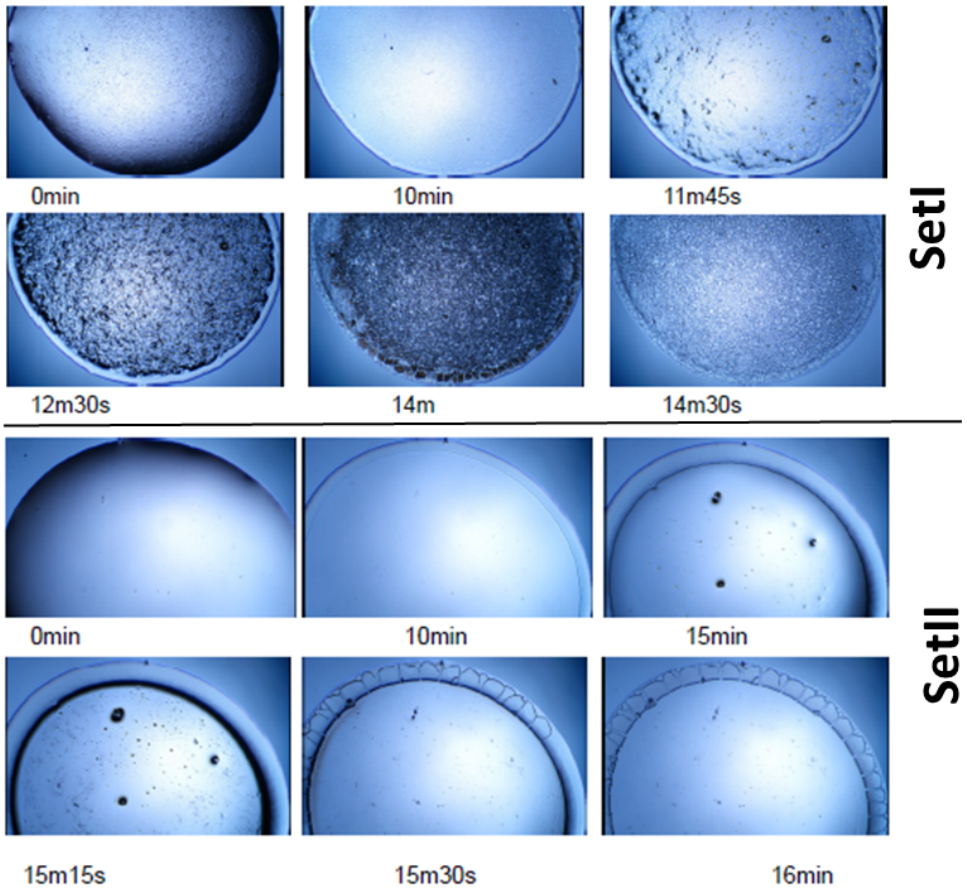

Figure 2.6: Time development of a drying droplet on glass substrate for both set of experiments

experiments was done with varying time from 5 minutes to 45 minutes in an interval of 5 minutes on both hydrophilic and hydrophobic substrate.

On acrylic substrate:

Figure 2.4 shows the final pattern of the dried pattern on a hydrophobic substrate with different ultrasonication times varying from 5 min-45 min. Examining Fig.2.4, it is seen that ultrasonication time increases from the lower to higher sonication time. Greater spreading of the droplet and hence the radius of the deposited is seen with the increase in sonication time instead of the same initial volume. For lower sonication time (say 5 minutes) deposition is thicker at the center of the droplet and thinner in deposition to the peripheral area. This results in the cracks at the central portion of the droplet being wider and thick than at the border.

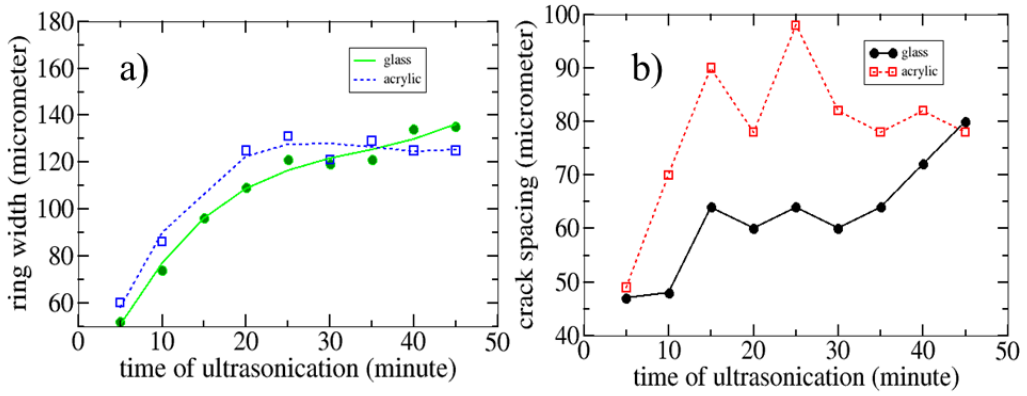

Figure 2.7: a) Variation of ring width at the TPCL with the variation of ultrasonication time. b) Variation of average crack spacing at the ring with the variation of ultrasonication time

The crack peds possess the gradient in size i.e. the peds are larger at the center and decreases in size at the TPCL. For greater sonication time (30-45 minutes) the reverse fashion is noticed with a thicker peripheral region than at the interior of the droplet. When the ultrasonication time is larger, the borders are wider and thick and hence cracks are seen. The cracks at the peripheral regions are periodic and confined between the inner and outer rings at the border. Finally examining the pattern of the droplet, ultrasonicated for 10 minutes, no discernible difference in thickness is seen at the TPCL and at the center of the droplet. A close comparison of this image to Fig.2.3a which is for the SetI experiment, shows the almost same pattern in their final deposition which indicates the same level of mixing of solute-solvent pair occurs i.e. degrees of paring down of aggregates are same for both cases. However, it is only after 30 minutes of stirring by ultrasonication, the identical deposition pattern is observed for both substrates. This leads to conclude for silica flake-water mixing, minimum time for making a stable solution for the reproducible pattern on the acrylic substrate is $t_{std} = 30$ minutes.

On glass substrate

Fig.2.5 shows the final pattern of the dried droplet of aqueous silica suspension on

a glass substrate with ultrasonication time varying from 5 minutes to 45 minutes. On a glass substrate, the spreading is greater for a higher ultrasonication time for the same initial volume of droplet. There is a border-like deposition for each case and the width of the border increases with an increase in ultrasonication time. This deposition at the border shows a distinct periodic pattern and periodicity increases with an increase in stirring time by ultrasonicator. For lower sonication time, 5-15 minutes, there is a crowd of small ped aggregates at the interior region to the droplet keeping a certain distinction from TPCL. As the sonication time increases the congregation at the center of the droplet disperses. For ultrasonication time of 30 minutes and after that the small aggregates vanish from the center and uniform deposition is observed with a thin annular ring-like pattern is observed with respect to the droplet center. Examining Fig.2.5 shows that, for glass substrate, ultrasonication time is 30 minutes for preparation of homogeneous solution of aqueous silica flakes. Considering both cases, it can be concluded that, t_{std}=30 minutes is the standard ultrasonication time for a stable solution of aqueous silica flakes.

The ring width of the deposition of the droplet is increased with an increase in ultrasonication time on both glass and acrylic substrates as shown in Fig.2.7. The ring width gets an almost constant value after a sonication time of 30 minutes which indicates there is no influence on solution characteristics for further ultrasonication when the other parameter is constant. It is clearly noticed from Fig.2.7 that levelling off is sharper for acrylic substrate than glass. Fig.2.7b shows the crack spacing at the periphery with respect to the ultrasonication time. Examining this figure, it is clear that the cracks are periodic i.e. there is a wavy pattern. If we notice the Fig2.6, 2.8, 2.9 then two sets of cracks with larger and smaller sizes are seen. Fig.2.7b shows the average crack spacing considering the larger cracks. A strong substrate effect is noticed in crack spacing at the periphery. Crack spacing is much higher for acrylic substrate than glass. In the case of the glass substrate, the strong pinning of the TPCL accumulates the stress. The release of stress is low and easily reaches the critical threshold of stress to crack. For acrylic substrate, the slipping tendency of

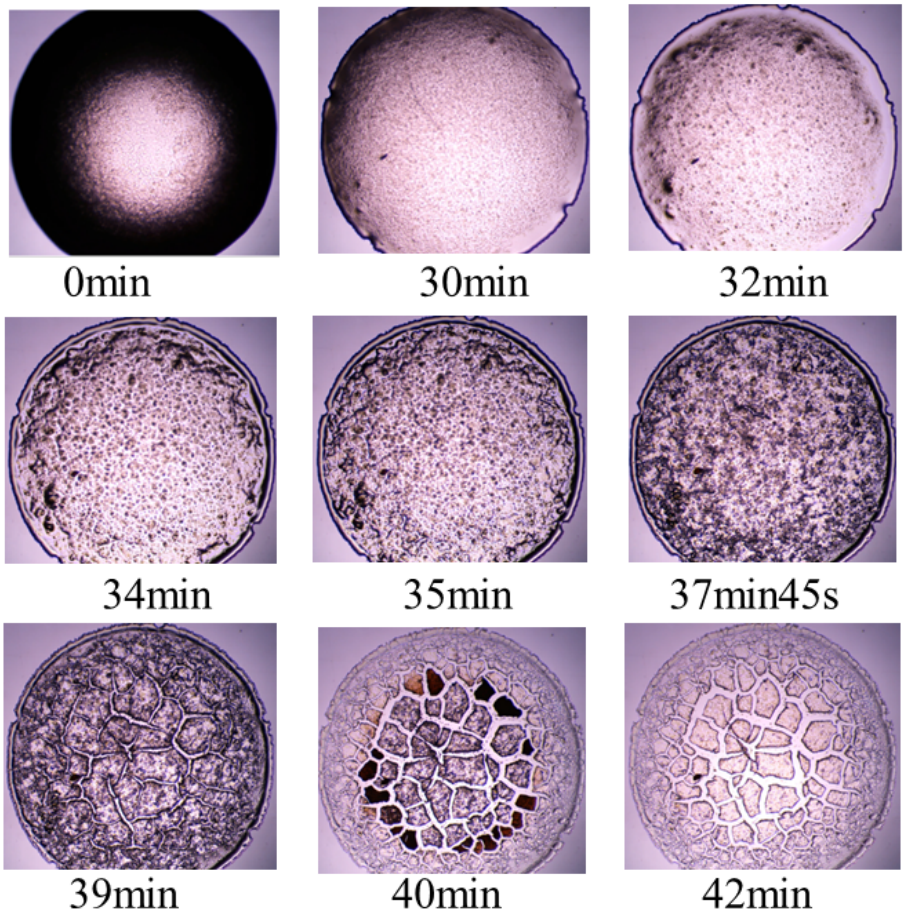

Figure 2.8: Time development of a drying droplet on acrylic substrate for SetI experiment

TPCL is seen and stress is released somehow and taking a longer time to reach the critical stress value and hence crack spacing is high.

2.6 Explanation

We have considered glass as a hydrophilic substrate with a small contact angle and acrylic as a hydrophobic substrate with a contact angle near about 90° throughout the experiments as well as the following discussions. Evaporation dynamics vary from substrate to substrate depending on the contact angle and spreading coefficient

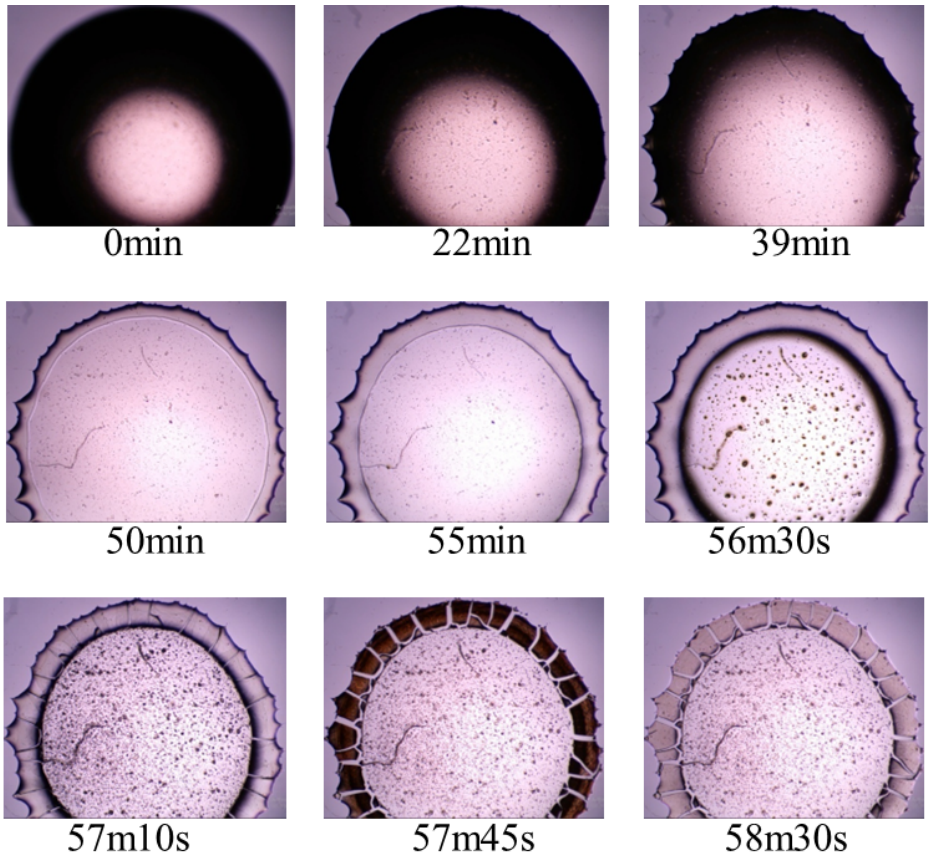

Figure 2.9: Time development of a drying droplet on the acrylic substrate for SetII experiment

which in turn change the deposition pattern of the drying droplet. In order to analyze the final pattern, it is important to understand the evaporation dynamics of a drying droplet. For the small value of contact angle say as in glass substrate the evaporation flux through the liquid-gas interface is given by[32]

$$J = \frac{2D(C_{sat} - C_c)}{\pi\sqrt{R^2 - r^2}} \tag{2.1}$$

and the free surface of the sessile droplet is parabolic in nature and the curvature is given by

$$h = \frac{\theta(R^2 - r^2)}{2R} \tag{2.2}$$

Where J= is the evaporation flux, D=diffusion coefficient of the vapour in the atmosphere, C_{sat}= saturation vapour concentration, C_c=constant vapour concentration

in the ambient condition far away from the droplet surroundings, R=radius of the droplet, r = radial distance at which the droplet height is h and θ= contact angle of the droplet.

From the above equation, it is clear that evaporation flux J is maximum [33] at the droplet TPCL where $r \sim R$. Due to the high evaporation flux at the TPCL, a radial convective flow is developed to the TPCL to create the famous phenomenon Coffee ring effect. Further approximation of the solute particles or aggregates as a sphere, the relative drag force of the solute particles during evaporation is given by

$$F = 6\pi\eta r v \tag{2.3}$$

where η is the viscosity of the fluid, r is the approximate radius of the aggregate and v is the velocity of the aggregates. Hence for smaller particles viscous drag force is less and easily carried to the TPCL of the droplet to form the coffee ring effect. During evaporation, some particles crowded themselves through the interface of the droplet and create a bridge through the droplet interface by submerging themselves partially inside the droplet. This solvent bridge holds the particles by a capillary force which is given by [34]

$$F_c = -\frac{4\pi r\gamma\cos\theta_1}{3} \tag{2.4}$$

where γ is the surface tension between solvent and air interface and θ_1 is the contact angle between solvent and particle. The evaporation of the solvent during drying gathers the aggregates to form skin to the interface. The particles also possess a long-range force which is known as Derjaguin- Landau-Verwey-Overbeek (DLVO) interactions or DLVO force. This DLVO force is the algebraic sum of the van der Walls and electrostatic forces. This force carries the aggregates toward the substrate with a velocity

$$V_D \sim \frac{2F_D}{12\pi\eta r} \tag{2.5}$$

Where F_D is the DLVO force [35]. Apart from these forces, there may be some forces that arises due to surface tension gradient which creates Marangoni circulating

during evaporation.

A close observation of Fig.2.1 shows that the rate of evaporation is higher for the SetII than the SetI experiment for hydrophilic substrate where the contact angle is low. The lower value of contact angle for hydrophilic substrate ensures the higher evaporation flux and small droplet height. In the case of the SetI experiment, stirring by a magnetic stirrer produces larger aggregates than obtained by the ultrasonication process. According to eqn.2.3 viscous drag force being higher for larger particles, a few particles are able to reach TPCL to form a very thin coffee ring pinned to the boundaries, and most of the aggregates remained suspended to the droplet. As the solvent evaporates, the larger particles are drawn to the droplet interface by capillary forces according to eqn.2.4 and form a crust to the droplet interface Fig.2.6 SetI and slow down the evaporation rate Fig.2.1. Fig.2.6 shows the time development of the droplet for SetI experiments for the hydrophilic substrate.

For hydrophobic substrate the contact angle being higher the ratio of droplet surface to the volume lower than hydrophilic substrate, a higher water retention is observed for hydrophobic substrate as shown in Fig.2.2a and b. Due to the high contact angle, height of the droplet is much higher at the droplet center than the height at the edge. Hence the heat transfer is higher at the droplet edge than the center of the droplet and a higher evaporation rate at the droplet edge generates a radial flow towards the TPCL forming a coffee ring pinned to the substrate. As the evaporation increases the droplet gets flattened by decreasing contact angle. As drying proceed the central light portion increases in size which suggests the flattening of the droplet. This in turns decreases the adhesion energy per unit area following the relation

$$\gamma_{lv}(1 + cos\theta) = W_{slv} \tag{2.6}$$

Where γ_{lv} is liquid-vapour interfacial energy and W_{slv} is the solid-liquid adhesion energy. This loss of energy creates the stick-slip motion of the droplet. This is the reason for decreasing the evaporation rate as shown in Fig.2.1b. Repulsion forces

between the droplet and substrate are sufficient for the hydrophobic substrate to move the TPCL. The time development of droplet evaporation for SetI and SetII experiments on the hydrophobic substrate (acrylic) are shown in Fig.2.8 and Fig.2.9. Time development on the acrylic substrate for SetII experiments shows a corrugated appearance at the TPCL which is a result of competition between surface energy force and frictional pinning force. The dark concentrated ring at the TPCL is evident in the stick-slip motion of the droplet.

The evaporation rate for SetII experiments is lower than SetI experiments for hydrophobic substrate as shown in Fig.2.1b. In this case, crust formation is happened to the interface by capillary forces given by eqn.2.4. As the particle size decreases the forces increase to form a closed-pack solid crust. Where the aggregates are larger in size the capillary force is lower and gets sufficient space that helps higher evaporation rate for SetI experiments. A rough crust is formed at the interface for SetI experiments due to a higher evaporation rate. Again the viscous drag force is higher due to the larger size of the aggregates, a thick crust is formed and developed crack formation just like mud crack.

Fig.2.2(a, b) show the substrate effect on evaporation rate. For SetI experiments, slower evaporation rate is noticed on a glass substrate. For glass substrate, surface to volume ratio is high and the capillary force that developed to the droplet interface is effective to shield and slow down the evaporation rate. For SetII experiments on acrylic substrate, the droplet height is more and latent heat transfer is low. The crust formation to the droplet interface reduces the evaporation rate.

Particles in colloidal solution are often smaller in size than the aggregation of solution. Stirring the solution changes the aggregate size depending on the degree of stirring and/or speed effect of stirring on the solution and hence changes the desiccation pattern. The desiccation pattern reaches a final pattern when the solution gets a standard homogeneous solution acquiring a critical size of the particles. With another degree of paring down the aggregates, a different critical size can be

reached and hence another desiccation pattern may be obtained. Stirring by ultrasonication process produces the solute particles of the order of nanosize. Due to very light particles, the convective force enables to carry the solute particles to the boundaries more strongly than DLVO forces. Most of the solute particles reached the peripheral border. The peripheral border gets thick and wide and a wavy crack is seen in Fig.2.6. For SetII experiments the peripheral border is fixed between two boundaries. Especially for a hydrophilic substrate the thick deposition at the border shows periodic wavy crack between two boundary lines. The decay length of the stress [36], [37] determines the crack nature. If the width of the pinned area of the droplet is very low then the cracks that occur to the boundary are straight line in nature. For uniform thickness, the released stress-energy can be estimated [38]. Cracks in the borderline get wavy due to oscillation of the stresses in the area of the boundary. Very near to the boundaries the stress components are almost parallel to the boundaries and hence the crack in the middle portion gets curved to the boundaries. The film just near the boundaries is thinner and maximum energy releases occur at $\pm 90^{\circ}$ in the vicinity of the two boundaries and in this way cracks deflect to the center line. Repetition of this process causes wavy cracks at the boundaries. If the central portion of the droplet is examined for SetII experiment, it can be seen that there is no crack. Most of the solute particles are deposited to the boundaries because of convective flow and thickness at the central portion is lower than the critical thickness and no such cracks are seen. In the case of SetI experiment, a thick crust is formed at the inner region of the droplet and cracks are observed.

2.7 Conclusion

In this work, the variation in the final dried pattern is shown by changing the mixing method of solute and solvent during solution preparation. The droplet drying dynamics during evaporation and the final pattern of the dried droplet are completely different for different substrates. It has been justified the observation in association

with the substrate properties and the flow dynamics that developed during drying for both sets of experiments. The variation in the result is very striking and interesting. In droplet drying experiments, a very common method of solution preparation is stirring by magnetic stirrer. It is shown that, if the same solution is prepared by stirring by ultrasonicator then the resulting drying dynamics and hence final dried pattern is completely changed for both hydrophilic and hydrophobic substrates. Not only that, time of stirring affects evaporation dynamics and the final pattern. This leads us to conclude that a minimum time is required to prepare homogeneous and standard solutions for any preparation protocol.

In most of the cases in the laboratory mixing of solute and solvent is done for constant time and for a particular stirring method. Practically it is ignored what will happen if the mixing time and method are changed. The difference in final dried patterns has led to conclude that the size of the aggregates in solution produced by different mixing methods and as well as the variation of degrees of paring down affect the size of the inclusions. The suitable explanation of the striking result leads to the proposal that particle size inside the solution as a function of time and preparation protocol and the substrate properties affect the drying dynamics. The protocol of preparation, especially for colloidal solution cannot be strongly intensified. In a colloidal solution, the solid inclusion size changes from μm to nm depending on the degrees of paring down. Again the size of the solute greatly affects the flow dynamics inside the droplet resulting in crack peds of different sizes. It is very important to establish and follow a particular preparation method in which the characteristics will be independent and then the prepared solution can be used with confidence in desired application to get a standard result.

Bibliography

[1] D. Zang, S. Tarafdar, Y. Y. Tarasevich, M. Dutta Choudhury and T. Dutta, *"Evaporation of a droplet: From physics to applications"*, *Physics Reports* **804**

1–56 (2019).

[2] D. Brutin, *Droplet wetting and evaporation: from pure to complex fluids*. Academic Press, 2015.

[3] F. Giorgiutti-Dauphiné and L. Pauchard, *"Drying drops: Drying drops containing solutes: From hydrodynamical to mechanical instabilities"*, *The European Physical Journal E* **41** 1–15 (2018).

[4] K. Sefiane, *"Patterns from drying drops"*, *Advances in colloid and interface science* **206** 372–381 (2014).

[5] T. Lim, S. Han, J. Chung, J. T. Chung, S. Ko and C. P. Grigoropoulos, *"Experimental study on spreading and evaporation of inkjet printed pico-liter droplet on a heated substrate"*, *International Journal of Heat and Mass Transfer* **52** 431–441 (2009).

[6] J. González-Gutiérrez, O. Moctezuma, V. Angeles, M. Rios-Ramirez, S. Zetina, A. Marin et al., *"Pattern formation by droplet evaporation and imbibition in watercolor paintings"*, *arXiv preprint arXiv:1909.09098*, (2019).

[7] Y.-Y. Yang, T.-S. Chung, X.-L. Bai and W.-K. Chan, *"Effect of preparation conditions on morphology and release profiles of biodegradable polymeric microspheres containing protein fabricated by double-emulsion method"*, *Chemical Engineering Science* **55** 2223–2236 (2000).

[8] R. D. Deegan, O. Bakajin, T. F. Dupont, G. Huber, S. R. Nagel and T. A. Witten, *"Capillary flow as the cause of ring stains from dried liquid drops"*, *Nature* **389** 827–829 (1997).

[9] H. Hu and R. G. Larson, *"Marangoni effect reverses coffee-ring depositions"*, *The Journal of Physical Chemistry B* **110** 7090–7094 (2006).

[10] R. D. Deegan, O. Bakajin, T. F. Dupont, G. Huber, S. R. Nagel and T. A. Witten, *"Contact line deposits in an evaporating drop"*, *Physical review E* **62** 756 (2000).

[11] B. M. Weon and J. H. Je, *"Capillary force repels coffee-ring effect"*, *Physical Review E* **82** 015305 (2010).

[12] P. J. Yunker, T. Still, M. A. Lohr and A. Yodh, *"Suppression of the coffee-ring effect by shape-dependent capillary interactions"*, *nature* **476** 308--311 (2011).

[13] V. R. Dugyala and M. G. Basavaraj, *"Control over coffee-ring formation in evaporating liquid drops containing ellipsoids"*, *Langmuir* **30** 8680--8686 (2014).

[14] R. Bhardwaj, X. Fang, P. Somasundaran and D. Attinger, *"Self-assembly of colloidal particles from evaporating droplets: role of dlvo interactions and proposition of a phase diagram"*, *Langmuir* **26** 7833--7842 (2010).

[15] M. Anyfantakis, Z. Geng, M. Morel, S. Rudiuk and D. Baigl, *"Modulation of the coffee-ring effect in particle/surfactant mixtures: the importance of particle–interface interactions"*, *Langmuir* **31** 4113--4120 (2015).

[16] R. Malinowski, G. Volpe, I. P. Parkin and G. Volpe, *"Dynamic control of particle deposition in evaporating droplets by an external point source of vapor"*, *The journal of physical chemistry letters* **9** 659--664 (2018).

[17] J. M. Baek, C. Yi and J. Y. Rhee, *"Central spot formed in dried coffee-water-mixture droplets: Inverse coffee-ring effect"*, *Current Applied Physics* **18** 477--483 (2018).

[18] A. K. Thokchom, A. Gupta, P. J. Jaijus and A. Singh, *"Analysis of fluid flow and particle transport in evaporating droplets exposed to infrared heating"*, *International Journal of Heat and Mass Transfer* **68** 67--77 (2014).

[19] H. B. Eral, D. M. Augustine, M. H. Duits and F. Mugele, *"Suppressing the coffee stain effect: how to control colloidal self-assembly in evaporating drops using electrowetting"*, *Soft Matter* **7** 4954--4958 (2011).

[20] C. Seo, D. Jang, J. Chae and S. Shin, *"Altering the coffee-ring effect by adding a surfactant-like viscous polymer solution"*, *Scientific reports* **7** 500 (2017).

[21] L. Cui, J. Zhang, X. Zhang, L. Huang, Z. Wang, Y. Li et al., *"Suppression of the coffee ring effect by hydrosoluble polymer additives"*, *ACS applied materials & interfaces* **4** 2775--2780 (2012).

[22] Y.-F. Li, Y.-J. Sheng and H.-K. Tsao, *"Evaporation stains: suppressing the coffee-ring effect by contact angle hysteresis"*, *Langmuir* **29** 7802--7811 (2013).

[23] X. Yang, C. Y. Li and Y. Sun, *"From multi-ring to spider web and radial spoke: competition between the receding contact line and particle deposition in a drying colloidal drop"*, *Soft Matter* **10** 4458--4463 (2014).

[24] B. Sharma, R. Verma, C. Baur, J. Bykova, J. M. Mabry and D. W. Smith, *"Ultra low dielectric, self-cleansing and highly oleophobic poss-pfcp aryl ether polymer composites"*, *Journal of Materials Chemistry C* **1** 7222--7227 (2013).

[25] J. Lee, P. K. Duy, S. C. Park and H. Chung, *"Development of hydrophobic surface substrates enabling reproducible drop-and-dry spectroscopic measurements"*, *Talanta* **153** 31--37 (2016).

[26] E. Kočišová, M. Procházka and H. Šípová, *"Thiol-modified gold-coated glass as an efficient hydrophobic substrate for drop coating deposition raman (dcdr) technique"*, *Journal of Raman Spectroscopy* **47** 1394--1396 (2016).

[27] M. Pack, H. Hu, D.-O. Kim, X. Yang and Y. Sun, *"Colloidal drop deposition on porous substrates: competition among particle motion, evaporation, and infiltration"*, *Langmuir* **31** 7953--7961 (2015).

[28] R. Dou and B. Derby, *"Formation of coffee stains on porous surfaces"*, *Langmuir* **28** 5331--5338 (2012).

[29] M. A. Hampton, T. A. Nguyen, A. V. Nguyen, Z. P. Xu, L. Huang and V. Rudolph, *"Influence of surface orientation on the organization of nanoparticles in drying nanofluid droplets"*, *Journal of colloid and interface science* **377** 456--462 (2012).

[30] Z. Cao and A. V. Dobrynin, *"Polymeric droplets on soft surfaces: From neumann's triangle to young's law"*, *Macromolecules* **48** 443--451 (2015).

[31] N. Saengchairat, C. K. Chua and T. Tran, *"Ink evaporation on soft substrates for additive manufacturing of stretchable electronic devices: experimental studies"*, .

[32] Y. O. Popov, *"Evaporative deposition patterns: spatial dimensions of the deposit"*, *Physical Review E* **71** 036313 (2005).

[33] H. Hu and R. G. Larson, *"Analysis of the effects of marangoni stresses on the microflow in an evaporating sessile droplet"*, *Langmuir* **21** 3972--3980 (2005).

[34] H. M. Van Der Kooij, R. Fokkink, J. Van Der Gucht and J. Sprakel, *"Quantitative imaging of heterogeneous dynamics in drying and aging paints"*, *Scientific reports* **6** 34383 (2016).

[35] O. Sardan, A. D. Yalcinkaya and B. E. Alaca, *"Self-assembly-based batch fabrication of nickel–iron nanowires by electroplating"*, *Nanotechnology* **17** 2227 (2006).

[36] L. Goehring, A. Nakahara, T. Dutta, S. Kitsunezaki and S. Tarafdar, *Desiccation cracks and their patterns: Formation and Modelling in Science and Nature*. John Wiley & Sons, 2015.

[37] M. Gao, X. Huang and Y. Zhao, *"Formation of wavy-ring crack in drying droplet of protein solutions"*, *Science China Technological Sciences* **61** 949--958 (2018).

[38] J. R. Rice, *"Some remarks on elastic crack-tip stress fields"*, *International Journal of Solids and Structures* **8** 751--758 (1972).

Chapter 3

Pattern formation of aqueous Laponite droplet on different substrates with varying pH

3.1 Introduction

Droplet physics is an interdisciplinary subject of fluid dynamics, transport phenomena, phase changes, interface science, properties of soft matters, etc [1], [2], [3], [4]. The pattern left by the droplet after completion of drying bears a significance of all the mentioned properties. That's why it has great importance for academic purposes also. It bears a great interest to scientists because of its application in medicine, diagnostic purpose, printing and painting technology, industry, etc. The sessile shape of a droplet of a complex solution is responsible for complex mass flow that developed inside a droplet during drying [5], [6]. Surface tension gradient, temperature, substrate properties, relative humidity, surfactant, etc. set up the competition between the different flows like convective flow, Marangoni flow, and the gravitational flow inside the droplet [7], [8]. These fluid flow carry the dissolved solutes and are deposited on the substrate in different patterns. The morphology of the residual

pattern of the dried droplet bears significance in the application. The shape of the particles and the presence of salt in the aqueous solution changes the final deposition pattern [9]. In most cases, the colloidal particles in the solution acquire an effective charge on its surface. The charged state of any particle is very sensitive to the pH of the solution. pH of the solution can affect the zeta potential of the solution and substrate which influence the electrostatic force. Zeta potential affects the DLVO forces. According to DLVO theory, this force is summed up by electrostatic forces between particle-particle and particle-substrate and van Der Walls force. In this study, we will discuss how the residual pattern of aqueous Laponite droplet changes with the change of pH of the solution from very acidic to basic pH.

Pure Laponite is a disk-shaped particle. In an aqueous medium, it possesses a net negative charge at its face surface and positive charges at the rim. When the pH of the aqueous Laponite solution is increased from the acidic range to basic, the nature of the charges of its rim changes from positive to negative charges at around pH 12. Depending on the pH of the solution Laponite particles arrange themselves to stack-coin arrangement or caged like house of card structure during drying to form. When the aqueous Laponite droplets of different pH are allowed to evaporate, the arrangement of the particle during drying is further perturbed by its complex mass transfer due to its uneven exposed surface. Thus the pattern left by aqueous Laponite droplets with varying pH on the substrates of different hydrophobicities. For hydrophobic substrate PMMA, the droplet shows the coffee ring effect in the acidic pH range. In a very acidic pH dried droplet on a hydrophobic substrate shows the dried droplet pattern indicates collapsed cavities that contain a ring of salts on its wall. In the basic range of pH on the same substrate, salt crystals gathered on the Laponite droplet. The same studies were done on hydrophilic substrates and quite different patterns of the result were seen. We have offered an explanation of the obtained results to justify on the basis of the particle-particle (PP) and particle substrate (PS) interaction in association with the pH of the solution.

3.2 Earlier work related to Laponite

Colloidal clays are emerged as a very compact subject because of their complex phase behavior, gel, and glassy state [10], [11]. This section contains the phase behavior of very known synthetic clay Laponite particles. The study of the phase behavior of Laponite particles goes through an intense debate after the revolutionary work of Thomson and Butterworth [12]. Mourchid and his group studied the phase diagram of colloidal disk-shaped charged particles. They showed that the colloidal suspension undergoes a sol-gel transition without macroscopic phase difference. They showed that ionic strength and concentration of the suspension are the key factor to control the sol-gel transition [13]. The study of the rheology of Laponite clay is very controversial. Jatav et.al studied the rheology of Laponite particles with varying particle and salt concentrations. They observed that all the rheological properties regarding sol-gel transition lead to percolated network as well as fractal nature. They showed that activation energy also changes with laponite as well as salt concentration [14]. Synthetic Laponite clay in an aqueous medium shows viscoelastic properties even in low concentrations. Gel formation is evidence of that property. Another observation shows no direct relation between the fractal dimension and viscoelasticity and they argued that Laponite solution forms a colloidal solution rather than gel [15]. Aggregation of the Laponite particle in the solution quickened with an increase in the ionic strength of the solution which helps to form gel [16].

3.2.1 Laponite particle and its characterization

Laponite particles are in a white powder state. Primary particles are platelet with aspect ratio $\sim 1:25$. One unit of Laponite particles is formed with one octahedron of magnesia and two tetrahedrons of silica and the tetrahedrons are on either side of the magnesia layer [17]. Upper valence atom lithium substitutes the magnesium ion from the octahedron to create the deficiency of positive charges. On the opposite

faces of the particle have excess electrons which are shared with the sodium atom. In the dry powder state, the sodium atoms are present inside the particles because the Laponite platelets are stacked form. When the particles are in aqueous solution the sodium atoms are dissociated into the bulk medium in the form Na^+ due to osmotic gradient. Due to this dissolution of sodium ion, the Laponite particles possess permanent negative charges in their face. This type of substitution is easy because of its smaller size. Normally in the powder state, the particles are in a neutral state because the cations from the atmosphere are adsorbed by the particles. These ions in the solution are responsible for the electrostatic interaction between the particles. The ionic state of the solution determines the morphology of the sol-gel, rheological properties of the gel, or electro-kinetic response to the electric field or magnetic field.

At very low concentrations the gelling of laponite is not observed. When the concentration reaches beyond 1%, soft solid-like consistency i.e. physical gelling is seen. There is the consent of Everyone that Laponite concentration up to 2% forms a space spanning attractive gel [18]. Beyond that concentration, a controversy exists amongst the researchers. The debate exists regarding the microstructure responsible for the solid-like property of Laponite. One group suggests that Laponite particles form repulsive glass where the particles are suspended in a stacked arrangement without touching each other due to repulsion between the negatively charged face surfaces [19], [18], [20]. Another group claimed that the Laponite particles in aqueous solution of concentration beyond 2% form a caged-like fractal structure by attraction between the negative face of one particle to the positive edge of the other particles [20], [21]. The interesting point is the concentration region between 1.8 to 2. It has been claimed that in this region Laponite particles may be either in a repulsive glass state or space-spanning attractive gel [22].

The edges of the Laponite particles consist of broken crystals of magnesium and silica. pH of the medium determines the nature of charges of the Laponite edge. The edge of the Lponite particle where MgOH crystals are present, possesses positive charges below pH 12 and above that pH, the edge holds negative charges. That's

why pH 12 is the Iso Electric Point (IEP) for MgOH crystal. Similarly, pH 2 is IEP for SiOH crystal [23]. There is a link between the face charges, charge of the edges, and pH of the medium [24], [25]. To maintain the positive charges to the edges, OH^- ions release to the bulk medium which increases the pH of the medium. Similarly, to render the negative charges on the edges of the particles, H^+ dissociates to the medium to decrease the pH. The H^+ ions available to the medium get adsorbed by the negative faces of the Laponite resulting in a decrease in the pH of the solution. Thomson and Butterworth [12] studied the effect of pH of aqueous Laponite solution with concentration up to 2%. pH of the aqueous Laponite is about 10. They proposed that Laponite particles in the pH limit < 9 disintegrate in the medium following the relation

$$Na_\alpha Si_8 Mg_\beta Li_\gamma O_{20}(OH)_4 + 12H^+ + 8H_2O \rightarrow 8Si(OH)_4 + \beta Mg^{2+} + \gamma Li^+ \quad (3.1)$$

where value of the variables α, β and γ can have a variation of ± 0.1 depending on the compositions. Mourchid and Levitz observed that Aqueous Laponite solution gets gel form in an open atmosphere faster than kept in a nitrogen atmosphere due to the absorption of carbon dioxide from the air. The absorbed CO_2 dissolved into the solution and forms weak carbonic acid. This carbonic acid increases the density of H^+ ion and leads to the release of the Mg^{2+} and Li^+ ions in solution according to eq.3.1 which speed up to gel fast [26], [27]. Mohanty et.al reported that pH does not have any direct impact on the degradation of Laponite Particle [28].

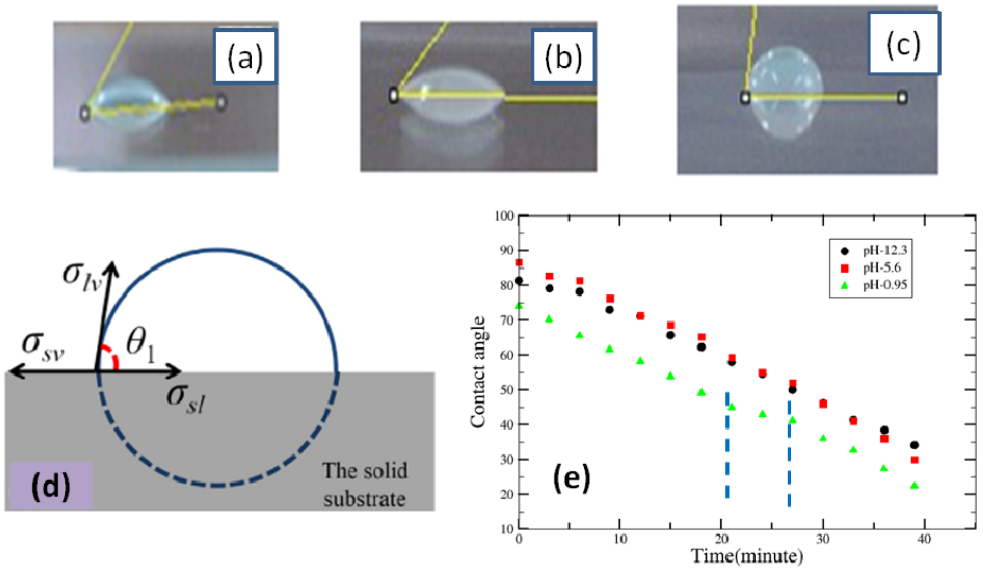

Figure 3.1: Contact angle of aqueous Laponite droplet on a)glass b)quartz and c)PMMA substrate. d) Surface tension at the TPCL. e)Rate of change of contact angle of Laponite droplet on PMMA substrate for different pH values. The region between the vertical and dotted lines is the time duration for constant contact angle.

3.3 Materials and Experimental Methods

The preparation protocol of a solution greatly affects the flow dynamics inside a droplet and hence the final patterns of residue [29]. Hence throughout the experiments, we follow the preparation methods described below faithfully to get the reproducible result and ensure that results are not a substantiation of the preparation protocol. Pure Laponite and deionized water were used throughout the experiments. The droplet of aqueous Laponite solution with varying pH is studied on PMMA, quartz, and glass substrates. In order to change the pH of the solution, a suitable amount of NaOH beads and 37% concentrated HCl are added to deionized water and kept it undisturbed for 30 minutes. This water is used for the preparation of the solution.

Laponite solution of 1% concentration is used for all experiments. 0.1 gm of Laponite powder is added to the 9.9 ml of water and stirred by ultrasonicator for 30 minutes.

Immediately after the preparation of the solution droplet of 5-7μl is deposited on PMMA, quartz, and glass substrate that was previously cleaned with extran detergent and then acetone and allowed to dry in an ambient condition of temperature 23-26°C and relative humidity 45-50%. The residue pattern of the dried droplet is photographed by a Magnus camera, fitted with an inverted microscope for further analysis.

The contact angle of the droplet for different substrates was measured by taking an image of the deposited droplet with a high-resolution camera (Canon700D). ImageJ software is used to measure the contact angle.

To make certain that no ageing effects of the aqueous solution of Laponite affect the result for the entire period of experiments, the solutions with all pH were put in the transparent glass bottle and kept for 90 hours, 3.2. These solutions were checked for transparency and liquid state.

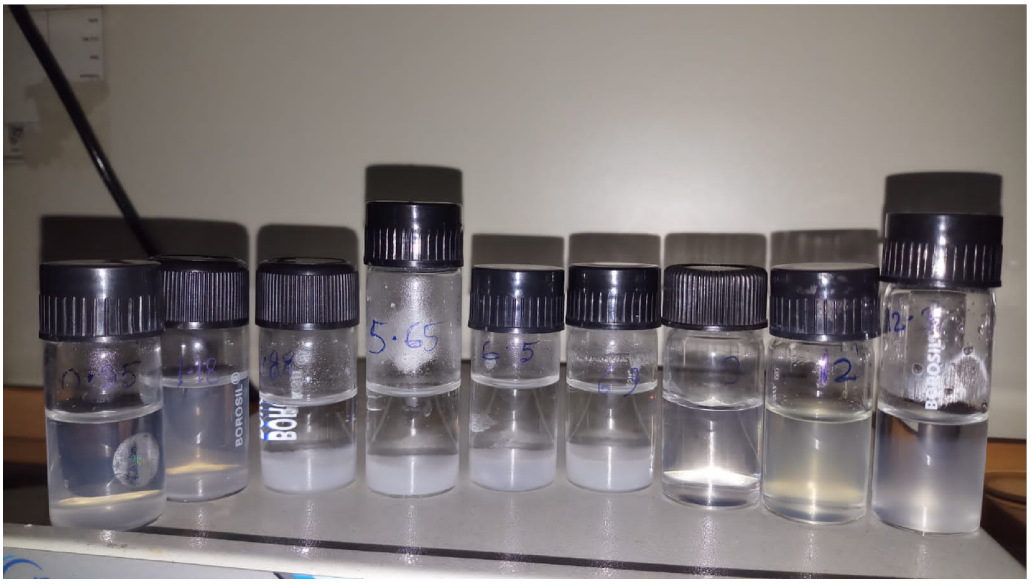

Figure 3.2: Bottles are contained with aqueous Laponite suspension with 1% concentration for different pH values, after 90 hours since sample preparation time. pH values are from left to right: 0.95, 1.18, 1.88, 5.65, 6.5, 7, 9, 12, 12.3.

3.4 Different forces at play

To analyze the residual patterns left by aqueous Laponite droplets with varying pH on different substrates, it is important to understand the forces at play during drying inside an evaporating droplet. The electrostatic force acts between the substrate and the colloidal particle are given by the following equation [30]

$$F_{el} = ae^{-\kappa z}n_z \tag{3.2}$$

where z=distance between the substrate and the particle, n_z= unit normal vector to the substrate, κ^{-1}=Debye length and 'a'= a constant factor which is a function of the surface potential, the interaction between the particle and substrate, and ambient temperature. Another force acting between the particle and substrate is the van Der walls attraction force which is given by [30], [31]

$$F_{vd} = \frac{Ad^3\alpha_{rt}n_z}{12z^2(z+d)^2} \tag{3.3}$$

where A= Hamaker constant, the value of this constant for water is 2.43×10^{-20}J [32], α_{rt}= retardation factor for van Der walls force which depends on the distance between the surface and particles. The DLVO force acting between the particle and the substrate is given by

$$F_{DLVO} = F_{el} + F_{vd} \tag{3.4}$$

Zeta potential is a function of pH and DLVO force is a function of zeta potential. So change in the pH of the solution changes the DLVO force as well. Iso-electric Point (IEP) for PMMA is $\sim$ 4 and zeta potential for this substrate is positive below pH 4 and negative above it [33]. IEP for glass and quartz substrate is almost the same and it is $\sim$ 2.8. The Zeta potential of Laponite also depends on the pH of the solution. IEP of Laponite is 12 and zeta potential becomes more negative with increasing pH of the solution [34], [35]. Hence the pH of the solution of Laponite particles becomes

the function of DLVO force which determines the particle substrate interaction. This force plays a serious role in the drying dynamics of an evaporating droplet on different substrates.

The sessile shape of the droplet is responsible for the complex mass flow inside the droplet during evaporation. Evaporation flux is uneven throughout the exposed surface but symmetric about the center of the droplet. For hydrophilic substrate glass and quartz, maximum evaporation happens at the TPCL and minimum from the droplet apex. Due to this gradient of evaporation flux a convective flow is developed from the droplet apex to the periphery of the droplet. This drives the solute particle to the TPCL resulting in the very known phenomenon of the Coffee ring. A different picture is seen in the hydrophobic substrate where more evaporation occurs from the droplet apex than the droplet TPCL. During the drying of an evaporating droplet, surface tension or thermal gradient may be developed inside the droplet which creates the solutal Marangoni flow or thermal Marangoni flow respectively. The interaction energy between the faces of the colloidal particles can be expressed by the DLVO force. It is the competition amongst the different forces that act inside the droplet during drying which is responsible for the final trajectory of the particles which creates the different patterns.

3.5 Experimental results and discussions

Contact angles on PMMA, glass, and quartz were measured for aqueous Laponite suspension using ImageJ software which are 83.6°, 30° and 38° respectively, Fig.3.1. Thus, PMMA is a 'hydrophobic substrate' whereas the glass, and quartz are treated as 'hydrophilic substrates'. Samples of all pH were prepared and kept in glass bottles to check the liquid state and clarity. After 90 hours of sample preparation, the transparency of the samples does not change with time, Fig.3.2. A close observation shows that after 2-3 hours of sample preparation, a white dreg was visualized at the

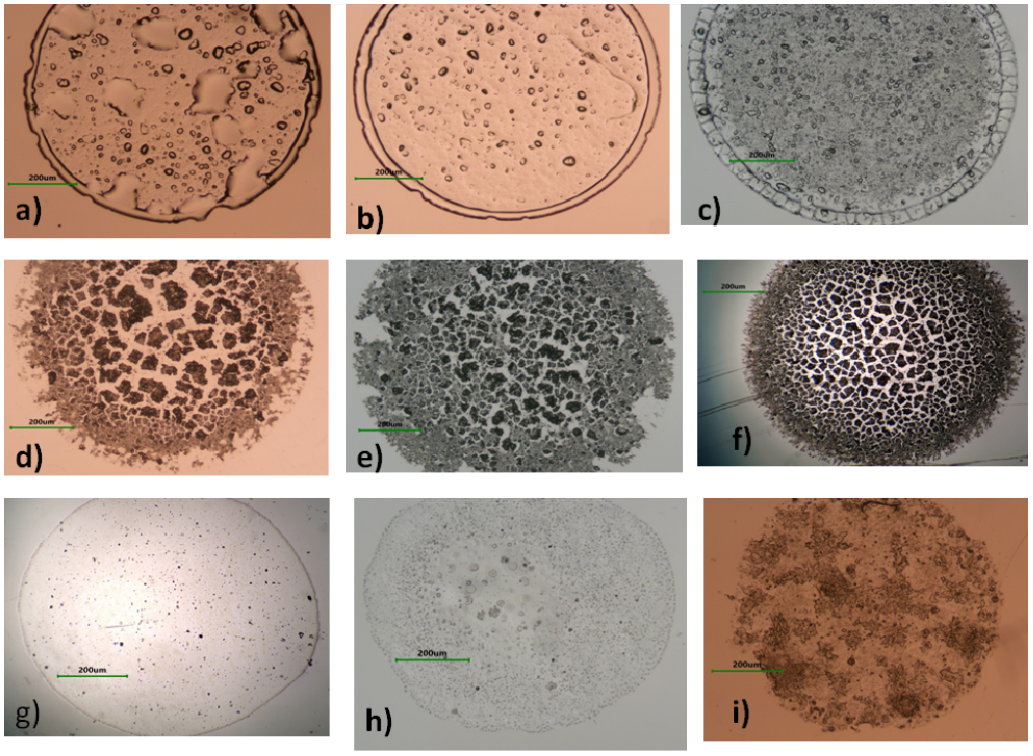

Figure 3.3: Final pattern of the dried droplet of aqueous Laponite droplet on PMMA substrate of different pHs a)0.95 b)1.18 c)1.88 d)5.6 e)6.5 f)7 g)9 h)12 i)12.3. The scale bars are of 200μm

bottom of the bottle for the sample of acidic range. This is the indication of the disintegration of Laponite in an acidic medium and leaching of Mg^{2+} and the white sediments are most probably $MgCl_2$. Cumins showed that for low concentration of aqueous Laponite solution, ∼1% concentration after some hours of preparation of the solution aging effect starts manifestation [36]. Since all the experiments were done just immediately after the preparation of solutions, we can consider the ageing effect to be very weak in the experiments as all the experiments in the drying droplet were completed within one hour. If there is some ageing effect, we can consider that it is uniform for all experiments, and evaporation dynamics or the final pattern of the dried droplet is the manifestation of the variation of pH of the solution. Aqueous Laponite suspension of low concentration initially behaves like a Newtonian fluid. Due to its very low concentration, its viscosity value is close to that of water [20]. Due to mass loss during evaporation in the surroundings, the quantity of solvent

decreases and the resulting viscosity increases gradually. All the experiments were done with constant concentration and under identical atmospheres with the same temperature and humidity, the rate of increase in viscosity during the drying of the droplet may be considered as constant. Change in viscosity may be developed due to variation of pH which can perturb the flow patterns during drying.

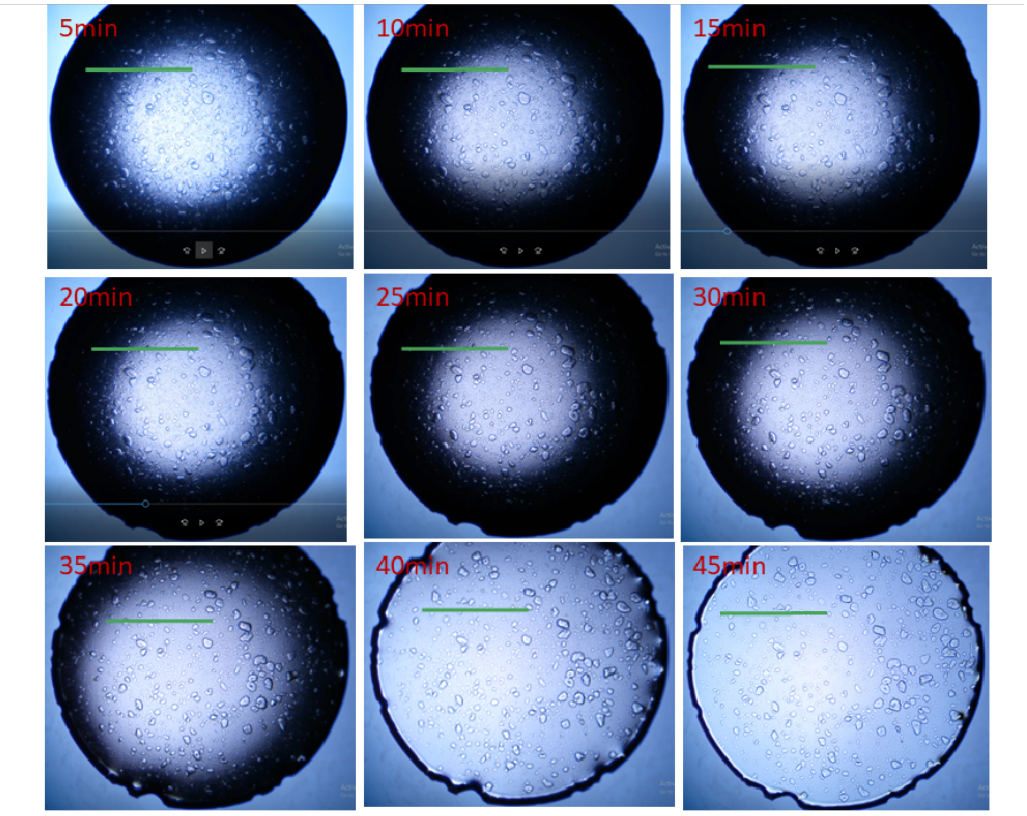

Figure 3.4: Time development of drying droplet of aqueous Laponite with pH value 0.95 on PMMA substrate. The scale bar mentioned in the figures is 200μm

3.5.1 Pattern formation on PMMA: Hydrophobic substrate

The dried deposition patterns of aqueous Laponite droplets with varying pH from acidic to basic on PMMA substrate are displayed in Fig.3.3. All the experiments were done for constant concentration and to keep all the parameters fixed. So, deposition in final patterns is ascribed to the variation in the pH of the solution.

The deposition pattern in the pH range 0.95 to 1.88 is a thin uniform layer with a thick ring at the droplet TPCL bounded by consecutive rings as shown in Fig.3.3(a-c). The thickness of the layer increases with an increase in pH. The zeta potential of the PMMA substrate is positive in the pH range below 4 and increasingly negative with higher pH [33]. PMMA substrate in the pH range < 4 shows particle-particle (PP) repulsion whereas particle substrate (PS) attraction force. Thus, the particles, which are close to the substrate are attracted to the substrate to form a uniform deposition. DLVO force is a short-range force of the order of Debye length, which is much less as compared to the droplet height, most of the particles are suspended to the droplet interface without being attracted to the substrate. The suspended particles are carried to the droplet interface by the fluid flow. Consecutive rings at the TPCL are seen which are the result of the convective flow inside the droplet. PMMA being a hydrophobic substrate, the height of the droplet is high and the contact area of the droplet is lower than the hydrophilic substrate for a droplet of the same volume. Evaporation flux is stronger at the droplet apex than at the droplet TPCL. The weak radial convective flow carried fewer particles to the droplet TPCL to form a thin ring at the droplet boundary. The consecutive ring at the droplet boundary is the result of the stick-slip motion of the droplet [30], [37]. For the stick motion, the droplet the TPCL is pinned at the initial stage and evaporates with CCR mode where the contact angle decreases keeping the contact area constant. As the evaporation proceeds, the contact angle decreases up to a limiting value such that $\sigma_{lv} cos\theta$ can exceed the value of σ_{sv} in the Neumann relation Fig.3.1d, the TPCL slips to a new position. For the slip process, the contact angle remains constant as indicated in the graph shown in Fig.3.1e in the time interval between 22-28 minutes on PMMA substrate in the very acidic pH range. Due to the high contact angle, evaporation is slower, and the rate of decrease in contact angle is slow and the depinning of the droplet takes a longer time. As a result, a consecutive ring is seen. During the drying of the droplet, the viscosity of the droplet increases which prohibits further movement of the particles. The strength of the PS interaction decreases near the IEP and particles are easily carried to the TPCL resulting in a

thick border at the boundary which cracks. Fig.3.3c shows a periodic crack between the consecutive ring having a wavelength of $47\mu m$.

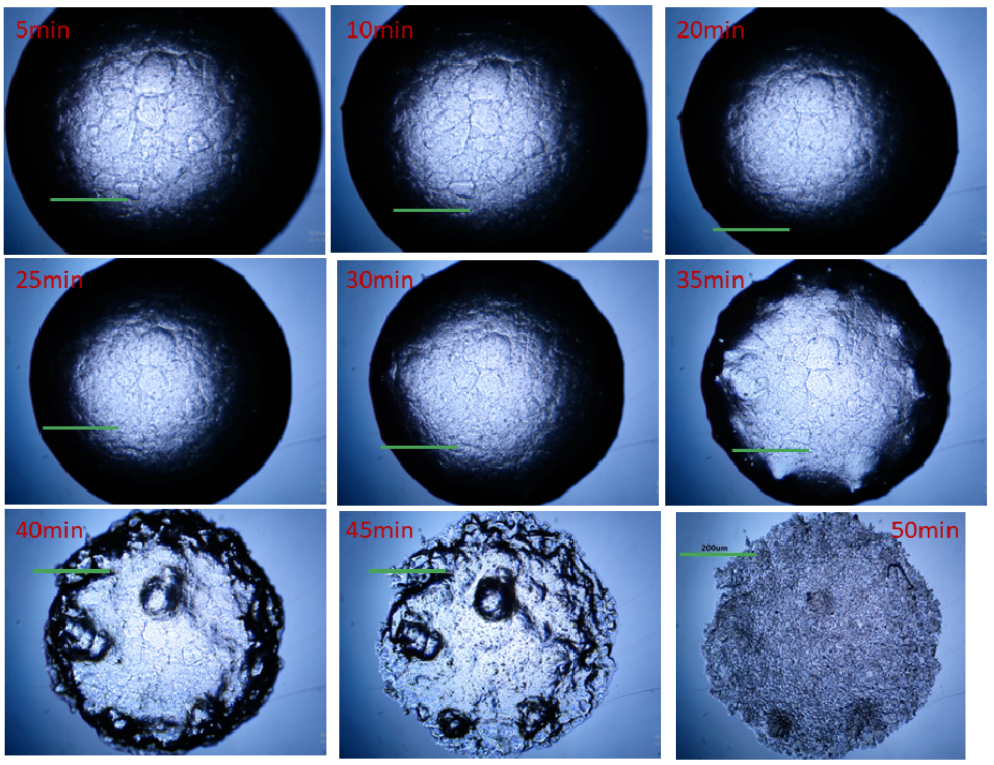

Figure 3.5: Time development of drying droplet of aqueous Laponite with pH value 12.3 on PMMA substrate. The scale bar mentioned in the figures is $200\mu m$

Fig. 3.3(d-f) shows a similar pattern left by the aqueous Laponite droplet with a pH range from 5.6-7. A close examination of the drying video of the droplet in this pH range shows the particles at the interface move towards the peripheral edge slowly and a slow swirling motion of the particles near the droplet edge is noticed. Normally a radial convective flow towards the contact line is developed during evaporation. With the high value of contact angle on the PMMA substrate, a thermal gradient is developed throughout the droplet interface. As a result, thermal Marangoni flow [38] moves the particles from the contact line to the droplet apex which interacts with the radial convective flow resulting in a slow swirling motion of the particle near the droplet contact line. The clear concentric ring at the boundary of the droplet is not developed here but the original trace of the sparse particles deposited at the ring is evident. The central portion of the droplet consists of small aggregates. In

this pH range PS interaction is negative and particles are not attracted much to the substrate and suspended particles are gathered at the droplet interface where they form a thick skin layer. At pH 5.6, the disintegration of Laponite particles forms SiO_2 which are very light and easily accumulated to the interface. This accumulation of the particles turns the interface thick and finally cracks. At neutral pH 7 disintegration of Laponite is much less, accumulation of the particles at the interface is less and a thin layer is formed and hence cracks numerous with small ped [39].

At pH 7 the droplet is deposited uniformly. At pH> 11.5, different pictures are noticed. At this pH range, the Laponite particles acquire negative charges at their edge as well as their face surface. Particle-particle and particle substrate interactions are repulsive in nature and the droplet slips and shrinks uniformly during drying. The droplet of pH 12 shows the crystallization inside the droplet instead of repulsive interactions Fig.3.7c. Most probably the recrystallization of NaOH occurs which is suspended inside the droplet. Due to this crystallization the flow dynamics were modified which is the reason for this pattern.

The drying droplet of the aqueous Laponite suspension is photographed from the top by a camera fitted with an inverted microscope. Time development of the drying droplet on PMMA substrate for highly acidic and highly basic pH, 0.95 and 12.3 are shown in Fig.3.4 and Fig.3.5 respectively. A common feature is seen in both cases. Initially, there appears a circular lighter patch at the center of the droplet surrounded by a dark broad ring. At later times of the evaporation the lighter circular patch increases with time. PMMA is a hydrophobic substrate, the droplet has more curvature initially. It is not possible to focus the entire droplet sharply at a time with a camera because of its height and curvature, thus the lighter patch corresponds to the focused area. As the drying proceeds, the droplet flattens due to decreasing its height with constant contact area, the focused area increases eventually. Fig.3.4 and Fig.3.5 show some differences in the textured interface of the

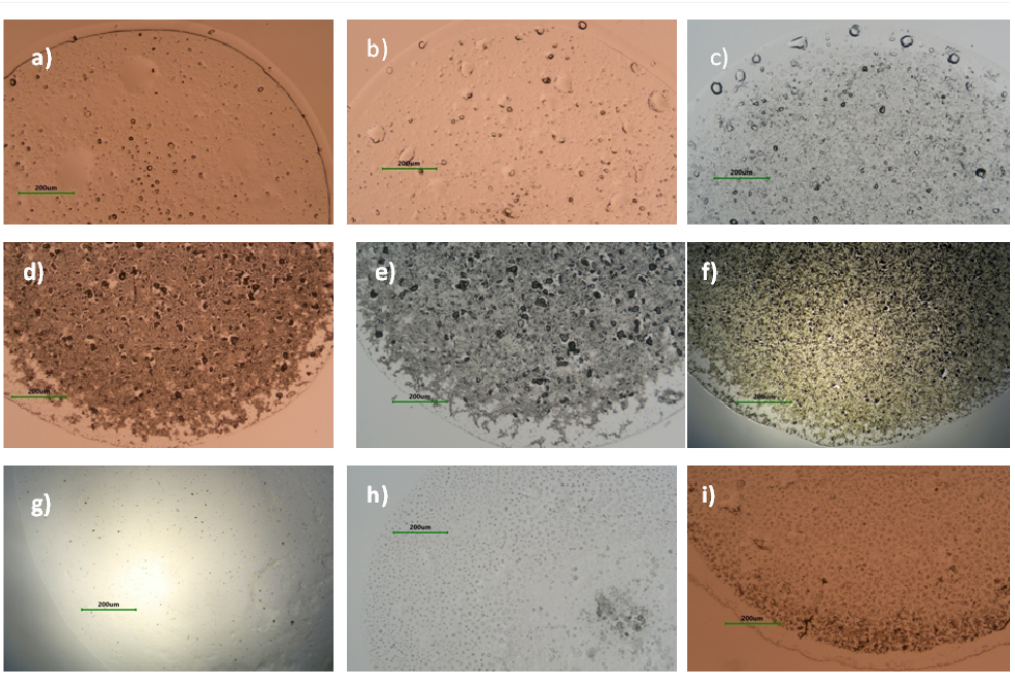

Figure 3.6: Final pattern of the dried droplet of aqueous Laponite droplet on the glass substrate of different pH values a)0.95 b)1.18 c)1.88 d)5.6 e)6.5 f)7 g)9 h)12 i)12.3. The scale bars are of 200μm

droplet which is only due to the difference in pH of the suspension. The zeta potential of the PMMA substrate is positive in a very acidic suspension. The Laponite particle in this solution is negatively charged, particle-particle interaction is negative and particle-substrate interaction is positive. More in this acidic pH leaching of the SiO_2 particles is responsible for the small crystallites which are visible on the droplet interface. In very basic pH 12.3, large aggregates are gathered in the droplet interior. As evaporation proceeds, rough crusty with salt crystals are developed gradually. The negative zeta potential of PMMA repels the negatively charged Laponite particles in the direction of the interface of the droplet. Recrystallization of NaOH occurs which helps to form the crusty surface at this high pH.

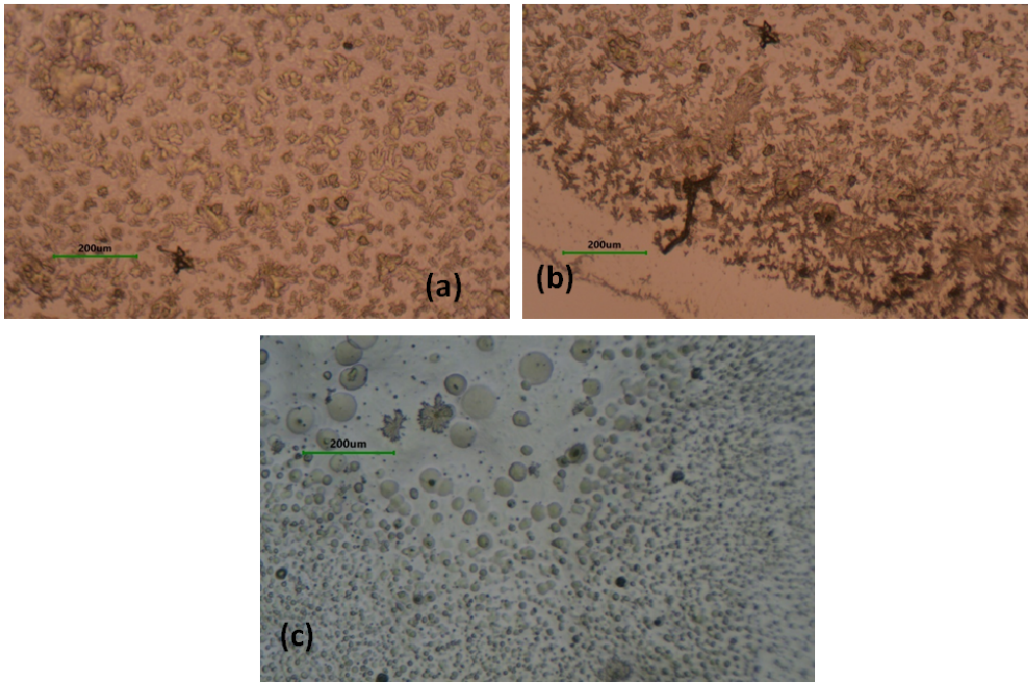

Figure 3.7: Deposition of crystal in a dried droplet of aqueous Laponite on glass substrate at pH=12.3 a) center of the droplet b) pattern near the contact line. c) crystalline deposit at pH 12.3 on PMMA substrate. The scale bars are of 200μm

3.5.2 Pattern formation on Glass and Quartz: Hydrophilic substrate

Glass and Quartz both are hydrophilic substrates because of their acute contact angle. The droplet with the same volume spreads more on these substrates than it spreads on the PMMA substrate. Droplet evaporation occurs on glass and quartz substrate in CCR mode, the contact angle decreases further during evaporation. Small changes in contact angle cannot be measured by ImageJ software of a droplet image. The main focus is to analyze the pattern formation of the droplet from the perspective of the hydrophobic and hydrophilic characteristics of the substrate. The unpredictability of contact angle variation will not influence the study of the pattern greatly.

The dried deposition patterns of aqueous Laponite droplets with varying pH from acidic to basic on glass substrate are shown in Fig.3.6. Glass substrate being hydrophilic, it has a lower curvature. The uneven evaporation flux, maximum at the TPCL and gradually decreases to the droplet apex, develops a strong convective flow towards the contact line. The zeta potential of the glass substrate is negative above pH 3 and decreases more with an increase in suspension pH. DLVO force between the substrate and particles is repulsive which makes it easier to transport the particles to the periphery. In the acidic range, Laponite particles disintegrate to release Mg^{2+} and Li^{+} ions with SiO_2 according to eqn.3.1 because of a surplus of H^{+} ions. The released SiO_2 particles being very light transported to the contact line by radial convective flow easily to form a ring at the periphery. The time taken to evaporate from the glass substrate is much less than in PMMA substrate because of contact angle is very low as well as the lower droplet height of the glass substrate. Hence evaporation is very fast and decreases the flux gradient quickly and does not get sufficient time to carry the particles to the contact line resulting in a thin ring at the TPCL.

The dried patterns of the droplets between pH values 5-7 on the PMMA substrate show the shrinkage of the deposition where the contact line is shifted inward. The comparison of the dried patterns with the pattern of PMMA substrate shows that no crack ped interior to the droplet is seen in the same pH regime. The differences in patterns are ascribed to the particle-substrate interaction of the two substrates which in turn perturb the DLVO forces in the droplet. In this pH range, the particle substrate interaction is repulsive. Hence most of the particles are suspended to the interface of the droplet and deposited on the substrate at the end of the evaporation.

The same picture is noticed as seen in the case of PMMA at pH=9, where uniform deposition is formed. When the pH of the solution exceeds 10, practically there is no disintegration of Laponite. The droplet above this pH dried with a fixed contact line. The original trace of the droplet is left as a thin circular line of tiny particles. Just like PMMA substrate, when the concentration of Na^{+} ion reaches a condition of

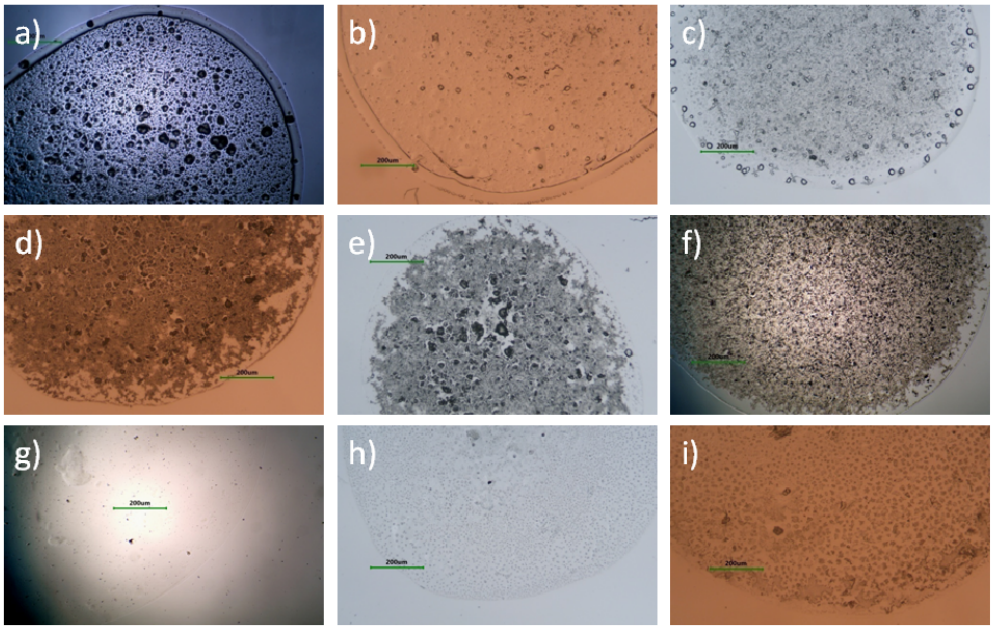

Figure 3.8: Final pattern of the dried droplet of aqueous Laponite droplet on a quartz substrate of different pH values a)0.95 b)1.18 c)1.88 d)5.6 e)6.5 f)7 g)9 h)12 i)12.3. The scale bars are of 200μm

saturation, recrystallization of NaOH crystal starts. The crystals are suspended at the droplet interface with increasing concentration there. The convective flow fails to carry the particles to the contact line. The increased concentration develops a solutal Marangoni flow which flows from the TPCL to the droplet apex. The crystals are finally deposited to the substrate at the end of drying. The dried deposition patterns of aqueous Laponite droplets with varying pH from acidic to basic on quartz substrate are shown in Fig.3.8. The quartz substrate shows the same picture as a glass substrate. The difference in contact angle is very low between glass and quartz substrates. The behaviour of Zeta potential for quartz substrate follows the same picture as a glass substrate. The difference pattern is seen for the pH value >10, where recrystallization of salt is not pronounced as in the case of glass. Hence the solutal Marangoni flow is not strong as glass and the border at the TPCL is not observed in the glass.

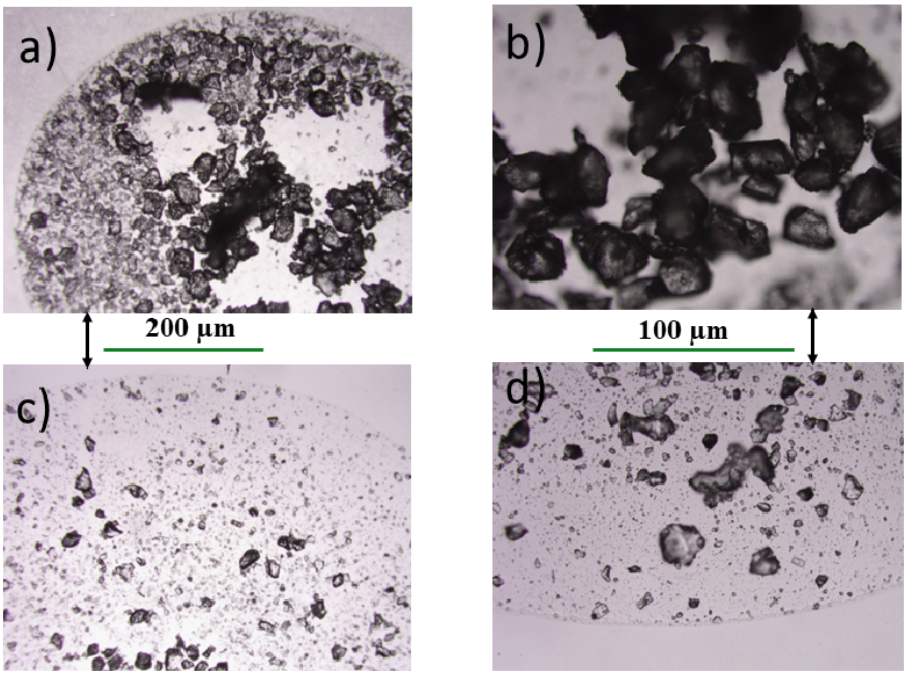

Figure 3.9: Pattern of aqueous Laponite droplet at pH 1.88 in different magnifications on different substrates. a) and b) pattern on PMMA substrate. c) and d) pattern formation on a glass substrate.

3.6 Cavity formation in acidic pH on PMMA substrate

Aqueous Laponite droplet shows very interesting features on PMMA, a hydrophobic substrate in very acidic pH under magnification. A close look in Fig.3.3a shows small aggregates of particles which are blotch of bubble-like structure in addition to uniform deposition. To examine carefully the patterns, the magnified images of the aqueous Laponite solution in an acidic medium (pH 1.88) on both hydrophobic PMMA substrate and hydrophilic glass substrate are shown in Fig.3.9. When the droplet dried on a hydrophilic glass substrate in the same pH value, no such cavitation is seen under high magnification Fig.3.9(c and d). Whereas the dried droplet on PMMA substrate at the same pH shows clear circular patches surrounded by crystals

of salt aggregation which is indicative of the cavitation formed during evaporation. For both substrates, pH was maintained constant, and kept all other parameters same. So, the different features observed in a particular substrate are attributed to the difference in DLVO forces plays in both cases. Cavitation can be formed in many colloidal solutions and in gel [40], [41]. The cavity is formed due to the gradient of osmotic pressure amongst the pores and enclosing shell or liquid droplet. Gels are normally porous samples for example Laponite gel. Sometimes bubbles are formed inside the gel and trapped inside the gel walls. A cavity may be developed inside the gel if the evaporation from bubbles is faster than the diffusion of solute particles from the bubble interface. In many cases, the cavity collapses due to a huge pressure difference between the interior and outside of the cavity. If the solution of salt is present inside the cavity, then evaporation from the cavity becomes very slow through the shell which in turns lead to saturation of that solution inside the cavity, hence salt crystals form to the inner wall of the cavity. Fig.3.9(a and b) show the salt crystals arranged themselves in circular form around empty spaces. At this pH, PS interaction is attractive in PMMA, the particles are attracted towards the substrate. During drying, a gel network is formed in the Laponite solution and it forms cavities by trapping the salts of the solution. Cavities collapse inside the gel at the end of the evaporation.

3.7 Conclusion

The dried residues of the aqueous Laponite droplet show interesting patterns with the variation of pH on different substrates with different hydrophobicities. We suggest an analysis to explain the patterns taking into consideration the aspect ratio of the Laponite particles, pH-dependent charge distribution on the face and edge of the particle, dissolution properties of the Laponite in the acidic medium, etc. The particle-particle and particle-substrate interaction forces change their nature with the pH of the suspension because of zeta potential of the substrate changes across

the Iso Electric Point. The competition amongst the different forces like, convective force, DLVO force, Marangoni forces, etc. which act during evaporation determines the final patterns of the droplet. The drying droplet of aqueous Laponite particles changes their pattern from a coffee ring at the border with multiple crack fractal deposition to a uniform deposition, to aggregation of salt crystals at the interface. PMMA being a hydrophobic substrate, the slower evaporation allowed for depositing a thick layer with periodic cracks at the periphery in an acidic range of pH. On hydrophilic glass and quartz substrates, the deposition at the contact line was not prominent as PMMA because of quicker evaporation of the droplet. Recrystallization of salt is more dendritic on the hydrophilic substrate than hydrophobic substrate in the regime of high pH. Collapsed cavitation pattern is noticed for acidic pH on PMMA substrate which is absent for glass or quartz substrate in the same condition. The collapsed cavities are bordered by a ring of salt crystals. These salt crystals are formed in the inner wall of the cavity due to the slow evaporation of the solution. The shell which slower the evaporation is formed due to the PS attraction force for the PMMA substrate.

Bibliography

[1] D. Zang, S. Tarafdar, Y. Y. Tarasevich, M. D. Choudhury and T. Dutta, *"Evaporation of a droplet: From physics to applications"*, *Physics Reports* **804** 1--56 (2019).

[2] D. Brutin and V. Starov, *"Recent advances in droplet wetting and evaporation"*, *Chemical Society Reviews* **47** 558--585 (2018).

[3] K. Sefiane, *"Patterns from drying drops"*, *Advances in colloid and interface science* **206** 372--381 (2014).

[4] S. Tarafdar, Y. Y. Tarasevich, M. Dutta Choudhury, T. Dutta and D. Zang, *"Droplet drying patterns on solid substrates: from hydrophilic to*

superhydrophobic contact to levitating drops", *Advances in Condensed Matter Physics* **2018** 1--24 (2018).

[5] R. D. Deegan, O. Bakajin, T. F. Dupont, G. Huber, S. R. Nagel and T. A. Witten, *"Capillary flow as the cause of ring stains from dried liquid drops"*, *Nature* **389** 827--829 (1997).

[6] R. D. Deegan, *"Pattern formation in drying drops"*, *Physical review E* **61** 475 (2000).

[7] R. Bhardwaj, X. Fang, P. Somasundaran and D. Attinger, *"Self-assembly of colloidal particles from evaporating droplets: role of dlvo interactions and proposition of a phase diagram"*, *Langmuir* **26** 7833--7842 (2010).

[8] V. R. Dugyala and M. G. Basavaraj, *"Control over coffee-ring formation in evaporating liquid drops containing ellipsoids"*, *Langmuir* **30** 8680--8686 (2014).

[9] S. Sircar, M. D. Choudhury, S. Karmakar, S. Tarafdar and T. Dutta, *"Crack patterns in drying laponite–nacl suspension: role of the substrate and a static electric field"*, *Langmuir* **34** 6502--6510 (2018).

[10] F. Sciortino and P. Tartaglia, *"Glassy colloidal systems"*, *Advances in Physics* **54** 471--524 (2005).

[11] E. Zaccarelli, *"Colloidal gels: Equilibrium and non-equilibrium routes"*, *Journal of Physics: Condensed Matter* **19** 323101 (2007).

[12] D. W. Thompson and J. T. Butterworth, *"The nature of laponite and its aqueous dispersions"*, *Journal of Colloid and Interface Science* **151** 236--243 (1992).

[13] A. Mourchid, A. Delville, J. Lambard, E. Lecolier and P. Levitz, *"Phase diagram of colloidal dispersions of anisotropic charged particles: equilibrium*

properties, structure, and rheology of laponite suspensions", *Langmuir* **11** 1942--1950 (1995).

[14] S. Jatav and Y. M. Joshi, *"Phase behavior of aqueous suspension of laponite: New insights with microscopic evidence"*, *Langmuir* **33** 2370--2377 (2017).

[15] D. Bonn, H. Kellay, H. Tanaka, G. Wegdam and J. Meunier, *"Laponite: What is the difference between a gel and a glass?"*, *Langmuir* **15** 7534--7536 (1999).

[16] T. Nicolai and S. Cocard, *"Light scattering study of the dispersion of laponite"*, *Langmuir* **16** 8189--8193 (2000).

[17] M. Kroon, W. L. Vos and G. H. Wegdam, *"Structure and formation of a gel of colloidal disks"*, *Physical Review E* **57** 1962 (1998).

[18] B. Ruzicka and E. Zaccarelli, *"A fresh look at the laponite phase diagram"*, *Soft Matter* **7** 1268--1286 (2011).

[19] P. Mongondry, J. F. Tassin and T. Nicolai, *"Revised state diagram of laponite dispersions"*, *Journal of Colloid and Interface Science* **283** 397--405 (2005).

[20] S. Jabbari-Farouji, H. Tanaka, G. Wegdam and D. Bonn, *"Multiple nonergodic disordered states in laponite suspensions: A phase diagram"*, *Physical Review E* **78** 061405 (2008).

[21] A. Shahin and Y. M. Joshi, *"Physicochemical effects in aging aqueous laponite suspensions"*, *Langmuir* **28** 15674--15686 (2012).

[22] S. Jabbari-Farouji, G. H. Wegdam and D. Bonn, *"Gels and glasses in a single system: Evidence for an intricate free-energy landscape of glassy materials"*, *Physical review letters* **99** 065701 (2007).

[23] W. Stumm et al., *Chemistry of the solid-water interface: processes at the mineral-water and particle-water interface in natural systems.* John Wiley & Son Inc., 1992.

[24] S. L. Tawari, D. L. Koch and C. Cohen, *"Electrical double-layer effects on the brownian diffusivity and aggregation rate of laponite clay particles"*, *Journal of Colloid and Interface Science* **240** 54--66 (2001).

[25] E. Tombacz and M. Szekeres, *"Colloidal behavior of aqueous montmorillonite suspensions: the specific role of ph in the presence of indifferent electrolytes"*, *Applied clay science* **27** 75--94 (2004).

[26] A. Mourchid and P. Levitz, *"Long-term gelation of laponite aqueous dispersions"*, *Physical Review E* **57** R4887 (1998).

[27] A. Mourchid, E. Lecolier, H. Van Damme and P. Levitz, *"On viscoelastic, birefringent, and swelling properties of laponite clay suspensions: Revisited phase diagram"*, *Langmuir* **14** 4718--4723 (1998).

[28] R. P. Mohanty and Y. M. Joshi, *"Chemical stability phase diagram of aqueous laponite dispersions"*, *Applied Clay Science* **119** 243--248 (2016).

[29] A. Khatun, S. Haque, S. Tarafdar and T. Dutta, *"Impact of varying preparation methods of colloidal suspensions on droplet desiccation patterns on hydrophobic and hydrophilic substrates"*, *Physica Scripta* **96** 025211 (2020).

[30] M. Kobayashi, H. Nanaumi and Y. Muto, *"Initial deposition rate of latex particles in the packed bed of zirconia beads"*, *Colloids and Surfaces A: Physicochemical and Engineering Aspects* **347** 2--7 (2009).

[31] C. Tien, *"Granular filtration of aerosols and hydrosols, vol. 1"*, 1989.

[32] P. C. Hiemenz and R. Rajagopalan, *Principles of Colloid and Surface Chemistry, revised and expanded.* CRC press, 2016.

[33] A. M. Gallardo-Moreno, V. Vadillo-Rodríguez, J. Perera-Nunez, J. M. Bruque and M. L. González-Martín, *"The zeta potential of extended dielectrics and conductors in terms of streaming potential and streaming current measurements"*, *Physical Chemistry Chemical Physics* **14** 9758--9767 (2012).

[34] P.-I. Au, S. Hassan, J. Liu and Y.-K. Leong, *"Behaviour of laponite gels: rheology, ageing, ph effect and phase state in the presence of dispersant"*, *Chemical engineering research and design* **101** 65--73 (2015).

[35] L. Priya and J. Jog, *"Journal of polymer science: part b: polymer physics"*, *Wiley Periodicals Inc* **40** 1682 (2002).

[36] H. Z. Cummins, *"Liquid, glass, gel: The phases of colloidal laponite"*, *Journal of Non-Crystalline Solids* **353** 3891--3905 (2007).

[37] M. Liu and X.-P. Chen, *"Numerical study on the stick-slip motion of contact line moving on heterogeneous surfaces"*, *Physics of Fluids* **29**, (2017).

[38] Z. Pan, S. Dash, J. A. Weibel and S. V. Garimella, *"Assessment of water droplet evaporation mechanisms on hydrophobic and superhydrophobic substrates"*, *Langmuir* **29** 15831--15841 (2013).

[39] A. Groisman and E. Kaplan, *"An experimental study of cracking induced by desiccation"*, *Europhysics Letters* **25** 415 (1994).

[40] F. Meng, M. Doi and Z. Ouyang, *"Cavitation in drying droplets of soft matter solutions"*, *Physical review letters* **113** 098301 (2014).

[41] P. T. A. Nguyen, M. Vandamme and A. Kovalenko, *"Collapse and cavitation during the drying of water-saturated pdms sponges with closed porosity"*, *Soft Matter* **16** 9693--9704 (2020).

Chapter 4

Role of pH and concentration on desiccation crack of aqueous Laponite suspension

4.1 Introduction

Interface cracking in the film of colloidal materials that develop upon desiccation is an area of surface science that has been an active and interesting research topic among scientists and engineers [1],[2],[3], [4], [5]. The importance of the study of desiccation cracks and fracture growth is widely accepted because of its wonderful application. It has been realized that we can produce different types of special textures on surfaces or cracks that can be controlled and tailored for useful nanofabrication. Crack patterns formed in drying in clay slurries have been studied in different drying conditions with different clays. Several external factors, such as solvent and solute [6], temperature [7], substrate [8], drying rate [9], layer thickness [10], and effects of the external field like mechanical [11], [12], electrical [13], etc. affect the desiccation crack formation. We have used Laponite clay for studying the desiccation crack formation. Laponite gets ionized in an aqueous medium. In this chapter,

we will discuss the much less studied factor: the role of pH on the desiccation of Laponite suspension. The details of the Laponite particle and its characteristics in pH medium have been discussed in Chapter 1 and Chapter 3.

The role of pH in the desiccation crack pattern in films of aqueous Laponite has been investigated experimentally. The pH of the colloidal solution varied between 0.445 - 13.45. The crack pattern changed from fractal to a hierarchical tree-like pattern as the solution pH changed from highly acidic to basic values. Cracks appear to be suppressed around the pH corresponding to zero charges of the Laponite particle in the solution. The changes in the crack pattern are analyzed for particle shape, changes in surface charge distribution, and aggregation geometry. As colloidal particle concentration in a solution determines the solution's net ionic strength, particle concentration's role in affecting desiccation crack patterns is also investigated for a fixed pH. For a particular combination of pH and particle concentration, the lace-like crystallization patterns were observed after the complete drying of the film.

4.2 Review of earlier related work

Several works on the desiccation of films of colloids or synthetic clay were done. Synthetic clays are used because of their known structure and characteristics in different conditions. One of the famous synthetic clays is Laponite. We are concerned about synthetic clay, specially Laponite clay, and its properties regarding desiccation cracks. Desiccation cracks happen due to drying the sample on a surface. The film cracks and may or may not be peeled off from the substrate. During the drying of a film, there is a competition between cracking and peeling off the film. A simulation study has shown that the competition is affected by the factor 'rate of drying' and 'roughness of the substrate' which affect the desiccation crack as well as the peeling off the substrate [14]. A study of crack patterns in Laponite gel has been done. The self-similarity of the patterns was studied regarding the crack width [15].

The desiccation of Laponite film for different thicknesses was studied. Depending on the thickness, the rate of drying and shrinkage of the film changes. In this case, also the self-similarity has been analyzed concerning crack width [16]. Patterns of desiccating films can be changed in character in a drastic manner by adding polymer with Laponite. The composition of Laponite and polymer changes the pattern from a fragmented network to a uniform film with no crack. The simulation study justified the patterns [17]. Several studies have been done on the desiccation crack pattern of Laponite clay in electric fields. Prof. Tarafdar and his group studied the desiccation crack pattern of Laponite clay. In an aqueous medium, Laponite clay is charged with a positively charged edge surface and a negatively charged face surface. hence, it has a quadrupole moment which interacts with a nonuniform electric field. They saw the crack starts from the positive electrode. The nonuniformity of the electric field was along radially [18], [13]. The effect of the AC field on the desiccation of the gel state of the Laponite particle was studied. The strength of the electric fields affects the characteristics of the crack patterns. With increasing the field strength, the bending of the crack increases with the curvature [19]. The effect of the electric field was studied for the Laponite droplet which gives interesting and highly reproducible results. Cracks appear after some dissipation of energy when a continuous DC field is applied. They find some empirical relations which show that Laponite clay has a memory of the field. The field strength reduces the microcracks inside the macro cracks [20]. The memory effect of the electric field was studied for Laponite particles. The electric field affects the crack pattern even after the field is removed after some time. Hence it carries a memory. The time of first crack appearance depends on the field strength and the time of exposure. This property is explained through a model using fractional derivatives [21]. The effect of nonuniform DC and AC fields on Laponite clay was studied by several groups. For both cases, the simulation was done using a randomized spring network model to explain the crack patterns observed under an electric field [22]. Crack always start from the strong end of the field. If the field strength and frequency are varied, the cracks tend to curve in the direction normal to the external field. [23]. The effect of crack

patterns of aqueous Laponite suspension is affected by NaCl salt. The crack pattern of aqueous Laponite-NaCl composition is studied on different substrates. The crack patterns induced by NaCl depend on the nature of the substrate. Another important observation was the crack pattern of this system under an electric field. NaCl has an important role in crack inhibition of aqueous Laponite in the presence of an electric field. This property can be used to suppress undesired cracks [24].

Aqueous laponite gel shows interesting tree-like crack patterns under a uniform DC field in a rectangular slab. Cracks emerge from the positive terminals and end to the negative electrode. The nature of the branched cracks looks like a hierarchical tree pattern [25]. Near the positive electrode, there are numerous peds with sizes varying from smaller to larger. The size of the peds increases gradually towards the negative electrode. A power law is obtained from the plot of the cumulative distribution of the ped's number up to a limiting area. This suggests the fractal properties of the observed pattern [26]. Magnetic-driven crack formation is seen in some magnetic colloids like, ferrofluid. Magnetic field changes the stress generated in the formation of gel and modifies the crack formation [27]. Crack pattern formation on ellipsoidal colloidal suspension is affected by the magnetic field. Orientation of the particles near the crack is aligned along the magnetic field [28]. Also the vibration can affect the crack pattern. The crack pattern in the paste can be controlled by external vibration which converts the perpendicular cracks into parallel in the direction of vibration [12]. Normally densely packed paste memorizes the external mechanical effect. Matsuo and his group found a charged paste that cannot remember the flow direction. If the charges of the paste are shielded by sodium chloride to screen the coulomb interaction, then the paste can remember the flow direction [11].

4.3 Materials and Experimental Methods

Pure Laponite and deionized water are used throughout the experimental studies. 37% HCl and NaOH beads are used to vary the pH of the suspension. Two sets of experiments were done. To vary the pH of the aqueous suspension, the required amount of HCl or NaOH beads is added to 20 ml of water and kept undisturbed for 30 minutes. 1.2 gm of Laponite powder is added to the 20 ml of water while it is on a magnetic stirrer and stirred for 30 seconds. Immediately after the preparation of the suspension, it is poured onto a polypropylene petri dish of 7.25 cm diameter and allowed to dry.

The second set of experiments is to study the desiccation pattern of aqueous Laponite with varying concentrations for a fixed pH value of $\sim$ 13.5. In order to gain this pH 0.3 gm of NaOH beads are added to 20 ml of deionized water and kept standing for 30 minutes. This water is used to prepare the suspension following the same preparation protocol and the prepared suspension was poured into a polypropylene petri dish of diameter 7.25 cm. Concentrations (w/w) of the suspension varied from 2% to 10%. The uniform films are allowed to dry in the relative humidity and temperature 30-35% and $21 - 25°C$ respectively for both sets of experiments. We have considered the concentration of water as $\frac{1000kg}{m^3}$.

Special care was taken to maintain the constancy of the initial thickness of the film. The same volume of prepared suspension was poured into the petri dish to fix the constant thickness.

The photographs of the dried films were taken by a digital camera, Canon700D for further analysis. ImagePro software was used to study the fractal nature of the dried films with crack patterns.

The conductivity of the suspensions was measured with a digital conductivity meter having platinum electrodes with an accuracy of $\pm$ 2 micro-siemens. pH of the suspension was measured with a digital pH meter having a hydrogen ion reversible

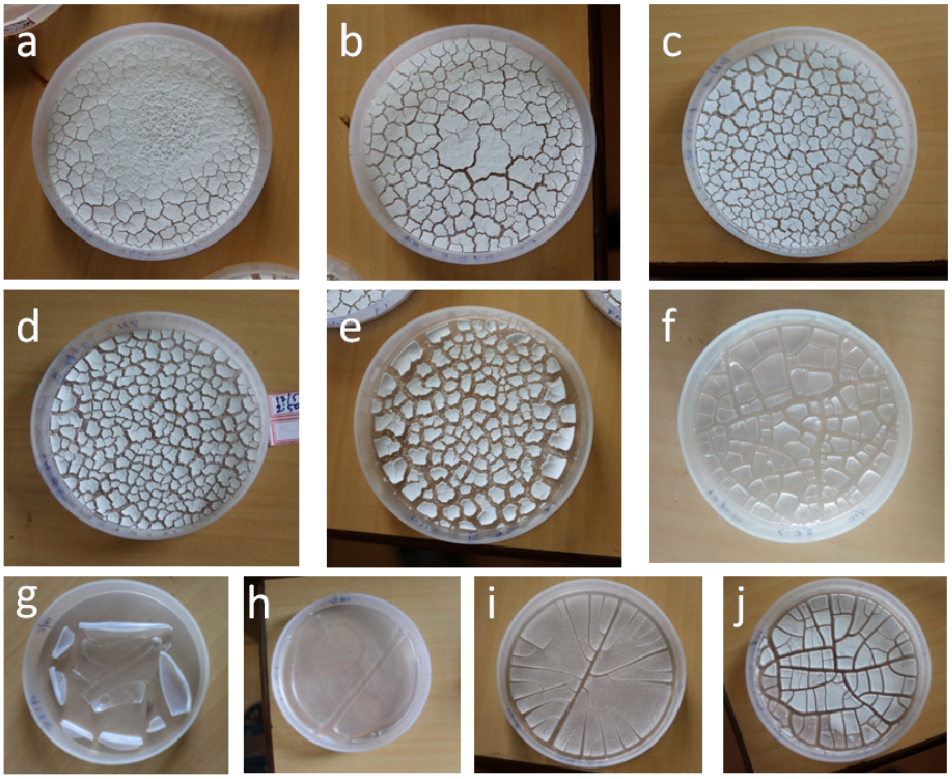

Figure 4.1: Desiccation crack patterns of aqueous Laponite suspension with varying pH. a)0.445 b)0.765 c)1.68 d)3.43 e)5.93 f)6.73 g)9.25 h)12.25 i)13.05 j)13.45

glass electrode. Both the pH meter and conductivity meter are of Systronics. SEM and EDAX were done using the dry and unpolished portion of the dried film.

4.4 Results and discussions

4.4.1 Variation of pH

The desiccation crack patterns form in an aqueous Laponite film of thickness 4.8 mm on a Polypropylene Petri dish is shown in Fig.4.1 for varying pHs ranging from very acidic to basic pH. We notice the prominent distinction of the patterns of the dried films in two different regions acidic and basic. In the acidic range, the films

show an opaque white appearance that changes to clear glassy looks at the basic pH range. Around the neutral pH 6.73, the film has translucent quality adhered to the substrate. We will discuss the two distinct regimes in two sections.

Films at the acidic pH range

At pH=0.445, the film has a white opaque appearance with a larger unbroken area surrounded by crack peds at the periphery of the petri dish. At this low pH, the maximum of the Laponite particles disintegrate because of high H^+ concentrations. When the pH increases to 0.765 the large unbroken area disappears and crack peds appear in its place which is distinctly more prominent in size. At the pH range 1.68 to 5.93, Fig.4.1(c-e), the cracks become smaller in size with numerous. At this highly acidic pH, the cracks look like wavy edges at the peds. When the pH increases, at pH=5.93, the crack peds get larger in size and the edges become linear. Also, the peds start curling up around the boundary of the petri dish. In the films near the neutral pH of $\sim$ 6.73, the peds become more prominent with a polygonal shape, Fig.4.1f. Examination of Fig.4.1, the textures of the films at the acidic pH range show uneven grainy surface textured on the peds with wavy edges. The grainy surface is most probably due to the aggregation of Laponite. At this pH range, the excess H^+ ions disintegrate the Laponite particles leading to the leaching lots of Mg^{2+} ions in the solution. The excess Mg^{2+} ions may inhibit the coagulation of the Laponite particles which increases the haziness of the suspension. Laponite particles possess a positively charged edge surface and a negatively charged face surface at the acidic medium. The Laponite particles form an attractive gel forming a house-of-cards structure with the attraction between the positive edges of one particle to the negative faces of another particle. Hence the particles form an aggregation in such a way that the cracks cannot propagate by breaking the structure and, uneven wavy edges of the peds appear, Fig.4.4a. This is responsible for the fractal edges of the crack peds. The fractal dimension of the peds increases from 1.1 to 1.6 with decreasing the acidity of the suspension.

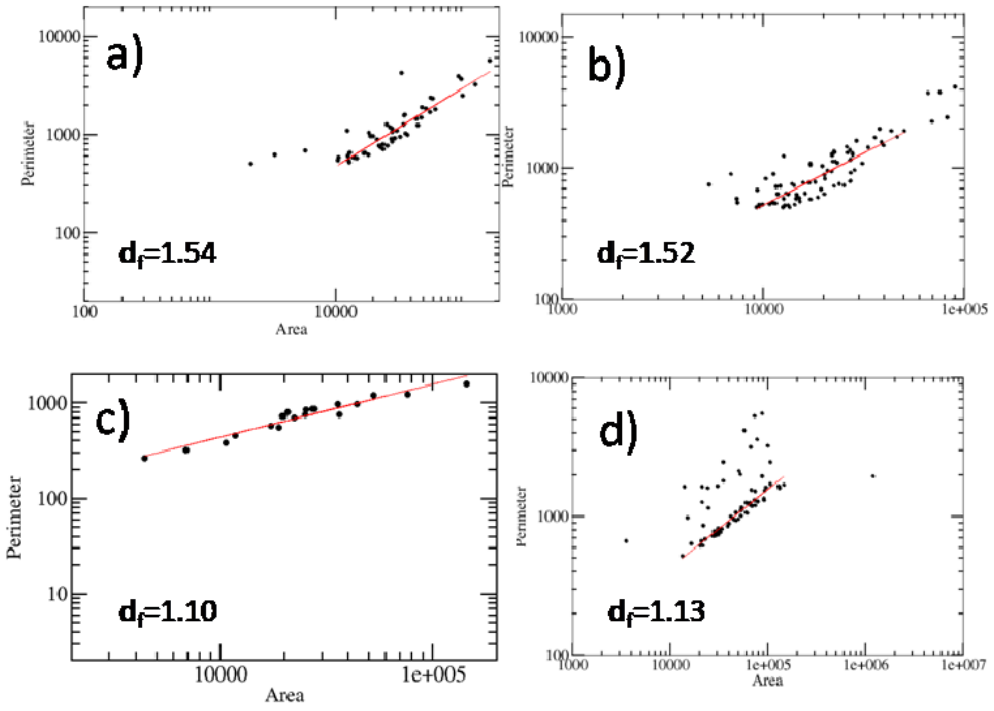

Figure 4.2: Area versus perimeter curve of the peds of the films for different pHs. a)pH=0.765 b)pH=1.68 c)pH=13.05 d)pH=13.45

Film at the basic pH range

At this pH range, the films show different patterns. At pH=9.25, Laponite particles acquire this pH in an aqueous solution of 6% concentration, which shows crack peds are fewer in number with a linear edge. Not only that, the peds are almost peeled off from the substrate, Fig.4.1g. At pH=12.25, a dramatic appearance is seen where almost total absence of crack is seen Fig.4.1h. The Iso Electric Point (IEP), the point of zero charges for Laponite particles is at pH 11.5 and the connection of the absence of a crack at this pH is notable. The point of zero charges for the broken crystal of $Mg(OH)_2$ indicates that the charges on the edges of the Laponite particles change from positive to negative in this pH range. Laponite particles behave as repulsive glass where the particles are suspended without touching each other. Now the crack lines propagate linearly to form a straight edge of the peds, Fig.4.4b. When the pH increases beyond the value of 13, the film patterns change distinctly. The peds

pH	d_f (Fractal dimension)	n (Relaxation coefficient)
0.765	1.54	- 8.111
1.68	1.52	- 8.538
13.05	1.10	- 57.00
13.45	1.13	- 43.154

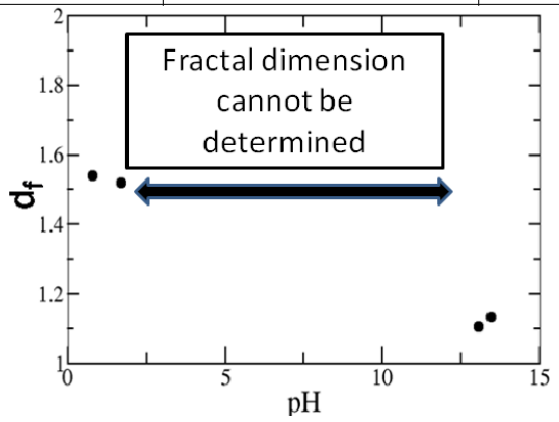

Figure 4.3: Variation of fractal dimension of the crack interface d_f with pH. Films of the pH range 3.43 to 12.25 are peeled off from the substrate. Calculation of d_f in this pH range is uncertain. The uncertain region is marked by an arrow line.

become polygonal in shape with radial hierarchical patterns with linear edges. The linear edge of the peds is noticeable at the pH=13.05, Fig.4.1i. At first cracks develop at the peripheral edge and join to the arterial one to make a Cayley Tree-like pattern and rounded in triangular form. At pH=13.45, the crack peds change to equispaced polygonal peds, Fig.4.1j, where the peds strongly adhere to the substrate. Fractal dimension can be measured for this desiccating film.

Characterization of the films

Several measurements have been done to characterize the films. The wavy nature of the edges of the peds in an acidic medium suggests the fractal nature of the textured having fractal dimensions between 1 and 2. At a high pH range, the film changes its appearance from an opaque surface to a clear glassy look. Fractal dimension has been measured with area perimeter curve as shown in Fig.4.2. In the cross-over

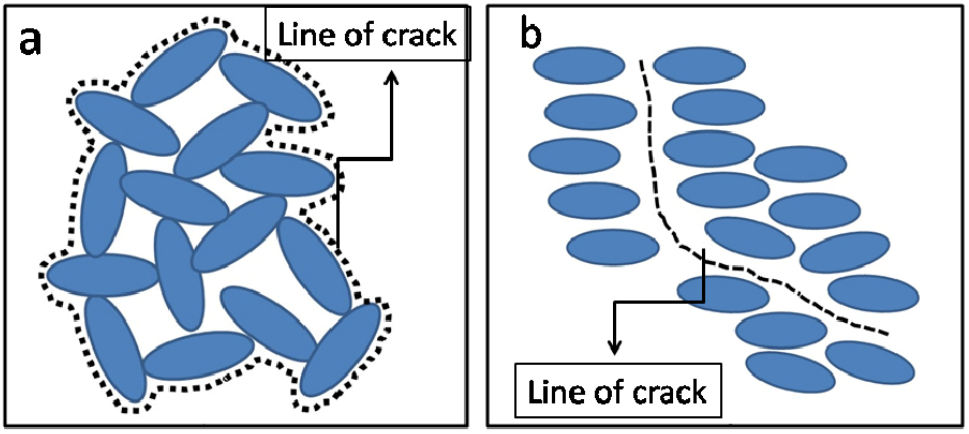

Figure 4.4: a)Schematic diagram of the crack formation of the films around a house-of cards structure at pH value < 11.5 b)Schematic diagram of the crack formation of the films around a stack-coin arrangements at pH value > 11.5

region between opaque appearance to clear hierarchical pattern, area, and perimeter measurement was not possible by ImagePro software because the peds are peeled off from the surface. The crack perimeter along the peds and the area of the peds were measured with ImagePro software. The interface fractal dimension d_f is measured from the slope of the area-perimeter plot, Fig.4.2 using the relation given by [17]

$$S = \frac{d_f}{2}$$

where S is the slope of the area perimeter curve. The variation of the fractal dimension with the pH of the suspension is shown in Fig.4.3. Muthukumar estimated the fractal dimension by analyzing the relaxation exponent [29] at the critical gel point of the gel system using the relation,

$$d_f = \frac{(2n - d)(d + 2)}{2(n - d)}$$

where n is the inverse of the relaxation time [30], [31]. Using the above relation, we have estimated the critical coefficient in Fig.4.3. d is the dimension of space, here taken as 3. Note the table given in Fig.4.3, which shows that the relaxation

exponent decreases with an increase in pH value. This suggests that the strength of elastic modulus increases compared to viscous modulus.

The time taken to crack the first time, t_f for the film is noted during experiments and plotted with the pH values, Fig.4.5b. t_f decreases with an increase in the pH value of the suspensions. For highly basic pH average time taken to crack first-time is almost constant. Fig.4.5c shows the variation of ionic conductivity with respect to the pH value of the aqueous Laponite suspension. It shows the minimum value at the pH value of 7. As the pH value decreases below 7, the leaching of Mg^{2+} and Li^{+} ions increase the ionic density. As pH increases above 7, the ionic concentration of negative charge increases which increases the conductivity. To characterize the crack pattern in the basic pH region, we have plotted the number of peds with pH, Fig.4.5a. The curve shows the minimum value at pH $\sim$ 11.5, which indicates the point of zero charge.

4.5 Effect of concentration variation on the crack pattern

The concentration of clay plays an important role in the cracking of a film. Viscosity increases with increasing solid concentration [32]. The rate of gelation of clay increases with solid concentration. An increase in solid concentration increases the ionic strength which reduces the energy barrier due to electrostatic repulsion between the faces of the Laponite particles. Fig.4.6 shows the crack patterns obtained for different concentrations varying from 2% to 10% of aqueous Laponite at pH 13.4-13.6. At this pH, the Laponite particle possesses both the face and edge negatively charged. The microstructure of the particle shows the stack coin arrangement to form the structure as repulsive glass. Examining Fig.4.6a, the film at a concentration of 2%, an opaque space is seen in the film. The microcracks are linear whereas the microcracks of the film at pH 0.445 shown in Fig.4.1a, are wavy in nature. The

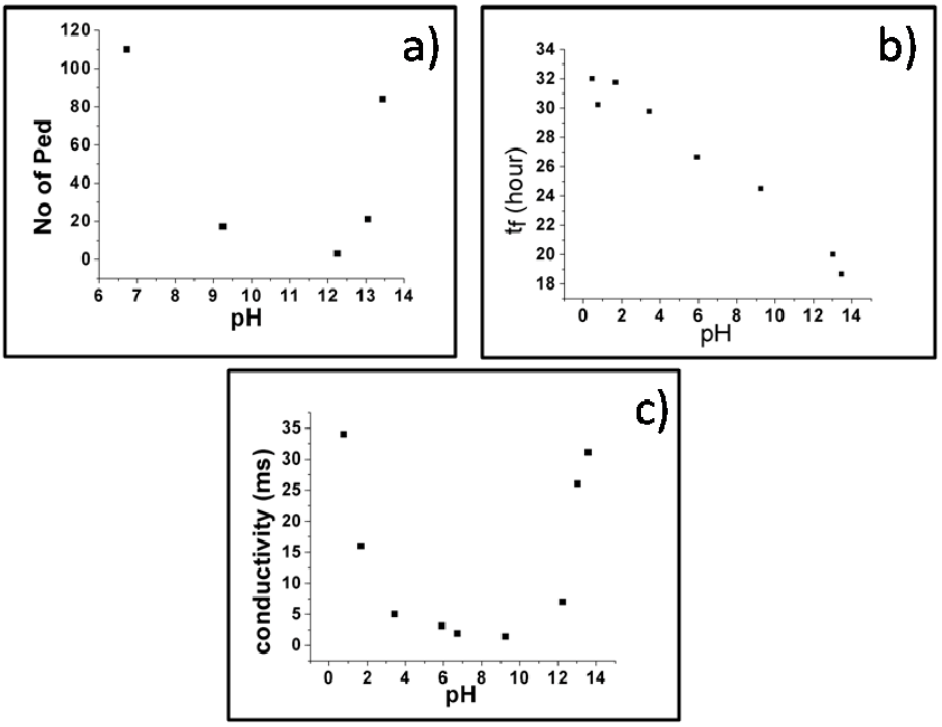

Figure 4.5: a)Variation of ped number of the films in the basic range of pH. b)Variation of time of first crack appearance of the films with pH. c)Variation of Conductivity of the suspensions with pH.

cracks are disjoint with each other and didn't form enclosed peds. This is in accordance with our expectations because of the stacked coin-like arrangements of the particles at high pH. A striation is seen on the film near the periphery of the petri dish. At a concentration of 3%, the cracks are prominent but disjoint with each other without forming an enclosed ped. The striations are seen where the films are adhered to the substrate. The central portion of the film peels off from the substrate where as the films near the periphery are adhered to it. This is the reason for the irregular crack formation in this case. At concentrations 4% and 6%, the cracks are seen like a radial hierarchical pattern where the cracks develop from the periphery towards the center. The arterial cracks join the primary cracks to form a hierarchical pattern. Maximum cracks occur at 6% concentration and the film becomes opaque. After this concentration, opacity as well as the cracks start to decrease.

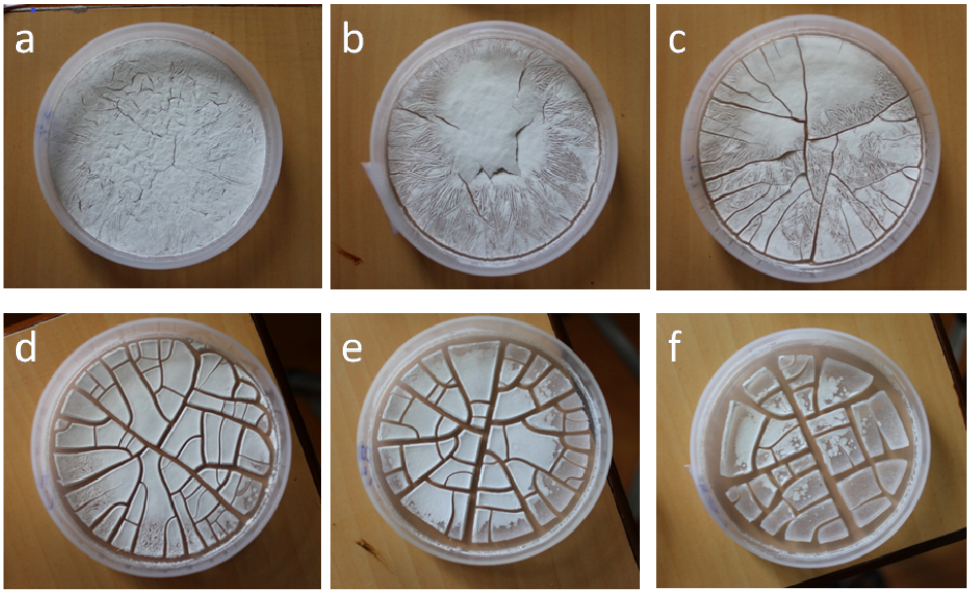

Figure 4.6: Desiccation crack pattern of aqueous Laponite suspension on Polypropylene petri dish of diameter 7.25 cm. (a)2% (b)3% (c)4% (d)6% (e)8% (f)10%.

The crack's width becomes wider and polygonal in shape. The films strongly adhere to the substrate at high concentrations.

Fig.4.7a shows the variation in the total crack length and the total number of peds that appeared after the complete drying of the film. Note that the maximum crack occurs at the concentration of 6%. We suggest this concentration as a threshold value for the maximum crack length and maximum in ped number. The maximum crack length and number in peds are due to small aggregates of the particles. However, the larger aggregates are responsible for wide cracks with well-defined boundaries.

Fig.4.7b shows the variation in the time of the first crack appearance at the film with the concentration of the suspension. It clearly shows that it decreases with increases in concentrations. The decrease in time of first-time crack-appearance t_f follows the quadratic relation of concentration c as below,

$$t_f = Ac + Bc^2$$

where A and B are the system constant.

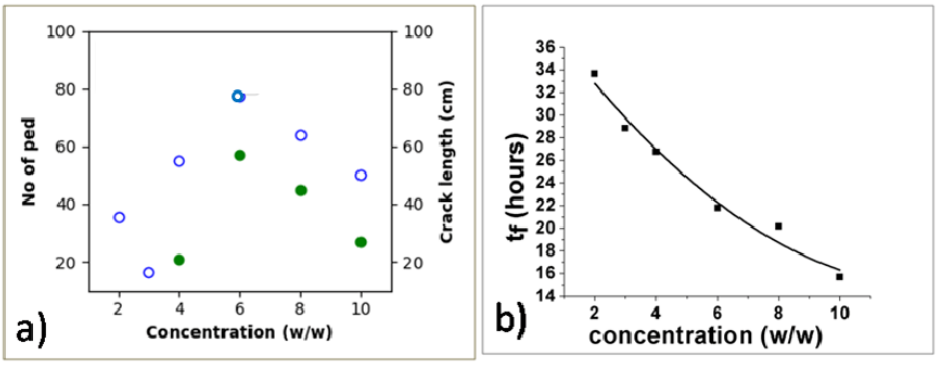

Figure 4.7: a)Variation of total crack length and ped number with the concentrations of the suspension. Solid green points represent the number of peds and open blue circle represents the crack length. b)Variation of the first crack appearance time with the concentrations of the suspension.

This can be explained by two reasons. Firstly, when the concentration of the particles are high, the aggregates have a greater chance to arrange themselves in the form of a stacked coin-like arrangement during gelation, Fig.4.4b. The regular arrangement decreases the amorphous state of the film. This arrangement decreases the homogeneous relaxation of stress that happens in a disordered system. Due to the regular arrangement of the film, the stress builds up along a particular plane that cracks easily. The second reason is the films strongly adhere to the substrate at higher concentrations. At lower concentrations, the ionic strength is comparatively low because of the DLVO force between the substrate and particles. At lower concentrations, particle-substrate interaction is repulsive, and hence the films tend to peel off from the substrate by releasing a substantial part of the stress that accumulates during desiccation. On the other side, when the films are adhered to the substrate, the stress develops along the film radially and release as an appearance of the cracks. Another observation is the decrease in opacity of the films with an increase in concentration. This can be explained by the decrease in ionization of carbonic acid to release H^+ ions.

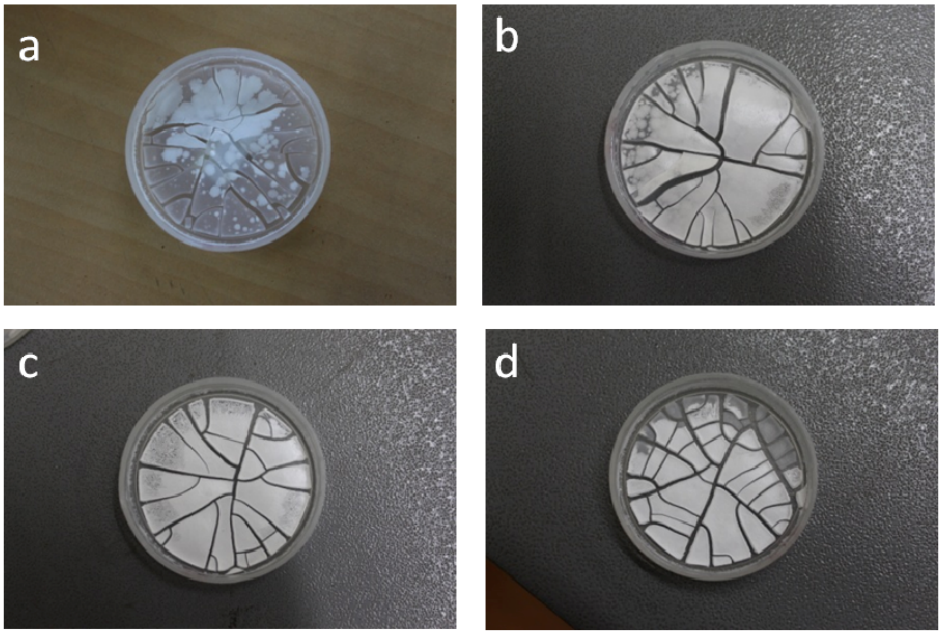

Figure 4.8: Desiccation crack formation of aqueous Laponite suspension of pH 13.3 on Polypropylene petri dish with varying thickness. (a)0.30 cm (b)0.35 cm (c)0.40 cm (d)0.45 cm . The diameter of the petri-dish is 7.25 cm.

Initial height of solution(cm)	Crack length (cm)	No of peds
0.30	40	22
0.35	37.9	20
0.40	40.02	22
0.45	53.31	41

Table 4.1: Effect of variation of initial thickness of the film

4.6 Effect of variation of film thickness

The variation in film thickness can cause a difference in the final crack pattern [10], [33], [34]. Serious care was taken to maintain the thickness of the film constant during the experiment. Despite the precaution regarding the maintaining constancy of film thickness, the final films may vary the thickness because of the variations in the concentration. We have tried to explore, how the thickness of the initial

deposition affects the final deposition pattern of desiccating film. To check this, an aqueous solution of Laponite at pH 13.3 with a 6% concentration is used. The thickness of deposition is varied from 0.3 to 0.45 cm on a petri dish of polypropylene. The final patterns of the dried film are shown in Fig.4.8. No such differences are seen in the films except for the peeling off from the substrate in the case of an initial height of 0.35 cm. The number of cracks peds and the number of crack lengths are obtained from the dried film as shown in table 4.1. only a variation of 50% of the initial thickness shows a significant difference in a dried film.

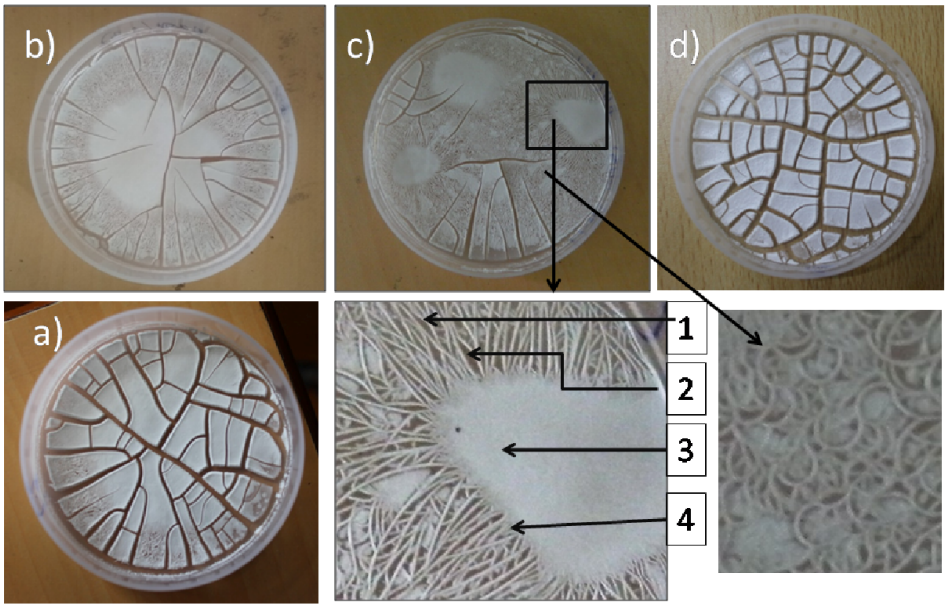

Figure 4.9: Absence of crystallization pattern at relative humidity of a)30% b)40% d)65%. c) Crystallization pattern at relative humidity 48%. Different magnified portions of the lace pattern are shown. 1) On the branch portion 2) Transparent portion between two branches 3) Lawn portion 4) Lawn portion from where it starts branching.

4.7 Lace crystallization pattern

Our experiment shows controlled evaporation of aqueous Laponite for a particular pH, developing a lace-like crystallization pattern after complete drying of the film.

When the aqueous solution of Laponite of 6% concentration is allowed to desiccate at relative humidity $50\% \pm 5\%$ and temperature $20 - 25°C$, the lace crystallization pattern is observed, Fig.4.9c. The formation of such crystallization is very sensitive to relative humidity. Other than the mentioned humidity, lace crystallization is not observed. The lace pattern disappears at higher concentrations. SEM image and EDAX have been taken for the different portions of the lace pattern. Fig.4.10 shows the SEM image and EDAX of the branch/lace portion and the base portion between the branch, shown in Fig.4.9c. EDAX of the branch shows the maximum contributions are from Na and O and the crystals are most probably NaOH. SEM image reveals the ellipsoidal crystal. It is to be mentioned that the evaporation of aqueous NaOH solution with the same conditions does not show such crystallization. So, we can argue that Laponite is the candidate, that is responsible for such a pattern. On the other hand, EDAX shows, the maximum contribution for the base portion comes from Si, O, and Mg. The SEM image and EDAX for the lawn-like portion and the part, where the lawn portion starts to branch, (Fig.4.9c) have been shown in Fig.4.11. The EDAX of that portions shows identical compositions but SEM images show some interesting differences. In the Lawn portion, part 3 of Fig.4.9c are most probably the NaOH crystals. The crystals are brought together with each other. In portion 4 of Fig.4.9c, the NaOH crystals start to align themselves, Fig.4.11.

A lace-like crystal formation is very sensitive to ambient conditions, the pH of the suspensions, and the concentration. A particular combination of the factors enables the crystallization of Na salt on the bed of the Laponite particles, which are leached to act as a seed in the formation of the crystal. Humidity controls the evaporation rate and a suitable evaporation rate helps the salt ions to gain the critical level of saturation that enables crystal seeds to form.

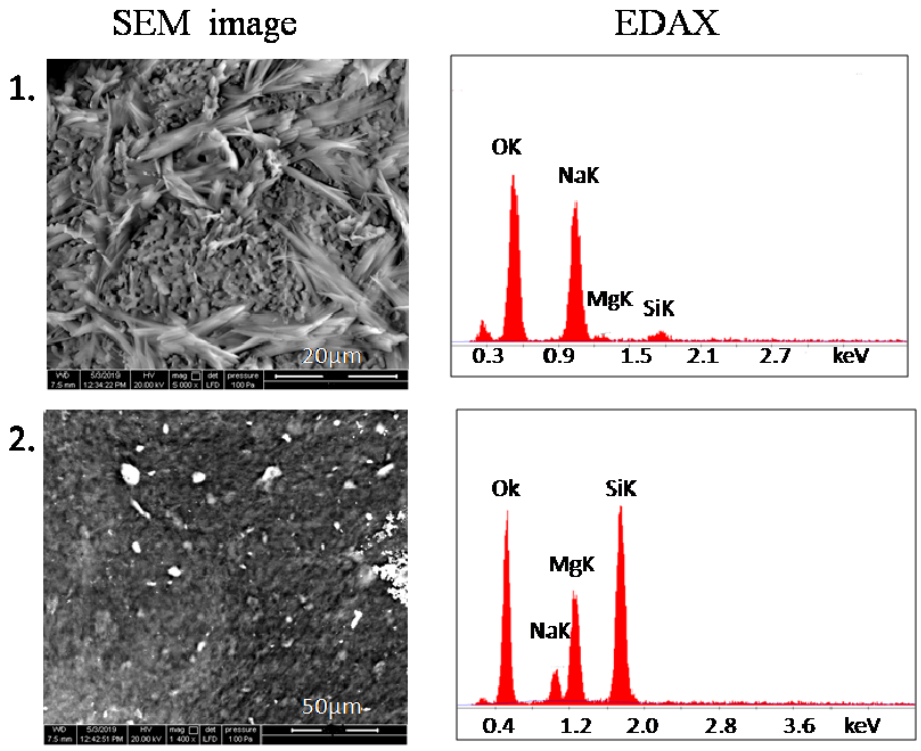

Figure 4.10: 1) Horizontal images at the top show the SEM and EDAX of the Branch portion as shown in Fig.4.9c. 2) Horizontal images at the bottom show the SEM and EDAX of the base portion between two branches as shown in Fig.4.9c

4.8 Conclusions

Desiccation crack patterns of aqueous Laponite particles show interesting patterns with the variation of pH of the suspensions. The different patterns are explained based on the anisotropic shape of the particles and the nature of charge distribution on the face and edge of the particles which depends on the pH of the medium. Important findings from this work are as follows.

At lower pH, the films exhibit crack patterns with the wavy edge of the peds with the grainy surface. The house of cards structure manifests the fractal nature of the surface. The film's opacity is attributed to the leaching ions and strong aggregation of the particles. At higher pH, cracks are polygonal in shape with even edges. The stack coin arrangement of the particles is the reason for the linear crack of the film.

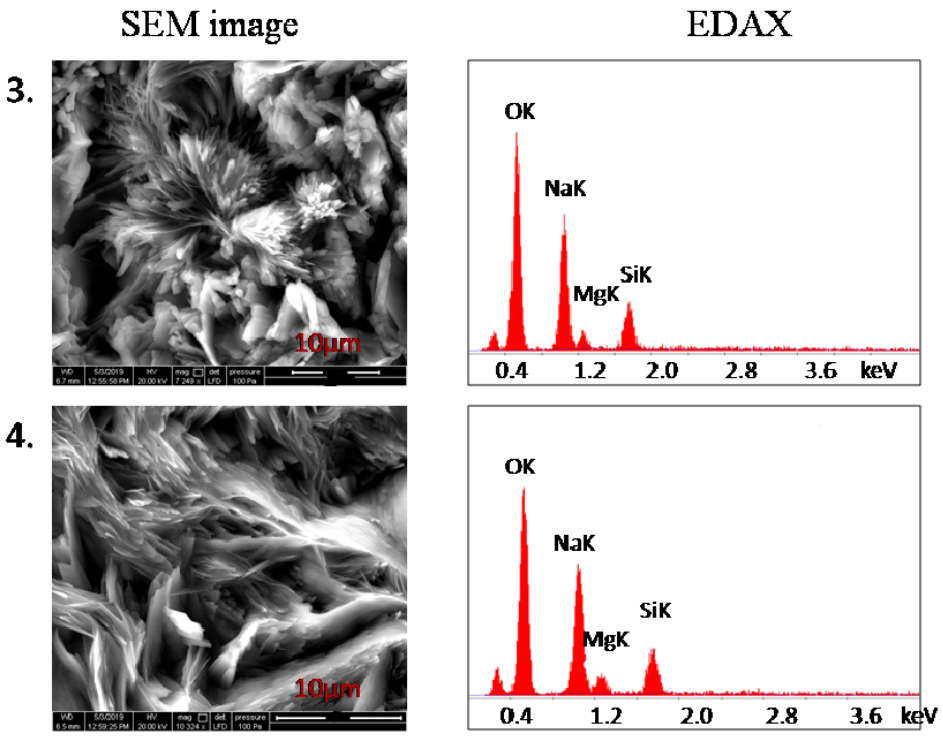

Figure 4.11: 3) Horizontal images at the top show the SEM and EDAX of the lawn like portion as shown in Fig.4.9c. 4) Horizontal images at the bottom show the SEM and EDAX of the lawn portion from where it starts branching as shown in Fig.4.9c

At pH $\sim$ 12, the absence of crack correspondence to the point of zero charges or the Iso Electric Point of the Laponite particles.

When the suspension pH $>$ 13, the concentration of the suspension can affect the crack pattern greatly. At lower concentrations, the cracks are linear but disordered. At higher concentrations, the cracks become ordered and the peds become polygonal and fewer in number. Also, the cracks are wider than at the lower concentration.

Dissolution of the Laponite particles is affected by the concentrations of the Laponite particles which affect the crack pattern and the opacity of the film.

For a critical combination of concentration, pH, and a small range of relative humidity, the desiccated films of Laponite particles show the crystallization of salts.

We have studied the SEM and EDAX of the film where crystallization is formed.

Bibliography

[1] R. Bandyopadhyay, D. Liang, H. Yardimci, D. A. Sessoms, M. A. Borthwick, S. G. Mochrie et al., *"Evolution of particle-scale dynamics in an aging clay suspension"*, *Physical Review Letters* **93** 228302 (2004).

[2] D. Saha, R. Bandyopadhyay and Y. M. Joshi, *"Dynamic light scattering study and dlvo analysis of physicochemical interactions in colloidal suspensions of charged disks"*, *Langmuir* **31** 3012--3020 (2015).

[3] R. Kumar, G. M. Coli, M. Dijkstra and S. Sastry, *"Inverse design of charged colloidal particle interactions for self assembly into specified crystal structures"*, *The Journal of chemical physics* **151**, (2019).

[4] S. Bohn, L. Pauchard and Y. Couder, *"Hierarchical crack pattern as formed by successive domain divisions."*, *Physical Review E* **71** 046214 (2005).

[5] L. Pauchard, F. Parisse and C. Allain, *"Influence of salt content on crack patterns formed through colloidal suspension desiccation"*, *Physical Review E* **59** 3737 (1999).

[6] K. Pasricha, U. Wad, R. Pasricha and S. Ogale, *"Parametric dependence studies on cracking of clay"*, *Physica A: Statistical Mechanics and its Applications* **388** 1352--1358 (2009).

[7] W. P. Lee and A. F. Routh, *"Temperature dependence of crack spacing in drying latex films"*, *Industrial & engineering chemistry research* **45** 6996--7001 (2006).

[8] F. Carle and D. Brutin, *"How surface functional groups influence fracturation in nanofluid droplet dry-outs"*, *Langmuir* **29** 9962--9966 (2013).

[9] Y. Y. Tarasevich, *"Simple analytical model of capillary flow in an evaporating sessile drop"*, *Physical Review E* **71** 027301 (2005).

[10] A. Groisman and E. Kaplan, *"An experimental study of cracking induced by desiccation"*, *Europhysics Letters* **25** 415 (1994).

[11] Y. Matsuo and A. Nakahara, *"Effect of interaction on the formation of memories in paste"*, *Journal of the Physical Society of Japan* **81** 024801 (2012).

[12] A. Nakahara and Y. Matsuo, *"Transition in the pattern of cracks resulting from memory effects in paste"*, *Physical Review E* **74** 045102 (2006).

[13] D. Mal, S. Sinha, T. Middya and S. Tarafdar, *"Field induced radial crack patterns in drying laponite gel"*, *Physica A: Statistical Mechanics and its Applications* **384** 182--186 (2007).

[14] S. Sadhukhan, J. Prehl, P. Blaudeck, K. Hoffmann, T. Dutta and S. Tarafdar, *"Desiccation of a clay film: Cracking versus peeling"*, *The European Physical Journal E* **27** 391--395 (2008).

[15] D. Mal, S. Sinha, S. Mitra and S. Tarafdar, *"Formation of crack networks in drying laponite films"*, *Physica A: Statistical Mechanics and Its Applications* **346** 110--115 (2005).

[16] D. Mal, S. Sinha, T. Dutta, S. Mitra and S. Tarafdar, *"Formation of crack patterns in clay films: desiccation and relaxation"*, *Journal of the Physical Society of Japan* **76** 014801 (2006).

[17] S. Nag, S. Sinha, S. Sadhukhan, T. Dutta and S. Tarafdar, *"Crack patterns in desiccating clay–polymer mixtures with varying composition"*, *Journal of Physics: Condensed Matter* **22** 015402 (2009).

[18] S. Tarafdar, D. Mal, S. Sinha and T. Middya, *"Crack patterns in laponite films dried in electrostatic field"*, *arXiv preprint cond-mat/0607787*, (2006).

[19] T. Khatun, T. Dutta and S. Tarafdar, *"Crack formation in laponite gel under ac fields"*, *Applied clay science* **86** 125--128 (2013).

[20] T. Khatun, T. Dutta and S. Tarafdar, *"Crack formation under an electric field in droplets of laponite gel: Memory effect and scaling relations"*, *Langmuir* **29** 15535--15542 (2013).

[21] S. Hazra, T. Dutta, S. Das and S. Tarafdar, *"Memory of electric field in laponite and how it affects crack formation: modeling through generalized calculus"*, *Langmuir* **33** 8468--8475 (2017).

[22] S. Sircar, T. Khatun, T. Dutta and S. Tarafdar, *"Alternating field induced crack patterns in desiccating laponite solutions: experiment and simulation"*, *Indian Journal of Physics* **90** 1355--1366 (2016).

[23] S. Sircar, S. Tarafdar and T. Dutta, *"Crack formation in desiccating laponite® films under ac field: Effect of varying frequency"*, *Applied Clay Science* **156** 69--76 (2018).

[24] S. Sircar, M. D. Choudhury, S. Karmakar, S. Tarafdar and T. Dutta, *"Crack patterns in drying laponite–nacl suspension: role of the substrate and a static electric field"*, *Langmuir* **34** 6502--6510 (2018).

[25] A. Ghosh, S. Sircar, T. Khatun, T. Dutta and S. Tarafdar, *"Tree-like crack patterns in clay dried in a uniform dc electric field"*, *Materials Research Express* **6** 026305 (2018).

[26] A. Ghosh, T. Dutta, S. Tarafdar and A. K. Ghosh, *"Branched crack patterns in layers of laponite® dried under electric fields: Evidence of power-laws and fractal scalin"*, *The European Physical Journal E* **43** 1--6 (2020).

[27] L. Pauchard, F. Elias, P. Boltenhagen, A. Cebers and J.-C. Bacri, *"When a crack is oriented by a magnetic field"*, *Physical Review E* **77** 021402 (2008).

[28] H. Lama, V. R. Dugyala, M. G. Basavaraj and D. K. Satapathy, *"Magnetic-field-driven crack formation in an evaporated anisotropic colloidal assembly"*, *Physical Review E* **94** 012618 (2016).

[29] M. Muthukumar, *"Screening effect on viscoelasticity near the gel point"*, *Macromolecules* **22** 4656--4658 (1989).

[30] A. Ponton, A. Bee, D. Talbot and R. Perzynski, *"Regeneration of thixotropic magnetic gels studied by mechanical spectroscopy: the effect of the ph"*, *Journal of Physics: Condensed Matter* **17** 821 (2005).

[31] S.-h. Hsu and T.-L. Yu, *"Dynamic viscoelasticity study of the phase transition of poly (n-isopropylacrylamide)"*, *Macromolecular Rapid Communications* **21** 476--480 (2000).

[32] Y. M. Joshi, G. R. K. Reddy, A. L. Kulkarni, N. Kumar and R. P. Chhabra, *"Rheological behaviour of aqueous suspensions of laponite: new insights into the ageing phenomena"*, *Proceedings of the Royal Society A: Mathematical, Physical and Engineering Sciences* **464** 469--489 (2008).

[33] V. Lazarus and L. Pauchard, *"From craquelures to spiral crack patterns: influence of layer thickness on the crack patterns induced by desiccation"*, *Soft Matter* **7** 2552--2559 (2011).

[34] T. Khatun, T. Dutta and S. Tarafdar, *"Topology of desiccation crack patterns in clay and invariance of crack interface area with thickness"*, *The European Physical Journal E* **38** 1--11 (2015).

Chapter 5

Fabrication of Transparent Conducting Sheet tailoring the pH-regulated desiccation crack network.

5.1 Introduction

Over the last two decades, scientists and researchers have invested much time and money in fabricating Transparent Conducting Sheet (TCS). The vast applications of TCS like Touch screens, solar cells, transparent heaters, etc. have drawn the attention of researchers and engineers [1], [2], [3]. Fabrication of Transparent Conducting sheet tailoring the pH-regulated desiccation crack network is new idea at all. All the applications need a high score for the efficiency of transparency and effective electrical and/or thermal conductivity. The challenging parts of this fabrication are maximum transparency as well as maximum conductivity. Achieving the maximum efficient TCS is compacted by some serious constraints of the brittleness [4] of the films, limited transparency near the infra-red region of the spectra [5], and high cost [6].

Different mechanisms are adopted to fabricate the transparent film. Sometimes desiccation cracks are used to obtain the desired network to obtain the TCS. Our objective is to make a low-cost and easily functional transparent film of desired conductivity and transparency. In this chapter, we propose a novel technique for the fabrication of TCS by modulating the crack network geometry. The crack network of the desiccated films which act as a template were changed vividly by changing the pH of the suspension. The desiccated crack networks can be changed by changing the pH of the suspension from very acidic to basic [7], [8]. Graphite powder of the order of a few µm is used as conducting material for filling the network. The use of graphite powder as the conducting part of the film lowers the expensive cost of the fabrication. The cost of conducting film has been addressed by the use of graphite powder deposited uniformly in the crack network. Hence this makes it economically feasible. The graphite powder has a lower chance to diffuse in the active material, unlike some metals which are used often to fill the network.

5.2 Review of earlier related works

Several mechanisms of fabrication of TCS have been explored in the last few years. Han et al invented a bio-inspired network for modern optoelectronic devices having high mechanical strength with good conductivity. They have invented two different networks for different applications. The networks are invented from leaf venation by chemical extraction and by metalizing spider's silk web [9]. Transparent electrodes are essential components for solar cells or touch screens. Metal-based deposition, such as ITO, has brittleness properties. A facile fabrication method of generating a network and metal-based nanotrough network is proposed [10]. Most of the metal-based network fabrications are high-cost. High-performance electrodes with low cost have been proposed using copper nanofiber. Cu wire has been used as an alternative to the very commonly used ITO. Highly interconnected cu wires have been fabricated on polyethylene terephthalate surface which exhibits low resistance [11].

The main advantages of copper nanofiber are highly flexible and stretchable [12]. Heaters with transparent plates or sheets have many applications in optoelectronic devices. Recently many advanced methods have been proposed in making transparent conducting electrodes based on different materials such as CNTs, graphene nanopowder, oxide nanoparticles, metal nanowires, metal meshes, and their hybrids [13]. The flat, flexible, and curved conducting film was prepared by spray coating Ag particles by vacuum evaporation with a crackle precursor on the desired network on a surface [14]. Lithography techniques have been invented to fabricate highly oxidation-resistant transparent conducting film. Roll and spray process by a solution process was used in crackle lithography process [15].

Desiccation cracks are narrow with the width of the cracks of the order of µm or less. These cracks on a transparent substrate are often used to generate transparent film by filling the crack network with metal atom deposition. In this context, it has focused on the suitable cracked network for making it most effective. Desiccation of a colloidal layer can result in cracks on a substrate because of stress developed due to solvent evaporation. A suitable mixture of solvent, water, and isopropyl alcohol of a colloidal suspension generates dense and narrow cracks on a transparent substrate. These crackle patterns are used as sacrificial templates to obtain metal meshes on this transparent surface [16]. The main challenging part of this fabrication is the high conductivity with good transparency. To find the optimal condition for maximum efficiency, a simulation study of the three-dimensional case has been done [17]. Recently some work has been done to study the topological properties against the electrical conductivity. Computational approaches revealed that electrical conductivity is proportional to the square root of the number density of cracks [18]. Cracked film lithography (CFL) is often used to fabricate metal grids for transparent contact in optoelectronic devices. CFL is basically controlled by the thickness of the film which modifies the areal crack density, crack spaces and width, etc. The modified template determines the final resistance of the template and transparency [19].

5.3 Fabrication of transparent conducting film by modulating the desiccation crack.

In this chapter, an interesting approach to designing network templates for the fabrication of TCS has been proposed by controlling the pH of the aqueous colloidal suspension. The pH of the aqueous Laponite suspension has been varied from 7.8 to 12.7 to design the different geometries and connectivity of the crack template on a glass substrate. The crack network was filled with micron-sized graphite powder by slow evaporation from the network. The conducting film is prepared after removing the clay completely. The resistance, reflectance, transmittance, and figure of merit have been analyzed in association with the pH of the suspension. Optical properties and electrical response are correlated to the topological measure where the graphite powder response for selective transmittance at certain pH values.

Euler characteristic is an important tool in algebraic topology and polyhedral combinatorics. It was originally defined for a polyhedron and is usually applied to prove various mathematical theorems. The original formula that was first used for polyhedrons is defined by

$$\chi = V - E + F \tag{5.1}$$

where V, E, and F represent no of Vertices, Edges, and Faces of a polyhedron [20]. This equation is known as Euler's polyhedron formula. For convex polyhedron $\chi = 2$, the simplest form of the equation for convex polyhedron becomes V-E+F=2. We are concerned here with binary images which are planners. Euler characteristic is very important because of its practical application. Its additive property allows analysis at a local level while drawing global inferences. We are interested in calculating χ from tessellations of binary images using the formula

$$\chi = N_b - N_w \tag{5.2}$$

where N_w and N_b are the number of white clusters and the number of black clusters accordingly [21]. The connectivity of the crack networks is addressed by the impact of χ for colloidal suspensions of different pH.

The electrical tortuosity τ_e [22] of a conducting path for a charged particle is defined as the first order [23], the mean free path l, travelled by the particle through the sample normalized by the sample characteristic length L i.e. τ_e=l/L. The resistance of the TCS is controlled by the tortuosity of the sample for different pH of the suspensions. So, the tortuosity, resistance, and pH of the suspensions are correlated with each other. The optical properties of the conducting film have been studied as a function of pH and have been characterized concerning their response in the wavelength of visible range. We have shown TCSs can behave as filters at certain pH values at wavelength $540nm$. This work provides a simple and cost-effective process to fabricate transparent conducting films of particular optical and electrical properties.

5.4 Fabrication method of Transparent Conducting Sheet (TCS)

Aqueous suspension of Laponite clay has been prepared following the preparation method faithfully. The desiccation crack network of aqueous suspension of Laponite clay has been obtained only in the basic range of pH. In order to change the pH, the required amount of NaOH or 37% HCl was added to 20 ml of water and kept for 30 minutes. 1.2 gm of Laponite powder is added to this water and stirred for 1 minute with a magnetic stirrer. Immediately after the preparation of the suspension, the sample is poured into a glass Petri dish which is already cleaned with extran detergent as well as acetone. The film was allowed to dry in an ambient condition of temperature $22-28^{\circ}$ degrees and $40-46\%$ relative humidity. Crack templates were prepared for different pHs in the basic range: 7.8, 8.7, 11.2, 11.8, 12.2, 12.5, and

12.7. Width of the cracks obtained from these films are in the range of μm. Crack templates obtained in the desiccation of aqueous Laponite suspension are used to fabricate the TCS. Width of the cracks can be obtained from this suspension in the range of nm at the acidic range of pH. However, the films in the acidic range are too brittle to be used for the fabrication of TCS.

Images of the crack network were taken by a NikonCool camera with a resolution of 1280 x 720. pH of the suspension was measured with a digital pH meter. Image analysis of the crack networks and peds was done by ImageJ software. The results reported in this section are performed at least 3 times for confidence.

A 2% concentrated graphite powder (from Merck; size $\sim 20\mu$m) suspension with the solvent 1,2 dichloroethane was prepared using an ultrasonicator. The solution is stirred for 30 minutes by an ultrasonicator to get a homogeneous suspension. Immediately after the preparation of the suspension, it is poured into crack geometry very carefully until the full network is filled up with the graphite suspension. The film with this suspension is kept standing to ensure homogeneous sedimentation due to gravity and evaporation of the suspension from the network. As the cracks are of the order of μm, there is no chance to set up turbulent motion inside the crack.

Once the suspension dries completely, the film of Laponite is removed carefully without touching the network which is filled with graphite. The resistance of the TCS is measured with a multimeter diametrically for different positions and averaged.

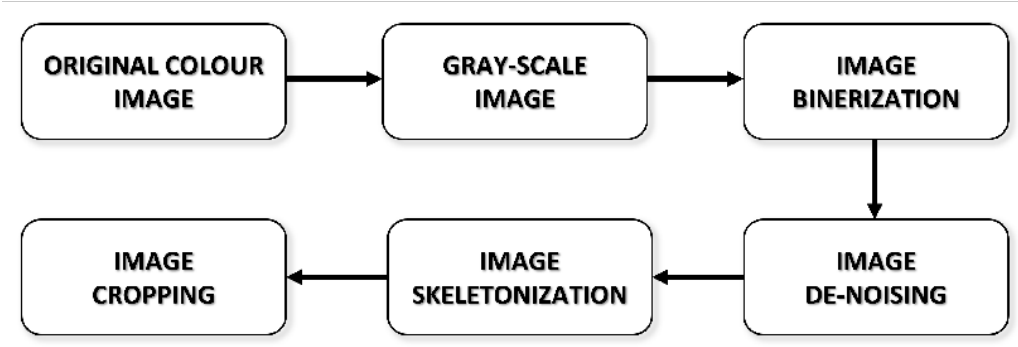

Figure 5.1: Flow chart: Image processing procedure of a crack template

5.4.1 Determination of optical properties of TCS

The optical properties, reflectance, and transmission for every TCS corresponding to all pHs were measured with MEEP (MIT Electromagnetic Equation Program) software. MEEP is an open-source software that simulates electromagnetism using the finite-difference time-domain (FDTD) method [24]. A necessary input for this software is a good-quality binary image. We have converted the images of TCSs for all pH into binary by ImageJ software. The flow chart followed in this procedure is shown in Fig.5.1. The thresholding of the grayscale should be chosen wisely for faithful binary images of the real images. All the measurements done by the MEEP software use these binary images. The important input for optical measurement is the refractive index of glass and graphite which are 1.5 and 2.71 respectively [25]. Reflectance and transmission of the TCSs are measured for normal incidence of the electromagnetic wave i.e. $\theta = 0$

5.5 Result

Transparent Conducting Sheets are obtained from the crack network formed in the desiccation of Laponite suspension and the networks filled with graphite are displayed in Fig.5.2. The crack network geometry depends on the pH of the suspension strikingly. There is a circular crack along the periphery of the petri dish corresponding to every pH due to stress developed because of the boundary.

Crack networks formed in the pH range of 7.8-11.8 are more random than the crack patterns formed at pH 12.7. The cracks are more ordered and the outlines are linear at pH 12.7 as shown in Fig.5.2g. The hierarchy of the patterns is evident here. The primary cracks start from the boundary while the secondary cracks form from the boundary and meet with the primary cracks at the T junction with a narrower crack comparatively. Tertiary cracks originate from the secondary one with the thinnest crack. The different hierarchies of the cracks are shown in Fig.5.2h with different

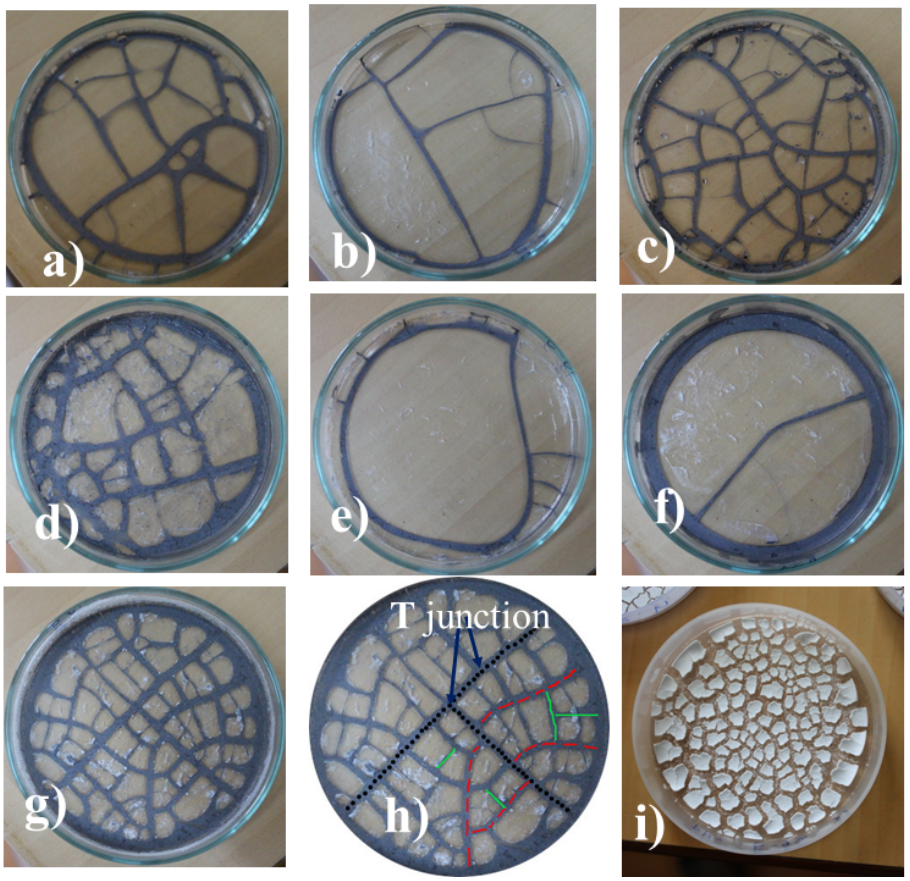

Figure 5.2: Images of the TCSs obtained from the crack template formed with the pH values (a) 7.8 (b) 8.7 (c) 11.2 (d) 11.8 (e) 12.2 (f) 12.5 (g) 12.7 (h)The hierarchical crack patterns are displayed for pH value 12.7. The black dotted lines represent the primary cracks, the red dashed lines represent the secondary cracks and the green lines are for tertiary cracks

colors. The minimum cracks are seen around pH 12, Fig.5.2(e-f), which corresponds to the Iso-electric Point of the Laponite particle. The cracks of nm order can be obtained from the films at acidic pH range. Nanometer order cracks can be obtained by drying thinner films slowly. However, the crack peds at the acidic range are too brittle to use for the fabrication of TCS. In this work, pH is the crucial point in designing crack geometry on a transparent slab to fabricate TCS. The optical properties of the TCSs are calibrated as a function of suspension pH. The variations of the transmission (T) and reflectance (R) of the TCSs are evaluated using MEEP with the pH of the suspension shown in Fig.5.3 a and b respectively. The average resistance of each TCS has been measured along diametrically for different positions.

The variation of the resistance with the suspension pH has been shown in Fig.5.4a. Variation of pH changes the crack network of the template vividly. So, the connectivity of the TCS is a function of pH. We have measured the topological invariant, Euler characteristics, and tortuosity of the network and addressed the variation of these measurements with the pH of the suspensions shown in Fig.5.4a and b.

5.6 Discussions

A close look at Fig.5.2 reveals that the cracks formed in the pH range 7.8-11.8 are more random than the crack formed in pH 12.7 where the cracks show hierarchy and linear crack. The nature of charge at the rim turns to negative from positive around the pH value 11.5 which corresponds to the point of zero charge [26], [27]. Around this pH, the Laponite particles change their structure of aggregation from a house of cards structure to a stack coin arrangement as shown in Fig.4.4(a and b).

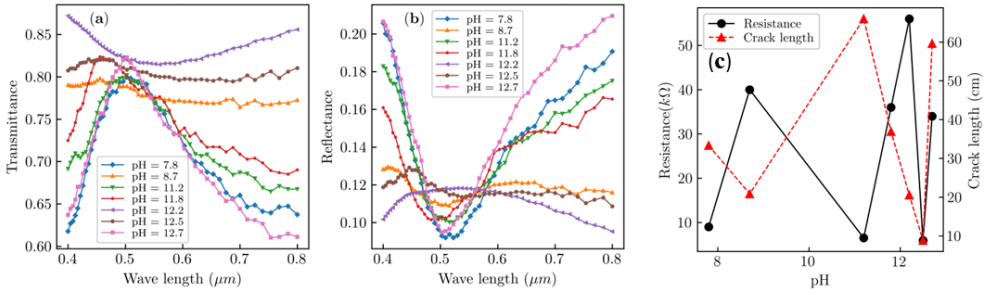

Figure 5.3: Variation of optical properties of TCSs with wavelength in the visible region. a) Variation of Transmittance of the TCSs with wavelength. b) Variation of Reflectance of the TCSs with wavelength. c)Variation of total total crack length and resistance with pH of the suspension.

Examining Fig.4.4a shows that the crack line cannot propagate by breaking the aggregates and the cracks are more random. This causes the random mosaic structure of the crack template at this pH range. However, the Laponite particles above this

pH behave as repulsive glass by arranging themselves in stack-coin arrangement as shown in Fig.4.4b, where the Laponite particles are suspended without touching each other and the cracks propagate along the stack structure to form the straight crack line. TCS obtained by prudent adjustment of the suspension pH shows interesting properties while measuring the optical properties like transmittance and reflectance using MEEP. The transmittance shows a maximum value at 0.54μm wavelength and dwindles at either side of that wavelength throughout the visible spectra for the pH values 7.8, 11.2, 11.8, and 12.7. As expected, the reflectance of the TCS for the mentioned pH value shows a dip at the wavelength 0.54μm and gradually increases on either side. A comparison of the crack networks shown in Fig.5.2 shows that the crack density is high for the pH values 7.8, 11.2, 11.8, and 12.7 which is is reflected in Euler Characteristic measurement. The more negative values correspond to the pH values other than 7.8, 11.2, 11.8, and 12.7. The high transmittance of the TCSs corresponding to pH values 7.8, 11.2, 11.8, and 12.7 can be attributed to the high-density crack network filled with graphite. Similar reflectance minima at 0.54μm wavelength was reported for graphite flakes in the plane (001) plane by Kwiecinskn et. al which supports our claim [28]. So, the transmission value of the TCSs is uniformly high for the entire wavelength range in visible spectra for the pH values 8.7, 12.2, and 12.5 while the reflectance is uniformly low. Thus, the TCSs fabricated with graphite can be used as a filter of green-blue light of wavelength 0.54μm tailoring the crack template by adjusting the pH value of the suspension. Similarly, graphite TCS can be produced for transmission of the entire wavelength of visible spectra by adjusting the pH of the suspension at 8.7, 12.2, and 12.5.

All the TCSs prepared by the modulation of pH of aqueous Laponite have a single connected path through the network as there is no isolated crack in the sample. So, the number of black clusters, N_b in eqn.7.4 is one in all cases. That's why the calculated value of χ is negative in all cases. The more negative value of χ is indicative of more fragmented interfaces because of the increase of the unbroken ped. Examining Fig.5.4b shows that $\chi \sim 0$ for 12.5 pH having average resistance is low

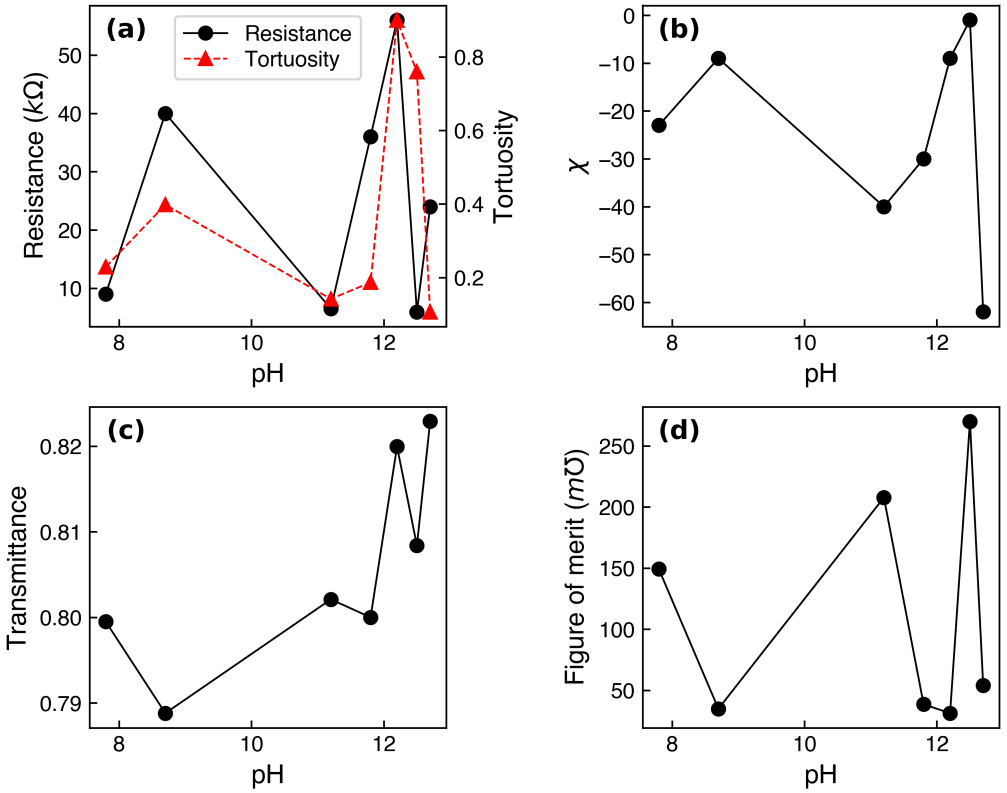

Figure 5.4: a)Variation of resistance and tortuosity with pH b)Variation of Euler number of TCS with pH c) Variation of transmittance of the TCS at 0.54μm d)Variation of Figure of Merit with pH

while χ is negatively very high and the resistance value is 40kΩ of pH 8.7. Thus, a greater branched template may be useful for touch screens but the resistance is high. Though the variation of resistance and Euler characteristic with the pH shows similar trends, the optical transport would choose the easiest path of the crack network. The tortuosity of a plane can be defined as the ratio of the mean free path to the characteristic length i.e.

$$\tau = \frac{l_m}{L}$$

The fabricated TCS are planer circles in this case. We take the mean free path as the shortest path through the crack geometry and the characteristic length is replaced by the total crack length. The shortest and easiest path travelled by a charged particle in a planar circle is along its diameter. At $\tau = 1$, is the most efficient electrical mode of transport. To investigate the mutual relation between

tortuosity, resistance, and pH of the solution we have calculated the tortuosity for each pH and plotted the variation of tortuosity and resistance with pH in a single plot as shown in Fig.5.4a. Although the two graphs don't follow the exact pattern, the trends of the graphs are almost the same which means there is dependency of resistance to the connectivity of the network. The efficiency of a conducting sheet is often measured by the Figure of Merit which is defined [29] by

$$F = \frac{188.5}{R(1/\sqrt{T_0.5} - 1)} \tag{5.3}$$

where $T_0.5$ is the transmittance at the wavelength 0.5μm. the variation of $T_{0.5}$ and figure of merit, F is plotted against the pH of the suspension in Fig.5.4(c and d). From Fig.5.4d, the maximum performance occurred at pH $>$ 12 which indicates the optimal DC connectivity at this pH range. Fig.5.3a shows the sharpness of the transmission at pH 12.7 for wavelength 0.54μm which is indicative of a sharp fall of the figure of merit. To understand the behavior of F at pH 12.7, we have calculated the total crack length of the sheet and plotted with pH value Fig.5.3c, which shows the maximum length is at pH 12.7. Thus, maximum conducting line of graphite density occurs at this pH value. Since the graphite shows the sharpest transmission at 0.54μm wavelength, the Figure of Merit falls sharply at this pH value. Spectral properties of the films are supposed to depend on the angle of the incident as expected from the disordered aperture structures [30], [31], [32]. This can help us to avoid the unjustifiable gleaming in the application of wide-angle displays. Our experiments help us to conclude that the most efficient TCS fabrication happens at the pH value 12.5, where the desiccated crack template shows minimum fragmentation with the least resistance and uniform transmittance at 0.54μm with a high Figure of Merit.

5.7 Conclusion

The desiccation crack network geometry of a glass sheet has been changed by modulating the pH of the suspension for the fabrication of a Transparent conducting Sheet. The crack network geometry so obtained by varying the pH of the suspension from almost 7 to 13 which serves as a template for the graphite network. The TCSs are calibrated for resistance as a function of pH. The connectivity of the networks has been measured in terms of the Euler characteristic and tortuosity of the sheet and we conclude that the similar variation of tortuosity and resistance is a function of pH.

The optical properties of the TCSs are measured for the wavelength range of visible spectra. The transmittance of the sheets is maximum for the wavelength 0.54μm and dwindles at either side of that wavelength throughout the visible spectra for all the pH except 8.7, 12.2, and 12.5. As expected, the reflectance of the sheets is minimal at the wavelength of 0.54μm and increases gradually on either side of the spectra. Thus, the TCSs fabricated with graphite can be used as a filter of green-blue light of wavelength 0.54μm by adjusting the pH value of the suspension to get proper crack geometry. Similarly, graphite TCS can be produced for transmission of the entire wavelength of visible spectra by adjusting the pH of the suspension at 8.7, 12.2, and 12.5.

TCSs fabricated by modulating the pH to get the crack geometry give a simple means of understanding the correlation of topological, electrical, and optical properties. This alternative technique of fabrication of TCS is economically viable which can help in further application.

Bibliography

[1] D.-S. Leem, A. Edwards, M. Faist, J. Nelson, D. D. Bradley and J. C. De Mello, *"Efficient organic solar cells with solution-processed silver nanowire electrodes"*, *Advanced materials* **23** 4371--4375 (2011).

[2] S. Walia, R. Gupta and G. U. Kulkarni, *"Disposable heater arrays using printed silver patterns on polyethylene terephthalate for multipurpose applications"*, *Energy Technology* **3** 359--365 (2015).

[3] C. Celle, C. Mayousse, E. Moreau, H. Basti, A. Carella and J.-P. Simonato, *"Highly flexible transparent film heaters based on random networks of silver nanowires"*, *Nano Research* **5** 427--433 (2012).

[4] S. Lee, Z. Gao and L. Hung, *"Metal diffusion from electrodes in organic light-emitting diodes"*, *Applied Physics Letters* **75** 1404--1406 (1999).

[5] X. Wang, L. Zhi and K. Müllen, *"Transparent, conductive graphene electrodes for dye-sensitized solar cells"*, *Nano letters* **8** 323--327 (2008).

[6] Z. Chen, B. Cotterell, W. Wang, E. Guenther and S.-J. Chua, *"A mechanical assessment of flexible optoelectronic devices"*, *Thin Solid Films* **394** 201--205 (2001).

[7] S. Haque, S. Tarafdar and T. Dutta, *"Desiccation cracks formed in laponite® suspensions of varying ph: aid to analyzing clay microstructure"*, *Physica Scripta* **95** 085703 (2020).

[8] S. Haque and T. Dutta, *"Role of ph and substrate on drying patterns of laponite® droplet"*, *Physica Scripta* **96** 125021 (2021).

[9] B. Han, Y. Huang, R. Li, Q. Peng, J. Luo, K. Pei et al., *"Bio-inspired networks for optoelectronic applications"*, *Nature communications* **5** 5674 (2014).

[10] H. Wu, D. Kong, Z. Ruan, P.-C. Hsu, S. Wang, Z. Yu et al., *"A transparent electrode based on a metal nanotrough network"*, *Nature nanotechnology* **8** 421--425 (2013).

[11] S. Kiruthika, R. Gupta, K. Rao, S. Chakraborty, N. Padmavathy and G. U. Kulkarni, *"Large area solution processed transparent conducting electrode based on highly interconnected cu wire network"*, *Journal of Materials Chemistry C* **2** 2089--2094 (2014).

[12] H. Wu, L. Hu, M. W. Rowell, D. Kong, J. J. Cha, J. R. McDonough et al., *"Electrospun metal nanofiber webs as high-performance transparent electrode"*, *Nano letters* **10** 4242--4248 (2010).

[13] R. Gupta, K. Rao, S. Kiruthika and G. U. Kulkarni, *"Visibly transparent heaters"*, *ACS applied materials & interfaces* **8** 12559--12575 (2016).

[14] R. Gupta, K. Rao, K. Srivastava, A. Kumar, S. Kiruthika and G. U. Kulkarni, *"Spray coating of crack templates for the fabrication of transparent conductors and heaters on flat and curved surfaces"*, *ACS applied materials & interfaces* **6** 13688--13696 (2014).

[15] S. Kiruthika, R. Gupta, A. Anand, A. Kumar and G. Kulkarni, *"Fabrication of oxidation-resistant metal wire network-based transparent electrodes by a spray-roll coating process"*, *ACS applied materials & interfaces* **7** 27215--27222 (2015).

[16] R. Pujar, A. Kumar, K. Rao, S. Sadhukhan, T. Dutta, S. Tarafdar et al., *"Narrowing desiccating crack patterns by an azeotropic solvent for the fabrication of nanomesh electrodes"*, *Langmuir* **35** 16130--16135 (2019).

[17] S. Sadhukhan, A. Kumar, G. U. Kulkarni, S. Tarafdar and T. Dutta, *"A spring network simulation in three dimensions for designing optimal crack pattern template to fabricate transparent conducting electrodes"*, *Bulletin of Materials Science* **42** 197 (2019).

[18] Y. Y. Tarasevich, A. V. Eserkepov and I. V. Vodolazskaya, *"Electrical conductivity of crack-template-based transparent conductive films: A computational point of view"*, *arXiv preprint arXiv:2307.01509*, (2023).

[19] C. P. Muzzillo, M. O. Reese and L. M. Mansfield, *"Fundamentals of using cracked film lithography to pattern transparent conductive metal grids for photovoltaics"*, *Langmuir* **36** 4630--4636 (2020).

[20] A. Roy, R. Haque, A. Mitra, M. D. Choudhury, S. Tarafdar and T. Dutta, *"Understanding flow features in drying droplets via euler characteristic surfaces—a topological tool"*, *Physics of Fluids* **32**, (2020).

[21] A. Roy, R. Haque, A. Mitra, S. Tarafdar and T. Dutta, *"Combinatorial topology and geometry of fracture networks"*, *Physical Review E* **105** 034801 (2022).

[22] H. Saomoto and J. Katagiri, *"Direct comparison of hydraulic tortuosity and electric tortuosity based on finite element analysis"*, *Theoretical and Applied Mechanics Letters* **5** 177--180 (2015).

[23] B. Nigro, C. Grimaldi, P. Ryser, F. Varrato, G. Foffi, P. J. Lu et al., *"Enhanced tunneling conductivity induced by gelation of attractive colloids"*, *Physical Review E* **87** 062312 (2013).

[24] A. F. Oskooi, D. Roundy, M. Ibanescu, P. Bermel, J. D. Joannopoulos and S. G. Johnson, *"Meep: A flexible free-software package for electromagnetic simulations by the fdtd method"*, *Computer Physics Communications* **181** 687--702 (2010).

[25] B. Stagg and T. Charalampopoulos, *"Refractive indices of pyrolytic graphite, amorphous carbon, and flame soot in the temperature range 25 to 600 c"*, *Combustion and flame* **94** 381--396 (1993).

[26] W. Stumm, L. Sigg and B. Sulzberger, *"Chemistry of the solid-water interface, john wiley&sons"*, *New York*, (1992).

[27] E. Tombacz and M. Szekeres, *"Colloidal behavior of aqueous montmorillonite suspensions: the specific role of ph in the presence of indifferent electrolytes"*, *Applied clay science* **27** 75--94 (2004).

[28] B. Kwiecinska, D. Murchison and E. Scott, *"Optical properties of graphite"*, *Journal of Microscopy* **109** 289--302 (1977).

[29] J. Kim and T. M. Truskett, *"Geometric model of crack-templated networks for transparent conductive films"*, *Applied Physics Letters* **120**, (2022).

[30] T. Qiu, B. Luo, F. Ali, E. Jaatinen, L. Wang and H. Wang, *"Metallic nanomesh with disordered dual-size apertures as wide-viewing-angle transparent conductive electrode"*, *ACS Applied Materials & Interfaces* **8** 22768--22773 (2016).

[31] X. Wen, X. Lu, C. Wei, J. Li, Y. Li and S. Yang, *"Bright, angle-independent, solvent-responsive, and structurally colored coatings and rewritable photonic paper based on high-refractive-index colloidal quasi-amorphous arrays"*, *ACS Applied Nano Materials* **4** 9855--9865 (2021).

[32] X. Chen, Y. He, X. Chen, C. Huang, Y. Li, Y. Cui et al., *"Non-iridescent metal nanomesh with disordered nanoapertures fabricated by phase separation lithography of polymer blend as transparent conductive film"*, *Materials* **14** 867 (2021).

Chapter 6

Summary and Future Outlook

Colloidal suspensions have profound implications in our daily life starting from human body fluids, to paint, pharmaceutical, food, printing, and many other industrial applications. The interesting pattern left by the colloidal particle during desiccation draws our attention to study the desiccation of a colloidal suspension. The shape and size of the colloidal particles affect the desiccation pattern depending on the spreading and wetting phenomena on a substrate. Most of our studies are on Laponite, which is a synthetic clay and available in pure form.

In this thesis, I have studied one of the lesser studied parameters-the role of pH that affect the desiccation pattern of colloidal suspensions, in particular aqueous Laponite. Existing as charged particles in the aqueous state, it is expected that changing the pH of the suspension will affect the charge distribution on the Laponite particle which exhibits a facial negative charge and a positive charge on the rim around the pH $\sim$ 10. As flow dynamics is very dependent on the interface geometry of the curvature, I have experimentally investigated the effect of varying pH on two geometries of the interface of aqueous Laponite suspension: (1) a desiccating droplet (2) desiccating film.

During our experiments, we discovered the importance of the preparation protocol of an aqueous solution in desiccation studies. Depending on the preparation protocol final dried pattern changes. The variation in the final deposited pattern is developed by different stirring methods namely, stirring by Magnetic stirrer and ultrasonication. Various degrees of stirring the solution during preparation, affects the aggregation process of particles that results in different drying patterns . We have established that a minimum stirring time is required to prepare a homogeneous solution for the reproducibility of any investigation. The homogeneous solution can be used in many applications for faithful results.

The anisotropic shape of Laponite clay possesses anisotropic charge density along its surface. Distribution and the nature of charge strongly depend on the pH of the medium. We have studied the role of the pH of the aqueous Laponite suspension on different substrates on the desiccation of different geometries. The pattern formation of aqueous droplets of Laponite particles shows interesting variations on both hydrophilic and hydrophobic substrates with pH variations. In an acidic medium, the droplet shows coffee ring formation on the hydrophobic substrate, and in a very acidic pH, 'the dried droplet pattern reveals collapsed cavities that contain a ring of salts on their wall'. In a basic range of pH, on the same substrate, salt crystals are gathered on the Laponite droplet. The same studies were done on hydrophilic substrates and quite different pattern of the result was seen. We have explained the result on the basis of the particle-particle (PP) and particle substrate (PS) interaction in tandem with the pH of the solution.

Desiccation of film of aqueous Laponite particles shows interesting patterns with the variation of pH of the medium. The films form a white opaque appearance which changes to a clear glassy look around the pH value 11.5 with increasing the pH from acidic to basic. The charge on the rim of the Laponite particles turns negative from positive around the pH value of 11.5 which is known as the Iso-electric Point. We have explained the patterns in association with the structure of the aggregation. The Laponite particle forms a house of cards structure in an acidic medium which

changes to a stack coin arrangement with a clear glassy look. The changes in the crack pattern are analyzed for particle shape, changes in surface charge distribution, and aggregation geometry.While the crack pattern is a fractal in the acidic range, the pattern is more ordered showing a hierarchical structure in the basic range. As colloidal particle concentration in a solution determines the solution's net ionic strength, particle concentration's role in affecting desiccation crack patterns is also investigated for a fixed pH.

Lastly, as an application of the role of pH in the desiccating film of aqueous Laponite, we have reported a novel technique for the fabrication of transparent conducting sheets. The crack network of different geometries has been used as the template for TCSs and was generated by modulating the pH of the suspension. The crack network was filled with graphite materials by sedimentations under gravity and uniform evaporation. Topological measure, Euler characteristics, and tortuosity of the template were measured and addressed in association with the suspension pH. We have measured the Transmittance as well as the reflectance of the sheets in the wavelength range of visible spectra. The fabricated TCSs show selective transmission for particular pH values of 8.7, 12.2, and 12.5. This simple technique of production of TCS is economically viable.

Future plans in continuation of the presented works in this dissertation are as follows:

My next target remains to study the effect of active matter in droplets or films of aqueous Laponite. There are pointers in the research field that certain bacteria can thrive in dilute solutions of Laponite to grow into colonies. Depending on the bacteria, the Laponite patches can be used effectively to clean and restore old frescoes, be used in medicinal practices such as treating certain dermatological problems and even used as capsules for targeted drug delivery. Before such applications can actually fructify in an economically viable way, there is a lot of systematic study waiting to done on the correct pairing of bacteria and the concentration and pH

of Laponite solution, the role of broth that provides food to the bacteria, in the desiccation pattern. Further, I hope to further my studies of pattern formation of colloidal suspensions like Laponite on soft substrates.

List of Publications

Haque, S., Tarafdar, S. and Dutta, T., **2020** Desiccation cracks formed in Laponite® suspensions of varying pH: aid to analyzing clay microstructure Phys. Scr. 95 085703

Khatun, A., **Haque, S.**, Tarafdar, S. and Dutta, T., **2020** Impact of varying preparation methods of colloidal suspensions on droplet desiccation patterns on hydrophobic and hydrophilic substrates Phys. Scr. 96 025211

Haque, S., and Dutta, T., **2021** Role of pH and substrate on drying patterns of Laponite droplet Phys. Scr. 96 125021

Haque, S., Bhattacharyya, S. and Dutta, T., **2021**. Aggregation patterns of copper sulphate salt via droplet drying: mediation by surface hydrophobicity and salt concentration. The European Physical Journal E, 44, pp.1-13.

Haque, S., Haque, R.A. and Dutta, T., **2023**. pH regulated desiccation crack network: a versatile template for Transparent Conducting Sheet fabrication. Physica Scripta, 98(8), p.085942.

Chapter 7

The end after ending: Aggregation patterns of copper sulphate salt via droplet drying: Mediation by surface hydrophobicity and salt concentration

7.1 Introduction

"The study of evaporation of droplets is an interesting and important feature in fundamental and applied sciences. Basic properties of fluids, fluid dynamics, phase transition and thermodynamics guide the mechanisms of mass and energy transport that occur at micro- and nano-scales of droplets during evaporation [1], [2], [3], [4]. These, coupled with the curvature of droplet interface, affect the wetting, spreading and the myriad patterns [5], [6] of the dry residue left by evaporating droplets. Important applications of droplet drying are found in industry [7], medical diagnosis [8], [9], transparent conductor fabrication [10] and in space research [11], to name a few.

If drying droplets contain dissolved salts, crystallization of salt may occur as evaporation proceeds and the solution concentration reaches super saturation. The presence of salt in colloidal solutions has been studied by several workers in the last two decades. From their observations of 'creeping' of salt crystallites outside the droplet boundary, Shahidzadeh et al. [12] have proposed that salt stains from drying droplets are a result of the wetting properties of crystals and the path they follow as they nucleate and grow, rather than the evaporation rate of the droplet and thermal conductivity of substrates. Misyura [13] has showed that at nucleate boiling of water and salt solution droplets, there are several characteristic regimes for heating, nucleate boiling, desorption without bubble formation, formation of the solid, thin crystalline hydrate film on the upper droplet surface and formation of the ordered crystalline hydrate structures during the longer time periods of the evaporation process. At high crystallization rates, complex structures of salt depositions occurred that facilitated the rate of water desorption from the surface of crystalline-hydrate film deposited. In later works, Misyura showed that the combined effect of gas convection, Stefan flow and vapour diffusion in the presence of high heat flux could cause the character of droplet evaporation of aqueous salt solutions to be fundamentally different from that of single-component liquids [14]. For droplet evaporation of salt solution, four regimes of different evaporation rates were identified, where in the last regime, the evaporation rate was significantly low as compared to aqueous solutions. In their study of drying droplets of salt solutions, Marin et al. [15] explained that ring deposits similar to coffee ring effects might be caused by flow reversal due to Marangoni effects. Pathak et al. [16] obtained different patterns formed by evaporating drops of solutions of BSA protein and two different salts. The patterns could be modulated by controlling the initial concentration of the components in the droplet. They proposed that the differential diffusion rates of components could lead to drastic changes in the final patterns. Microscopic features like dendritic crystals in the pattern were reported to be a result of the local drying of trapped solvent. Studies on droplet evaporation of salt solutions have led to the understanding that the orientation and aggregation of salt crystals during droplet

evaporation of salt solution are determined by flow dynamics as well as electrostatic and vander Waals interaction [17] between the particles and substrate. The inclusion of gelatin, starch or polymers usually increases the viscosity of the solution which can modify the substrate residual pattern after drying. This technique has been used to tune the crystal growth [18], [19], [20], [21], [22], [23] during droplet evaporation. Several studies indicate that diagnosis of different diseases can be effectively done by investigating crystallization modes in drying drops of biological fluids [24], [25], [26].

The role of substrate on droplet evaporation has been studied by several researchers. In comparison with hydrophilic substrates, hydrophobic substrates make larger contact angles with the droplet at the line of contact. This changes the evaporation flux gradient at the droplet interface, and the total evaporation time for a droplet on a hydrophobic substrate increases in comparison with that on a hydrophilic substrate [27], [28]. The lifetime of the evaporating droplet has an important impact on the salt patterns left upon complete drying as it determines the time scope for competing flow processes like diffusion, convection and Marangoni effects to take effect. There is much work on the effect of substrate temperature on the lifetime of an evaporating droplet [29], [30], [31], [32]. In such cases, the thermal conductivity contrast between substrate and droplet solution can greatly affect the droplet drying dynamics and the residue pattern at the completion of drying.

This work reports the effect of substrate and salt concentration on the dry residue left behind by the drying droplet. The substrates-glass, quartz and polypropylene, have different hydrophobicities. All experiments reported in this work have been performed on substrates kept at room temperatures. The novelty of this work is that starkly different patterns are obtained with the same salt solution just by changing the substrate hydrobhobicity. The authors explain the differences in the patterns with respect to the substrate effect on the evaporation process. The effect of variation of salt concentration on the dry pattern is also reported. Similar looking crystallization patterns have been reported earlier, but with different combinations

of salt-substrate. There are no reports to the knowledge of the authors, of such a variety of crystallization patterns obtained with a single salt solution with systematic variation of substrate hydrophobicity, and their explanation. The patterns of the dry deposits are characterized by the variation in their morphology. While a common practice is to analyse residue patterns with respect to geometrical parameters such as fractal dimension, topological analysis of the deposition patterns has not been reported. In this work, the authors measure the geometry of the deposition patterns in terms of the fractal dimension of the deposits, determined through the box-counting method. In addition, the authors demonstrate that a simple topological measures as the Euler Characteristic χ can be used to quantify desiccation patterns of evaporating droplets. The Euler Characteristic provides a useful tool for correlating desiccation patterns of salt deposits to the factors guiding droplet evaporation.

The topology of the deposits has been studied through the variation of the Euler characteristic, a topological measure, for the different substrates and salt concentrations. The Euler characteristic χ is an important and useful topological property in the field of image processing as it remains invariant under any arbitrary rubber-sheet transformation, i.e. stretching, shrinking, rotation etc. The concept of characterization of systems through Euler characteristic has been used successfully in many fields, analysis of soil crack patterns [33], [34], fast reading of car number plates [35], automatic signature matching [36] and in wetting and spreading problems in surface science and crystal growth [23]. It is an important feature that can be used to describe and understand the topological connectivity structure of a binary image, as has been used by the authors to analyse the salt deposition patterns reported here. Finally the geometry and topology of the patterns have been interpreted on the basis of the different forces that control the drying dynamics for the different substrates and concentrations studies.

In the following sections, we describe the experimental methods and the underlying forces that guide fluid dynamics in an evaporating droplet. The geometrical and

topological features are then analysed and the results interpreted and discussed. Since the methodology of the analysis is based on the images of the patterns, this has been discussed in tandem to the results. Finally we conclude highlighting the main findings of our work."

7.2 Materials and Methods

"The protocol of solution preparation of a droplet can greatly affect the final pattern of the dried deposit as has been reported by Khatun et al. [37]. In our experiments, we have faithfully followed the protocol described below, thereby ensuring that the results are not manifestations of preparation methods.

1. Glass, quartz and polypropylene slides are cleaned with Extran detergent, and deionised water successively and finally dried using acetone.

2. Hydrated copper sulphate (molecular weight: 249.72 g/mol) is used as solute/-experimental salt. 0.36 g and 0.6 g of dry copper sulphate are used to prepare 3% and 5% (w/w) strength of aqueous copper sulphate solution, to form a final amount of solution of 12 g. The prepared solution is stored in glass beakers cleaned by the same procedure as the glass slides.

3. 0.3 g of dry gelatin (used for bacteriology) is added in each glass beaker. The mass content in each beaker is stirred by magnetic stirrer at 510 rpm, for 45 minutes at 50°C, to get a homogeneous gel. After stirring, the whole mass is allowed to cool for 1 hour to attain the room temperature of 24°C. The relative humidity of the ambient was maintained between 50% and 52%.

4. From each beaker, 10 μl of solution is dropped on the glass, quartz and PP slides, successively.

5. After 10 to 15 sec from time of deposition, every droplet was photographed for measurement of angle of contact by digital camera (model:Canon 700D).

6. Rate of evaporation was also noted using a digital balance having least count of 10^{-4}4g.

7. The surface tension of each fluid sample is measured by Kruss Tensiometer K9. The droplets are allowed to evaporate at 24°C with humidity 50%.

The angle of contact was measured by photographing a drop of fluid placed on the substrate, cleaned carefully with methanol. The angle was measured for both left and right ends of the image of the drop and is averaged over several drops. Dried droplets on these three substrates were observed at microscopic level $\sim$ scale 500μm, using inverted microscope [Magnus MagCam MU 2.3 MP Camera with 0.5 $\times$ C—Mount Adapter]".

7.3 Theory

"The sessile shape of the droplet on a substrate is responsible for a gradient of evaporative flux that is symmetric about the central axis of the droplet. For hydrophilic substrates as glass and quartz, evaporation flux increases from the drop apex to the peripheral line of contact [38]. For hydrophobic substrates as PP, evaporation flux is greatest at the droplet apex and lowest at the Three-Phase Contact Line (TPCL) [27]. For low contact angles between droplet and substrate, the increased evaporation at the line of contact results in a convective flow field in the radially outward direction that drives the fluid from the centre to the edge in order to replenish the evaporating fluid. The outward capillary flow carries solute to the pinned contact line and is responsible for formation of the "coffee ring".

Surface tension gradients may develop on the droplet-air interface either due to temperature or concentration gradients giving rise to thermal or solutal Marangoni flow respectively [39], [40]. The interaction energy between the faces of colloidal particles is a resultant of electrostatic (usually repulsive) and van der Waals (attractive)

forces between the particles, and is determined by the DLVO (Derjaguin, Landau, Verwey and Overbeek)theory. The electrostatic force between a particle and the substrate is calculated using the expression, [41],

$$\boldsymbol{F_{el}} = a \exp\left(\frac{-z}{\kappa^{-1}}\right)\boldsymbol{n_z} \tag{7.1}$$

where z is the distance between the particle and the substrate, $\boldsymbol{n_z}$ is the unit vector normal to the substrate, κ^{-1} is the Debye length and a is function of the surface potential of particles and substrate and the ambient temperature. The van der Waals attraction force between the substrate and a particle is given by [42],

$$\boldsymbol{F_{vdw}} = \frac{1}{12} A d_p^3 \frac{\alpha_{rtd}}{z^2(z+d_p)^2}\boldsymbol{n_z} \tag{7.2}$$

where A is the Hamaker constant, $A = 2.43 \times 10^{-20} J$ for water [43] and α_{rtd} is the retardation factor for van der Waals force which depends on the distance between particle and substrate. The total DLVO force between a particle and the substrate is,

$$\boldsymbol{F_{DLVO}} = \boldsymbol{F_{el}} + \boldsymbol{F_{vdw}} \tag{7.3}$$

It is the competition between these flows that determine the final trajectory of solute particles in the evaporating droplet.

As droplet drying proceeds, the concentration of the solution usually increases, in turn increasing the viscosity of the solution. At the TPCL, the viscosity contrast between the gaseous and the liquid phase may give rise to Saffmann-Taylor instability that is manifested as viscous fingers" [44].

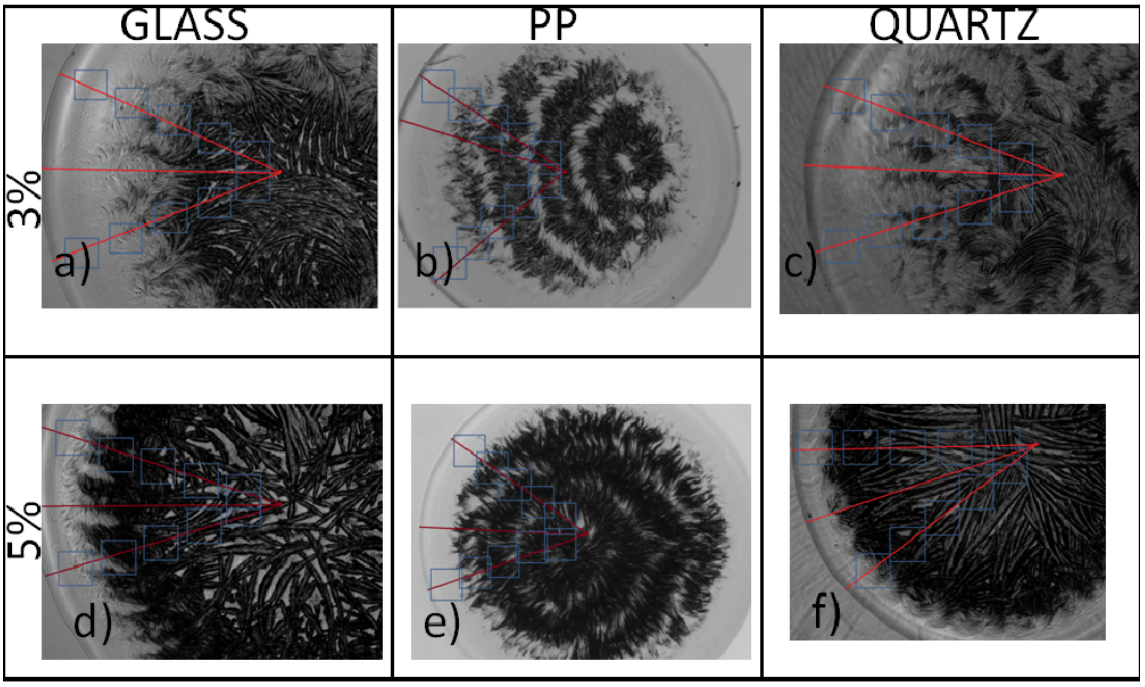

Figure 7.1: Droplet deposition pattern of 3% salt solution on different substrates: glass, quartz and polypropylene (PP) are displayed column-wise. The rows display the pattern for two salt concentrations-3% and 5%

7.4 Results and Discussions

"The salt deposition pattern observed on the substrates for two 3% and 5% salt concentrations, after complete drying of droplet, is displayed in Fig.7.1. The deposition patterns for hydrophilic and hydrophobic substrates show a rough circular symmetry but are distinctly different. For the hydrophilic substrates, glass and quartz, the deposition pattern has a general branched-vein look arranged around the droplet centre. The branches are composed of clusters of crystals, Fig.7.1d, f, and are reminiscent of diffusion limited aggregation (DLA) growth with curved branches. The outer periphery of the deposition pattern for both glass and quartz shows a tooth-like serrated deposition pattern. These features are present for both the salt concentrations in general. The deposition pattern on PP shows interesting periodic

circular deposition of salt. The circular salt depositions are off-centred slightly with respect to the droplet point of symmetry. The morphology of the deposition patterns is characterized by through topological and geometrical characterization of the deposits".

7.5 Characterization through Euler characteristics

"In a two-phase system, let the two phases be named black(B) and white(W). In a two-dimensional image, the Euler characteristic may be defined simply as the difference between the number of 'connected components' and the number of 'holes' in an image. Then the Euler characteristic (also referred to as the Euler number) can be most simply defined as

$$\chi = N_b - N_w \tag{7.4}$$

where Nb are the number of black clusters and Nw are the number of white clusters.

In the cases of deposition patterns of dry droplets of complex fluids as in the cases discussed here, one may think of an underlying two-dimensional square lattice on which the deposition occurs. The images are grey-scaled suitably so that the most faithful binary images of the real system are obtained. Every site on the underlying lattice will be labelled either black(B) or white(W), depending upon whether it houses phase 1 or phase 2. In the cases studied here, the crystalline salt deposits are labelled B-sites and the absence of the salt, labelled as W-sites. If sites of the same phase are connected by their first nearest neighbours, they are said to belong to the same cluster. A 'cluster' definition may extend upto a 'r-neighbourhood' about the centre of a grid [45]. In a square or triangular lattice, their can be a certain ambiguity regarding connectivity of clusters through vertices, which is usually resolved by assigning a certain probability to the vertex neighbours of being connected [46].

Once all the clusters are counted and numbered, the Euler characteristic is calculated following Eq.7.4".

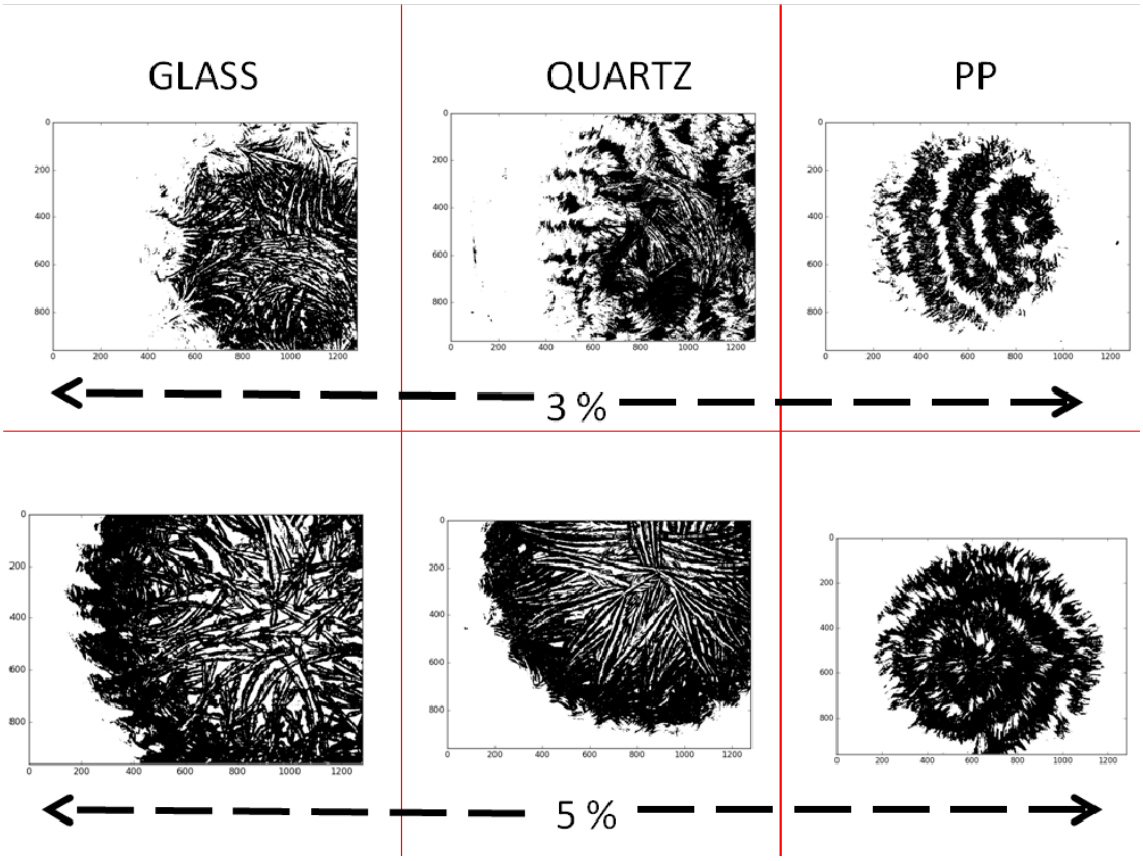

Figure 7.2: Binary images of deposition pattern after optimal thresholding of images. The upper row depicts images for 3% salt concentration and the lower row shows images for 5% salt concentration, The columns denote the different substrates.

"To summarize, the Euler characteristic analysis of the deposition images for each substrate and salt concentration was done following the protocol enumerated:

1. The image files are optimally grey-scaled and converted to binary files.

2. With image centre as origin, boxes of length l are placed one after another, at a distance r from the origin , and along an arbitrary radial direction.

3. The number of black clusters N_B(r), and white clusters, N_W(r), are counted in every box at a distance r.

4. The above two steps are repeated for several arbitrary directions about the origin, and the average N_B(r) and N_W(r) computed.

5. χ(r) is determined for every r following Eq.7.4.

6. The variation of χ(r) with r plotted.

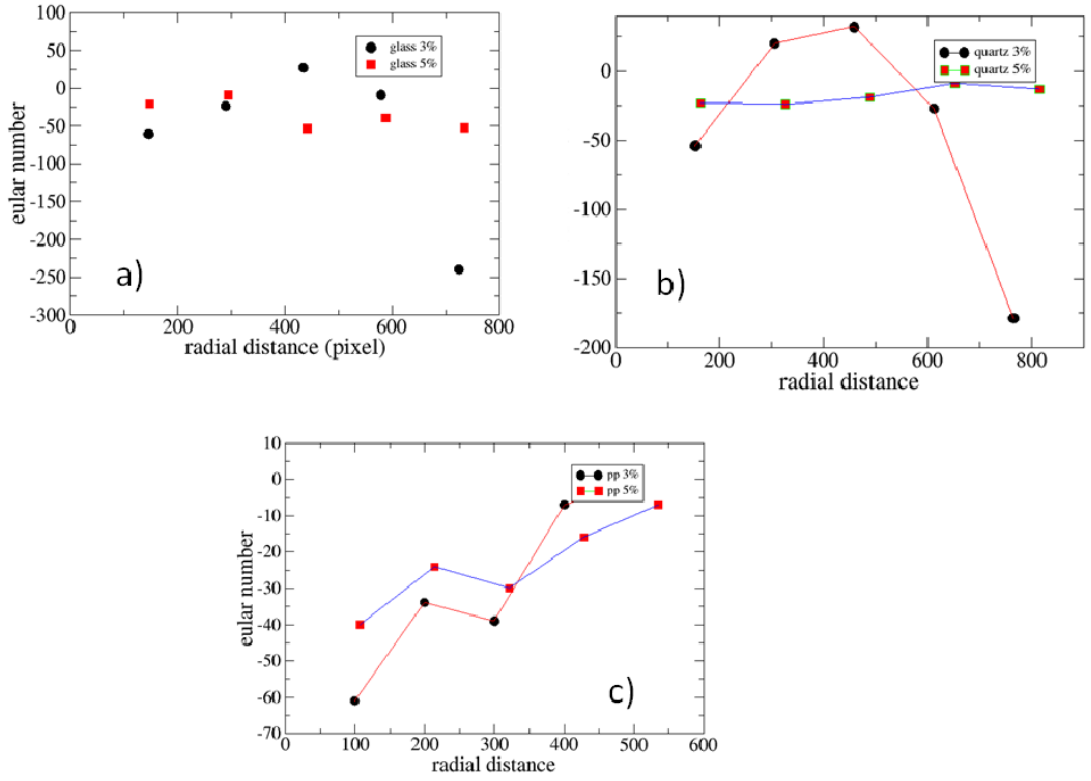

Figure 7.3: Variation of Euler characteristic χ(r) with r (pixel) for 3% and 5% salt concentration. Figures a, b and c indicate the variation for glass, quartz and PP substrates, respectively

The variation of Euler characteristic χ(r) with distance r as measured from the deposit centre of symmetry is plotted for both hydrophilic and hydrophobic substrates, and for both salt concentrations as shown in Fig.7.3.

As one moves from droplet centre to periphery for hydrophilic substrates, glass and quartz, χ(r) is confined to between 0 to -50, Fig.7.3 a, b. At the droplet periphery, r $\sim$ 800, there is a sharp drop in χ(r) to almost $\sim$ -200 for the patterns on hydrophilic

substrates. However, this drop occurs for 3% concentration on glass and for 5% concentration on quartz, implying that the deposition of crystals is determined by a combination of hydrophobicity and salt concentration. From Eq.7.4, it follows that the difference between the number of crystallite clusters and their absence is small, implying an almost uniform deposition on the substrate. The dendritic growth that is visible under the microscope is manifested within the cluster number variation contained in the small range between 0 to -50. Moreover, though the general nature of the variation of Euler characteristic with distance is similar for glass and quartz, for a particular substrate, say quartz, there is a marked difference in $\chi(r)$ with r as the salt concentration is varied. For a 5% salt concentration, the dendritic pattern of crystal deposition is thick and spread almost uniformly on the substrate, manifested in a uniform value of $\chi(r)$ with r. For 3% salt concentration, most of the deposition occurs away from the TPCL indicating that solutal Marangoni flow predominates over radial convective flow and guides the deposition process.

In comparison, for hydrophobic substrate as PP, $\chi(r)$ shows a pronounced oscillation within the same range, Fig.7.3 c. From Eq.7.4, it follows that there is a periodicity in the number of crystallite clusters as we move from droplet centre to the periphery. As the periodic variation in $\chi(r)$ is only a function of r, the crystallite deposition patterns must be concentric rings about the droplet centre. The variation of the Euler characteristic with r implies that a stick-slip movement of the TPCL has occurred during drying".

7.6 Wetting and Drying

"Contact angles between fluid and substrates were measured with profile photographs of the droplets displayed in Fig.7.4.

The measured values of the contact angles between substrate and solution pre- pared with different concentrations of salt, are summarized in Table.7.1.

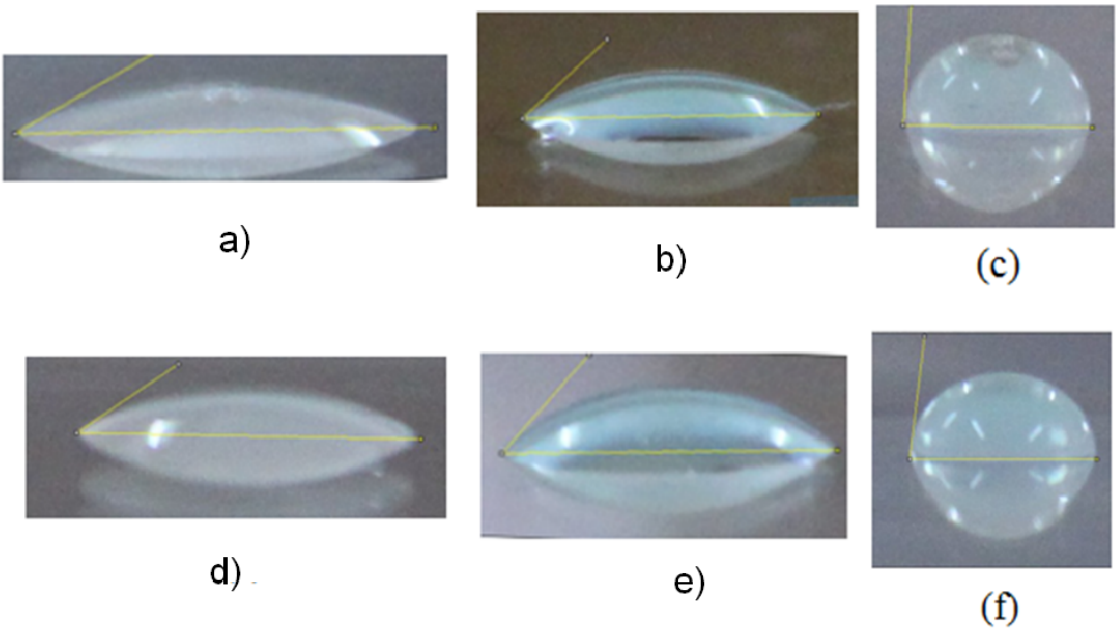

Figure 7.4: Droplet profile of 3% salt solution on different substrates: (a) glass (b) quartz (c) polypropylene(PP). Droplet profile of 5% salt solution on different substrates: (e) glass (f) quartz (g) polypropylene(PP).

While both glass and quartz are hydrophilic, PP is clearly hydrophobic with respect to $CuSO_4$ substrate. Quartz has a hydrophobicity in between that of glass and PP. It was observed that the contact angle of the salt solutions with all the substrates increased with an increase in the salt concentration. The contact angle with glass changed by $\sim$ 39%, while for quartz, the increase was 16%, for a concentration change of 2%. In case of PP, the contact angle however decreased by $\sim$ 2

Evaporation rates of the drying droplet for both salt concentrations and all the substrates was measured and the results are displayed in Fig.7.5.

As the hydrophobicity of a substrate increases,i.e., as the contact angle increases, the ratio of height to base area of a droplet increases for the same volume of fluid. The highest evaporation flux shifts from the droplet Triple Phase Contact Line(TPCL)

Substrate	Salt concentration 3%	Salt concentration 5%
Glass	26.6	36.9
Quartz	40	46.4
Polypropylene	83.7	82

Table 7.1: Contact angle for different substrates and salt concentrations

to the droplet apex. Total evaporation time decreases with increase in hydrophobicity as seen in Fig.7.5(a)for salt concentration of 3%. The evaporation decreases quadratically with time, with the plot showing distinct broken lines indicative of a stick-slip motion of the TPCL. When the contact line shifts to a new position and the contact angle increases, the droplet height increases too. This results in a sudden lowering of evaporation rate which picks up gradually as the droplet evaporates in constant contact angle (CCA) mode. For PP substrate, it is evident that the TPCL remains pinned for a much longer time compared to either glass or quartz. This enables greater growth of crystallites at the TPCL which is the region where salt reaches its highest supersaturation. This stick-slip motion of the TPCL is manifested in the alternate prominent periodic circular rings of salt deposit seen in this case.

In Fig.7.5 b, for 5% salt concentration, the evaporation rate decreases almost linearly for all three substrates. However the rate of decrease on glass substrate is substantially lowered in the higher salt concentration and equals the rate of evaporation on PP. This can be reconciled to the observation that a change in the salt concentration from 3% to 5%, resulted in an increase of 39% in the contact angle for glass. Here too the time of 'stick' of the TPCL is highest for PP substrate. As the salt concentration is higher, there is greater density of crystalline deposition at the TPCL as seen the deposition patterns.

The high evaporation flux at the TPCL for hydrophilic substrates is responsible for strong convective flow from droplet interior to the TPCL. As evaporation occurs,

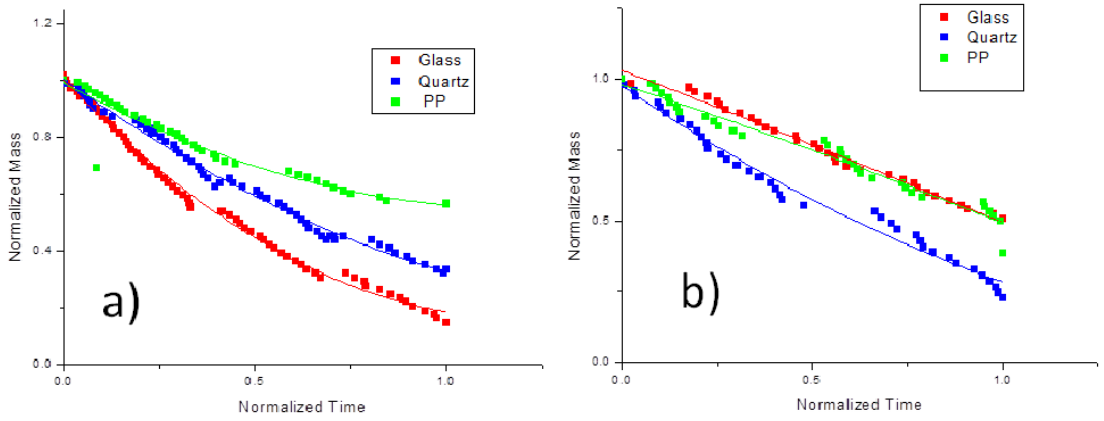

Figure 7.5: (a)Rate of evaporation for 3% salt concentration. (b)Rate of evaporation for 5% salt concentration.

the solution at the TPCL reaches the critical supersaturation necessary for crystallisation. Solutal Marangoni flow sets in because of increase in salt concentration and drives the flow inside the droplet from region of lower to higher surface tension, i.e. from the TPCL to the droplet apex. However with crystallization, the salt concentration in the immediate vicinity of the crystallization sites decreases. This in turn causes diffusion of solute to these areas. Therefore crystallization proceeds from the TPCL to the droplet interior. The thicker deposition of crystallites at the TPCL due to the higher evaporation flux here, results in much depletion of solute in the droplet at the later stages of evaporation. This is conducive to DLA like growth pattern observed in these cases

As the water evaporates and more and more crystallization occurs, the viscosity of the solution increases and flow is slowed down. In the case of PP, this is manifested

in broader bands of crystalline deposition as one moves from TPCL to apex as seen from the images for both concentrations.

For the hydrophilic substrates as in glass and quartz, the lower contact angle together with increase in viscosity, is responsible for a Saffman-Taylor instability that shows up as viscous fingers at the TPCL. This causes deposition pattern in the form of 'fingers', evident from the images in Fig.7.2. The salt 'fingers' are very stark for glass substrate at 5% and for quartz at 3% salt concentrations. The salt fingers occur with a periodicity of 66μm in the former and 75μm in the latter. Conversely in terms of the salt 'finger' thickness, for glass substrate at 5% concentration, the finger thickness is 98μm , with the thickness being 37μm on quartz. It is well established that prominent viscous fingers are a result of a suitable viscosity contrast, η_c, between two fluids at thee interface. It is interesting to note that the prominent fingers on glass substrate occurs at a higher salt concentration whereas the fingers are more prominent on quartz at the lower salt concentration. Again while both glass and quartz are both hydrophilic, glass has a lower contact angle than quartz. The lesser the contact angle, greater is the radial convective flow that is manifested in thicker fingers at the TPCL; the higher the salt concentration, the thicker is the salt finger deposit. For lower contact angles, fingering deposition was observed at higher salt concentration which enhanced the viscosity of the solution. This in turn impedes the convective flow at the TPCL, thereby enabling the growth of viscous fingers. As the contact angle increases, the evaporation flux gradient between droplet apex and TPCL weakens, resulting in a slower radial convection. This again enables the formation of viscous fingers despite the lower viscosity at lower salt concentration. Thus we propose that the appearance of salt fingers at the TPCL of a drying salt solution is determined by an optimal radial convection velocity v_{opt} that is a function of contact angle and salt concentration for a given ambient condition. If the evaporation flux at the TPCL is very high, the resulting convective flow of salt may be too fast to allow the viscous fingers to form well. However if the flow velocity can be tempered by increasing the viscosity of the fluid sufficiently, (in our

case the higher salt concentration does the trick), fingering can be obtained. With increase in hydrophobicity, the weakening effect of the radial convective flow at the TPCL can be compensated by a lower viscosity of the solution".

7.7 Conclusion

"Self-assembled aggregates of $CuSO_4$ deposits are achieved through droplet drying of the salt solution on hydrophilic and hydrophobic substrates. The deposited patterns are found to be starkly different for the two categories of substrates. The patterns were examined for two different concentrations of salt solution.

Topology of the salt aggregates in the dried droplet was measured as the variation of Euler characteristic χ versus r, for the different combinations of substrate and salt concentrations. The homogeneous distribution of salt for hydrophilic substrates was reflected in the almost steady value of χ with r. However, the periodicity of circular deposition of salt aggregates for hydrophobic substrates was evident as oscillations in the χ value with r. The denser deposits of salt aggregates at higher salt concentrations showed up in the higher χ values in this case.

The presence of prominent 'viscous finger' like salt deposition at the TPCL was observed at certain combinations of substrate contact angle and fluid viscosity. We proposed that prominent salt fingers are determined by an optimal radial convection velocity v_{opt} that controls the rate at which salt is transported from the droplet interior to the periphery. Thus, where the contact angle is smaller, fingers are observed at higher salt concentrations, whereas higher contact angles require low salt concentrations for the appearance of 'fingers'. The formation of viscous fingers in context to substrate hydrophobicity and salt concentration has not been reported earlier as far as the knowledge of the authors

Thus, the self-assemblage of salt crystallites in a micro-litre droplet of a colloidal solution shows a variety of patterns that are guided by choice of substrate and salt

concentration. A suitable choice of these parameters can be used to fine-tune pattern formation obtained in evaporating droplets. The authors propose that the analysis techniques used in this work can be adopted for quantification of both geometrical and topological features of complex patterns of drying droplet. With a sufficiently large repository of data, measures may be identified with features of deposition patterns that are atypical of well-understood drying processes".

Bibliography

[1] D. Zang, S. Tarafdar, Y. Y. Tarasevich, M. D. Choudhury and T. Dutta, *"Evaporation of a droplet: From physics to applications"*, *Physics Reports* **804** 1--56 (2019).

[2] D. Brutin and V. Starov, *"Recent advances in droplet wetting and evaporation"*, *Chemical Society Reviews* **47** 558--585 (2018).

[3] K. Sefiane, *"Patterns from drying drops"*, *Advances in colloid and interface science* **206** 372--381 (2014).

[4] S. Tarafdar, Y. Y. Tarasevich, M. Dutta Choudhury, T. Dutta and D. Zang, *"Droplet drying patterns on solid substrates: from hydrophilic to superhydrophobic contact to levitating drops"*, *Advances in Condensed Matter Physics* **2018** 1--24 (2018).

[5] R. D. Deegan, O. Bakajin, T. F. Dupont, G. Huber, S. R. Nagel and T. A. Witten, *"Capillary flow as the cause of ring stains from dried liquid drops"*, *Nature* **389** 827--829 (1997).

[6] R. D. Deegan, *"Pattern formation in drying drops"*, *Physical review E* **61** 475 (2000).

[7] A. Shimoni, S. Azoubel and S. Magdassi, *"Inkjet printing of flexible high-performance carbon nanotube transparent conductive films by "coffee ring effect""*, *Nanoscale* **6** 11084--11089 (2014).

[8] V. Shabalin and S. Shatokhina, *"Diagnostic markers in the structures of human biological liquids"*, *Singapore medical journal* **48** 440 (2007).

[9] E. Rapis, *"A change in the physical state of a nonequilibrium blood plasma protein film in patients with carcinoma"*, *Technical Physics* **47** 510--512 (2002).

[10] B. Roy, S. Karmakar and S. Tarafdar, *"Self assembled transparent conducting network of multi-walled carbon nanotubes formed by evaporation"*, *Materials Letters* **207** 86--88 (2017).

[11] D. L. Dietrich, V. Nayagam, M. C. Hicks, P. V. Ferkul, F. L. Dryer, T. Farouk et al., *"Droplet combustion experiments aboard the international space station"*, *Microgravity Science and Technology* **26** 65--76 (2014).

[12] N. Shahidzadeh-Bonn, S. Rafaı, D. Bonn and G. Wegdam, *"Salt crystallization during evaporation: impact of interfacial properties"*, *Langmuir* **24** 8599--8605 (2008).

[13] S. Y. Misyura, *"High temperature nonisothermal desorption in a water–salt droplet"*, *International Journal of Thermal Sciences* **92** 34--43 (2015).

[14] S. Y. Misyura, *"Evaporation and heat and mass transfer of a sessile drop of aqueous salt solution on heated wall"*, *International Journal of Heat and Mass Transfer* **116** 667--674 (2018).

[15] A. Marin, S. Karpitschka, D. Noguera-Marín, M. A. Cabrerizo-Vílchez, M. Rossi, C. J. Kähler et al., *"Solutal marangoni flow as the cause of ring stains from drying salty colloidal drops"*, *Physical review fluids* **4** 041601 (2019).

[16] B. Pathak, J. Christy, K. Sefiane and D. Gozuacik, *"Complex pattern formation in solutions of protein and mixed salts using dehydrating sessile droplets"*, *Langmuir* **36** 9728--9737 (2020).

[17] L. Pauchard, F. Parisse and C. Allain, *"Influence of salt content on crack patterns formed through colloidal suspension desiccation"*, *Physical Review E* **59** 3737 (1999).

[18] R. Chen, L. Zhang, D. Zang and W. Shen, *"Adv. colloid sci"*, 2016.

[19] S. Bhattacharyya, B. Roy and M. D. Choudhury, *"Pattern formation in drying drops of colloidal copper sulphate solution on glass surface"*, *Journal of Surface Science and Technology* **32** 79--84 (2017).

[20] S. Bhattacharyya, B. Roy and S. Tarafdar, *"Aggregation of crystalline copper sulphate salt in a gelatin medium"*, *Fractals* **25** 1750038 (2017).

[21] M. D. Choudhury, T. Dutta and S. Tarafdar, *"Growth kinetics of nacl crystals in a drying drop of gelatin: transition from faceted to dendritic growth"*, *Soft Matter* **11** 6938--6947 (2015).

[22] T. Dutta, A. Giri, M. D. Choudhury and S. Tarafdar, *"Experiment and simulation of multifractal growth of crystalline nacl aggregates in aqueous gelatin medium"*, *Colloids and Surfaces A: Physicochemical and Engineering Aspects* **432** 127--131 (2013).

[23] M. D. Choudhury, T. Dutta and S. Tarafdar, *"Pattern formation in droplets of starch gels containing nacl dried on different surfaces"*, *Colloids and Surfaces A: Physicochemical and Engineering Aspects* **432** 110--118 (2013).

[24] M. Buzoverya, Y. P. Shcherbak and I. Shishpor, *"Quantitative estimation of the microstructural inhomogeneity of biological fluid facies"*, *Technical Physics* **59** 1550--1555 (2014).

[25] Y. Y. Tarasevich and D. M. Pravoslavnova, *"Segregation in desiccated sessile drops of biological fluids"*, *The European Physical Journal E* **22** 311--314 (2007).

[26] Y. Y. Tarasevich, I. Vodolazskaya and O. Bondarenko, *"Modeling of spatial–temporal distribution of the components in the drying sessile droplet of biological fluid"*, *Colloids and Surfaces A: Physicochemical and Engineering Aspects* **432** 99--103 (2013).

[27] J. M. Stauber, S. K. Wilson, B. R. Duffy and K. Sefiane, *"Evaporation of droplets on strongly hydrophobic substrates"*, *Langmuir* **31** 3653--3660 (2015).

[28] J. M. Stauber, S. K. Wilson, B. R. Duffy and K. Sefiane, *"On the lifetimes of evaporating droplets"*, *Journal of Fluid Mechanics* **744** R2 (2014).

[29] F. G. Schofield, D. Pritchard, S. K. Wilson and K. Sefiane, *"The lifetimes of evaporating sessile droplets of water can be strongly influenced by thermal effects"*, *Fluids* **6** 141 (2021).

[30] F. Schofield, S. Wilson, D. Pritchard and K. Sefiane, *"The lifetimes of evaporating sessile droplets are significantly extended by strong thermal effects"*, *Journal of Fluid Mechanics* **851** 231--244 (2018).

[31] G. Dunn, S. Wilson, B. Duffy, S. David and K. Sefiane, *"The strong influence of substrate conductivity on droplet evaporation"*, *Journal of Fluid Mechanics* **623** 329--351 (2009).

[32] S. David, K. Sefiane and L. Tadrist, *"Experimental investigation of the effect of thermal properties of the substrate in the wetting and evaporation of sessile drops"*, *Colloids and Surfaces A: Physicochemical and Engineering Aspects* **298** 108--114 (2007).

[33] T. Khatun, T. Dutta and S. Tarafdar, *""islands in sea" and "lakes in mainland" phases and related transitions simulated on a square lattice"*, *The European Physical Journal B* **90** 1--6 (2017).

[34] H.-J. Vogel, H. Hoffmann and K. Roth, *"Studies of crack dynamics in clay soil: I. experimental methods, results, and morphological quantification"*, *Geoderma* **125** 203--211 (2005).

[35] W. Al Faqheri and S. Mashohor, *"A real-time malaysian automatic license plate recognition (m-alpr) using hybrid fuzzy"*, *International Journal of Computer Science and Network Security* **9** 333--340 (2009).

[36] M. Vatsa, R. Singh, P. Mitra and A. Noore, *"Signature verification using static and dynamic features"*, in *Neural Information Processing: 11th International Conference, ICONIP 2004, Calcutta, India, November 22-25, 2004. Proceedings 11*, pp. 350–355, Springer, 2004.

[37] A. Khatun, S. Haque, S. Tarafdar and T. Dutta, *"Impact of varying preparation methods of colloidal suspensions on droplet desiccation patterns on hydrophobic and hydrophilic substrates"*, *Physica Scripta* **96** 025211 (2020).

[38] Y. O. Popov, *"Evaporative deposition patterns: spatial dimensions of the deposit"*, *Physical Review E* **71** 036313 (2005).

[39] H. Hu and R. G. Larson, *"Analysis of the effects of marangoni stresses on the microflow in an evaporating sessile droplet"*, *Langmuir* **21** 3972--3980 (2005).

[40] H. Hu and R. G. Larson, *"Marangoni effect reverses coffee-ring depositions"*, *The Journal of Physical Chemistry B* **110** 7090--7094 (2006).

[41] M. Kobayashi, H. Nanaumi and Y. Muto, *"Initial deposition rate of latex particles in the packed bed of zirconia beads"*, *Colloids and Surfaces A: Physicochemical and Engineering Aspects* **347** 2--7 (2009).

[42] C. Tien, *"Granular filtration of aerosols and hydrosols, vol. 1"*, 1989.

[43] P. C. Hiemenz, *"Principles of colloid and surface chemistry. 2nd edn. new york: M"*, 1986.

[44] S. Tarafdar, S. Sinha, S. Nag and T. Dutta, *"Fingering and pressure distribution in lifting hele-shaw cells with grooves: A computer simulation study"*, *Physical Review E* **80** 026315 (2009).

[45] A. Roy, R. Haque, A. Mitra, M. D. Choudhury, S. Tarafdar and T. Dutta, *"Understanding flow features in drying droplets via euler characteristic surfaces—a topological tool"*, *Physics of Fluids* **32**, (2020).

[46] S. Dutta, S. Sen, T. Khatun, T. Dutta and S. Tarafdar, *"Euler number and percolation threshold on a square lattice with diagonal connection probability and revisiting the island-mainland transition"*, *Frontiers in Physics* **7** 61 (2019).